Diagnosis of Historical and Future Flow Regimes of the Bow River at Calgary Using a Dynamically Downscaled Climate Model and a Physically Based Land Surface Hydrological Model

Final Report developed under Agreement #AP744 for the
Natural Resources Canada Climate Change Adaptation Program

Centre for Hydrology Report No. 18

Zelalem Tesemma, Kevin Shook, Dan Princz, Saman Razavi, Howard Wheater, Bruce Davison, Yanping Li, Alain Pietroniro and John W Pomeroy

Centre for Hydrology, University of Saskatchewan
101-121 Research Drive, Saskatoon, Saskatchewan S7N 1K2

Disclaimer

This report was prepared by scientists from the University of Saskatchewan Centre for Hydrology between March 2018 and August 2020 with financial and in-kind assistance from Natural Resources Canada, Alberta Environment and Parks, the City of Calgary, Environment and Climate Change Canada and the Global Water Futures program. The finding of the report reflects the best judgment of the authors considering the knowledge, model, information, and data available at the time of preparation. Any use which a third party makes of this report, or any reliance on or decisions to be made based on it, are the responsibility of such third parties. The authors accept no responsibility for damages, if any, suffered by any third party because of decisions made or actions based on this report.

Executive summary

This report assesses the impacts of projected climate change on the hydrology, including the flood frequencies, of the Bow and Elbow Rivers above Calgary, Alberta. It reports on investigations of the effects of projected climate change on the runoff mechanisms for the Bow and Elbow River basins, which are important mountain headwaters in Alberta, Canada. The study developed a methodology and applied a case study for incorporating climate change into flood frequency estimates that can be applied to a variety of river basins across Canada. This research was carried out by scientists from the University of Saskatchewan Centre for Hydrology, under contract to Natural Resources Canada and Alberta Environment and Parks with contributions from the City of Calgary, Environment and Climate Change Canada and the Global Water Futures program.

A high resolution, enhanced version of Environment and Climate Change Canada's MESH (Modélisation Environnementale Communautaire - Surface Hydrology) land surface hydrological model was set up at a spatial resolution of approximately 4 km by 4 km to correspond to the resolution of dynamically downscaled Weather Research Forecast (WRF) atmospheric model outputs for current and future climates in the region. This convection-permitting WRF product used ERA-Interim reanalysis product boundary conditions over 2000 - 2015 to produce realistic, high resolution weather simulations. Other available meteorological forcings were evaluated at the lower resolution of approximately 10 km by 10 km for which MESH is normally run. Prior to this study, MESH did not consider the impact of slope and elevation on meteorological forcings below the resolution of the data, which is not a reasonable assumption in mountains. Here, incoming solar radiation was calculated as a function of terrain slope and aspect. Also, precipitation, temperature, pressure, humidity and longwave radiation were corrected for elevation. The necessary cold regions processes (blowing snow, intercepted snow, sublimation, frozen soil infiltration, slope/aspect impacts on melt rates, glacier ice melt) and water management processes needed to simulate the natural and reservoir-managed streamflow hydrographs in the basin were modelled. Most model parameter values were set based on remote sensing, land surveys and the results and understandings from previous regional hydrological investigations, however forest root depth and stomatal resistance, and soil hydraulic conductivity and channel routing model parameters were calibrated using measured (2006 - 2015) streamflows on the Bow River at Banff, and evaluated (2000 - 2005) at the same stream gauging station. The pseudo global warming (PGW) approach to dynamical downscaling of future warming projection under RCP8.5 (2086 - 2100), used WRF bounded by ERA-Interim outputs that were perturbed by the mean outcomes of an ensemble of Coupled Model Intercomparison Project Phase 5 (CMIP5) climate model projections.

The simulation results show that, by the end of the century, snowmelt runoff events are projected to increase by up to six events per year, an approximately 20% increase, in the highest elevations of Central Ranges of the Canadian Rockies, primarily in Banff National Park (BNP), and to decrease by up to fourteen events per year, a decrease of approximately 100% in the lower elevation foothills. Snowmelt runoff itself would virtually cease at the middle to lower elevations of the basins. Rain-on-snowmelt events are projected to become more frequent at all elevations (100%-200% increase), particularly in Banff National Park, the Kananaskis and Elbow river

headwaters, and the agricultural lands in the eastern part of the basins, but less frequent in the foothills where they will drop by 50%. The future reduction in frequency of rain-on-snowmelt events in the foothills is associated with a substantial shortening of the snow-covered period and its increase at medium to high elevations and on the plains is due to more frequent rainfall in winter on the plains and spring in the high mountains. Compared with the historical period, rainfall-runoff events are projected to become more frequent and widespread. They currently cause more than four events per year only in the foothills and eastern part of the basins, this will decline dramatically in the agricultural areas as soil become drier. However, overall, there will be an increase of four events per year for the Bow River Basin, particularly in the foothills, but also in the high mountains, as the warmer climate increases the proportion of precipitation falling as rain. Glacier contributions to runoff will decline dramatically at high elevation locations with concomitant deglaciation, providing notable declines in late summer streamflow above Banff. This is projected to cause a reduction in annual streamflow volumes of less than 2% for the Bow River at Calgary and will have no impact on the Elbow River.

A novel way was devised to use bias correction from streamflow observations to reduce the uncertainty of modelled and projected flow duration curves. The effects of climate change on future streamflow is likely to reduce the highest streamflows and to increase the medium and low flows. A detailed examination of historical floods in June of 2005 and 2013 and how such events may shift under future climates showed increases in flood event flow volumes for the Bow River at Banff, but reductions in flood event flow volumes at Calgary in both the Bow and Elbow rivers. These shifts can be attributed to changes in the precipitation regime, and to reduced rain-on-snow runoff and antecedent snowmelt runoff from the Front Ranges – both are consequences of warmer conditions. The increase in rainfall runoff components of the events that causes higher flow volumes at Banff is unable to compensate for the decrease in snowmelt runoff and rain-on-snowmelt runoff components in the Front Ranges and so overall, the flood event flow volumes are smaller at Calgary.

A companion report, Centre for Hydrology Report No. 17 incorporates future climate uncertainty from RCMs into subsequent WRF-MESH modelling exercises and should be considered along with this foundational report as part of the comprehensive case study of how to estimate future flood streamflows using coupled climate and hydrological models.

Table of contents

1. Introduction

The impacts of climate change on water resources and flooding are of paramount importance to Canadians and are of particular interest to Calgary, Alberta where Canada's most expensive riverine flooding event occurred in June, 2013 with some loss of life as well as over $6B in economic damage and where a city of over 1.2M and a large downstream irrigation district rely on the flows of the Bow and Elbow rivers for municipal supply and food production. Besides being a reliable "water tower" for water resources and occasionally a source of major flooding, the Canadian Rockies headwaters of the Saskatchewan River system have been subject to rapid climate warming and deglaciation over the last 50 years. This has created uncertainty in assessments of flood potential for current and future climates. Natural Resources Canada and Public Safety Canada have jointly established a Technical Subcommittee on Climate Change and Floodplain Mapping which has noted the challenges in floodplain mapping under non-stationarity due to the impacts of a changing climate on hydrology. The Technical Subcommittee was interested in obtaining a case study of the impacts of climate change on the hydrological regime and flooding on the Bow River at Calgary. This study will feed into other research and into development of updated hydraulic modelling of the river and will thus lead to reductions in uncertainty for floodplain delineation in a time of changing climate.

This report assesses the impact of projected 21st Century climate change on the hydrology, including the flood frequencies, of the Bow and Elbow Rivers above Calgary, Alberta. The report investigates the effects of projected climate change on the runoff mechanisms for the partially glaciated Bow and the Elbow River basins. It then develops a methodology and applies a case study for incorporating climate change into flood frequency estimates that can be applied for a variety of river basins across Canada. This research was carried out by scientists from the University of Saskatchewan Centre for Hydrology between March 2018 and August 2020 with financial and in-kind assistance from Natural Resources Canada, Alberta Environment and Parks, the City of Calgary, Environment and Climate Change Canada and the Global Water Futures program.

1.1 Background

The Bow River Basin above Calgary (including the Elbow River tributary) is one of the most important river basins in all of Canada. The economies of the three Prairie Provinces depend on flows from this basin. Conversely, when floods occur, damages can occur in all three provinces (Pomeroy et al., 2015; Shook, 2016).

The basin contains the largest city in Alberta, which is responsible for much of the province's economy. It also contains a national park and several provincial parks and other protected wilderness areas that constitute a UNESCO World Heritage site. Runoff originating in the headwaters of the Bow River Basin forms streamflow that supplies cities and towns in Alberta, most importantly the city of Calgary, as well as in Saskatchewan and Manitoba. This water is also used for irrigation in southern Alberta,, the largest irrigation district in Canada and a major food

supply and economic driver, - and contributes to irrigation in Saskatchewan. The Bow River Basin is responsible for much of Alberta's hydroelectric generation and contributes to hydroelectric generation in Saskatchewan and Manitoba. Importantly, the water provides the basis for aquatic and riverine ecosystems from the lakes and streams of Banff National Park downstream to Lake Diefenbaker. It influences the aquatic ecosystems of the Saskatchewan River, Lake Winnipeg, the Nelson River and discharges into Hudson Bay. The sediment, nutrients, temperature and water levels in this system contribute to ecosystem services across three provinces.

The Bow River Basin above Calgary is a complex assembly of agricultural, grassland, forest, alpine, lake and glaciated terrain whose semi-arid to alpine climate has already shown sensitivity to the changing climate. Flows in this region are generated by snowmelt, rainfall, melt of accumulated snow on glaciers (Bash and Marshall, 2014) and glacier wastage (Hopkinson and Young, 1998; Bash and Marshall, 2014), all of which are strongly affected by climate change. The 2005 and 2013 floods devastated many communities within the basin and downstream (Shook, 2016; Pomeroy et al., 2015), and have naturally led to increased interest in how climate change will affect flooding within the basin. So far, traditional statistical techniques are unable to reliably estimate changes in flood frequency due to the temporal clustering of events and differences between the mechanisms that generate large floods and those that generate annual peak flows (Whitfield and Pomeroy, 2016).

Studies have been carried out on the effects of climate change within the region on future precipitation and streamflow extremes (Gizaw and Gan, 2016; Whitfield and Pomeroy, 2016), and there have also been several modelling studies of the same. However, none of the studies carried out to date have combined sophisticated, high-resolution downscaling of future climate scenarios, with sophisticated, distributed hydrological models capable of modelling the cold-region processes which affect this region.

1.2 Previous modelling studies

Many models have been developed which attempt to represent the Bow River Basin above Calgary. Some models have been concerned with water management within the basin (Sheer et al., 2013), rather than attempting to model the headwater hydrology. Other, data driven, models have only attempted to model the discharges at a point from flows at other locations, without attempting to simulate the basin hydrology (Veiga et al., 2015). Bash and Marshall (2014) conducted sophisticated glacier modelling of the glacial contributions to the Bow and Elbow Rivers, but did not extend their modelling to other components of the basin hydrology, nor did they extend the modelling to account for the effects of future climates.

Some researchers have attempted to evaluate the effects of climate change on streamflows within the Bow and Elbow basins above Calgary, but these attempts have been undermined by the use of models which were not capable of modelling the appropriate cold-region processes. Valeo et al. (2007) used Canadian Regional Climate Model (CRCM) data to force a SSARR Watershed model of the Elbow River. The SSARR model does not contain physical representations of cold-region processes; indeed, it contains virtually no physics.

Tanzeeba and Gan (2012), Islam (2013) and Islam and Gan (2014) modelled the effects of climate change on flows on the South Saskatchewan River basin, of which the Bow Basin is a headwaters tributary. However, the MISBA model used, although capable of physically based snowmelt calculations, does not incorporate such important cold-region processes as infiltration to frozen soils, nor the erosion, deposition or sublimation of snow by blowing snow. Nor does it contain any modules for the simulation of glaciers. Therefore, the model results are difficult to extrapolate to changing climate conditions and extreme events.

Farjad et al. (2015) modelled the Elbow River basin, using the MIKE SHE/MIKE 11 model. Although MIKE 11 has quite sophisticated hydraulics, MIKE SHE is completely unsuited to the modelling of cold-regions basins. The single-layer snowmelt model is not sufficient for deep mountain snowpacks, the model cannot simulate the interception of snow by forest canopies or sublimation losses, it cannot simulate infiltration to frozen soils, and in cannot simulate the effects of blowing snow redistribution. It does not have a glacier model.

There are several studies on water resource management under climate change, for instance, Nazemi and Wheater (2014) have explored the potential impact of climate change and assessed water resource vulnerability for the Oldman River basin in Alberta, Canada. Islam and Gan (2014) simulated the operation of reservoirs, but Tanzeeba and Gan (2012) simulated only natural flows. The Elbow River has a reservoir near Calgary, but the Bow River has several reservoirs between Banff and Calgary. The Elbow River can be considered unregulated above Sarcee Dam and the Bow River considered unregulated above Banff.

The hydrological processes which govern runoff and streamflow in cold mountain regions are complex. All of the processes are affected by energy fluxes and storages, so models which do not represent the energetics properly cannot give good results under changing climate conditions. As a simple example, the majority of hydrological models represent snowmelt as a simple cumulative function of air temperature, when it is actually based on all of the fluxes of energy (largely driven by solar radiation) and energy storage within the snowpack. Any model which cannot simulate major the fluxes and storages correctly will inevitably give incorrect results under changing conditions.

None of the models mentioned above are capable of simulating the horizontal fluxes of snow and water vapour driven by blowing snow. These fluxes are important in governing the redistribution of snow within alpine, glacier, grassland and agricultural zones of a river basin and are extremely sensitive to precipitation, wind speed, humidity and air temperature. Although the models used in the studies in the listed above may have produced acceptable streamflow synthesis under the current conditions for which they were heavily calibrated, they cannot be assumed to give good results in the future, or for the current hydrological cycle, as they do not adequately represent the processes which affect streamflows.

Harder et al. (2015) demonstrated the complexities of the response of Marmot Creek, a small catchment within the Kananaskis Valley of the Bow River Basin, to changes in climate and forest

management. Despite large changes in forest cover and climate forcing, there was little change in Marmot Creek discharge volumes, extremes or timing of flows over a period of 51 years, although the fluxes and storages of water within the catchment changed greatly. Similar complexities of mountain basins have been demonstrated at other mountain basins in Canada, the US and Spain (Rasouli et al., 2015; López-Moreno et al., 2013), showing non-linear responses to changes in forcings. Rasouli et al. (2019) and Fang and Pomeroy (2020) showed modest changes to annual streamflow discharge volume but much earlier freshet and peak flows in Marmot Creek, despite large changes in hydrological processes associated with climate change to mid-century respectively. They showed some evidence of compensatory processes causing apparent resilience to the impacts of climate change on streamflow.

1.3 Objectives

There is a need for a study based on a model capable of simulating all of the cold regions processes which affect the Bow River Basin's hydrological response, and which also incorporates the operation of the many dams within the region that influence downstream flows, to demonstrate the effects of changes in local climate on the flows of the Bow and Elbow rivers at Calgary. It is essential that the model be forced with future climate simulations which are downscaled sufficiently well to represent the spatial variability of precipitation caused by convection and mountain orography. Fortunately, both an appropriate modelling tool, and finely downscaled future climate data have become available in the last few years, due in large part to work by Environment and Climate Change Canada and the Global Water Futures program at the University of Saskatchewan.

This study has two primary objectives:

1) to estimate the changes in flood frequencies of the Bow River at Calgary (including the Elbow) under climates of the mid to late 21st Century using a physically based, spatially detailed hydrological model driven by downscaled global atmospheric models.
2) to develop a novel methodology for incorporating climate change into flood frequency estimates, based on state-of-the-art physically based hydrological and water resource modelling, applicable to the wide range of river basins across Canada.

2. Methodology

Data required to operate the hydrological model includes meteorological forcing data to drive the model and streamflow data to calibrate and validate it. These data sets require pre-processing and conversion/formatting before they can be used for modelling. All pre-processing was done using Geographical Information Systems (GIS), the open-source language R (Ihaka and Ross, 2007), and MATLAB.

2.1 Description of the study area

This project models the Bow and Elbow River Basins at Calgary in Alberta (Figure 1). The upper Bow River Basin at Banff has an area of 2207 km^2 with elevations ranging from 1376 to 3455 m.a.s.l. (metres above sea level).

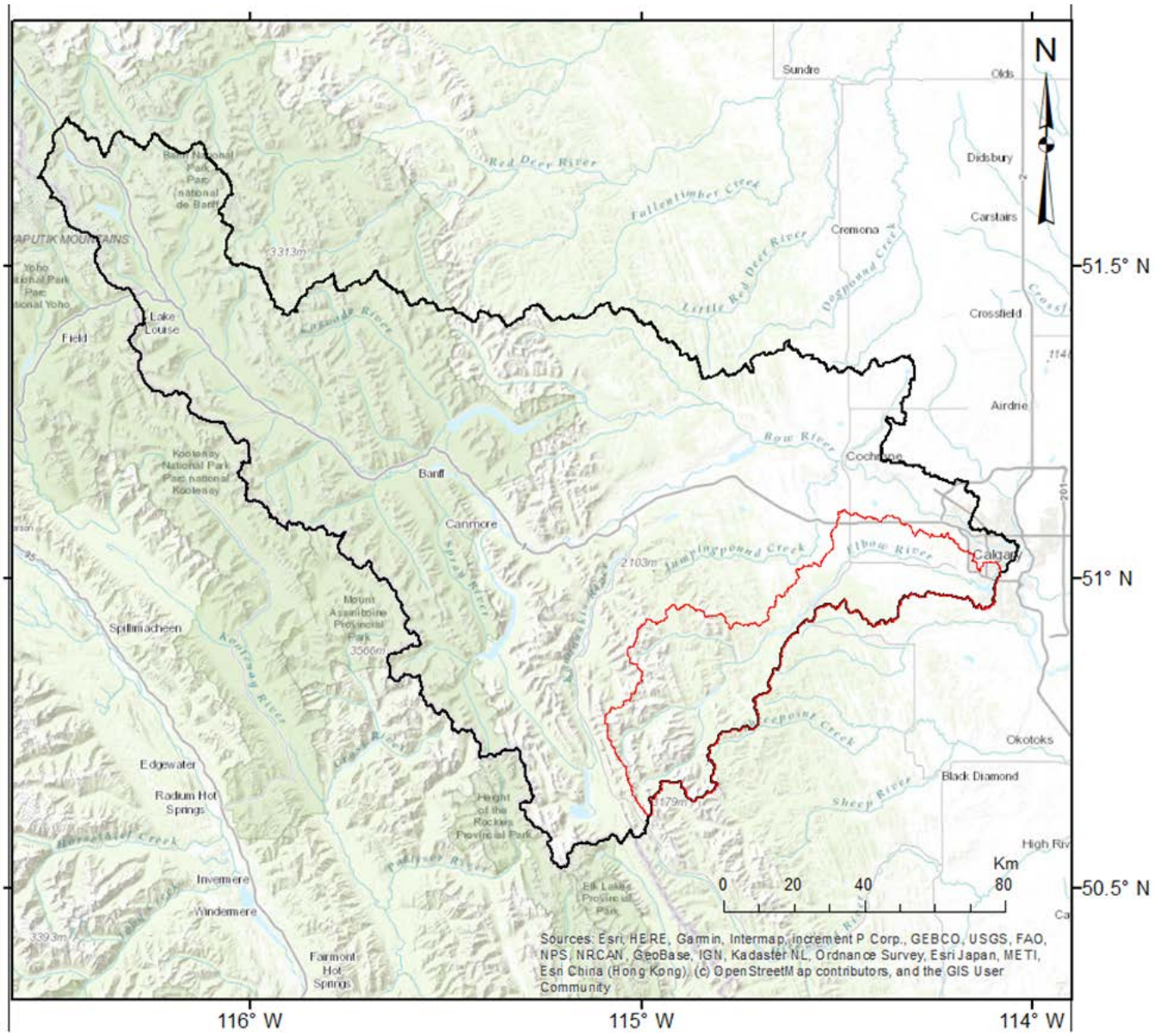

Figure 1. The Bow and Elbow River Basins above Calgary. The Elbow River Basin is shown in red.

The Elbow River Basin above Sarcee Bridge has an area of 1190 km^2 with elevations ranging from 1054 to 3065 M.A.S.L. The combined area of the Bow and Elbow River basins at Calgary is 9116 km^2, with an elevation that varies from 1025 to 3459 M.A.S.L. The Elbow River joins the Bow River in the city of Calgary and the combined river later joins the Oldman River, forming the South Saskatchewan River.

The weather in the Upper Bow River basin is remarkable for its season-to-season, day-to-day, and even hour-to-hour variability (Whitfield and Pomeroy, 2016). Due to the large variation in elevation within the basins above Calgary, a correspondingly large spatial variability is found in the precipitation from the top of the mountains towards the valleys at seasonal and monthly scales. The majority of the precipitation in the basin is derived from convection events (in summer) and frontal events (in spring, fall and winter), which include persistent westerly storms and periodic heavy precipitation upslope events that focus the greatest depth of precipitation on the Front Ranges (Whitfield & Pomeroy, 2016). Based on the revised Köppen-Geiger climate classification system (Peel et al., 2007), the Upper Bow River Basin lies in the Dfc climate type, having a cold climate, and cold summer with no distinct dry season. The Upper Elbow River Basin has the Dfw climate type, which is a similar climate region except having a warm summer. The coldest month is both basins is January, which has a mean daily minimum air temperature ranging between -20°C and -15°C in the mountains; the hottest month is July, with mean daily maximum air temperature varying between 20°C and 25°C. Other climatic variables: radiation, temperature, precipitation, cloud cover, wind, etc. show significant variations with elevation. The climates of the east-west valleys differ from those of the north-south valleys and the microclimates of south-facing slopes differs from those of north-facing slopes.

The landscape of the Bow River Basin shows heterogeneity with various land covers such as glaciers, forest, grasslands, cultivated fields, water bodies and developed areas. Vegetation varies from foothills forests, to prairie grasslands and wetlands. Subalpine fir, Engelmann spruce and Lodgepole pine are the dominant forest species in the upper Bow River basin. There are a number of glaciers in the basin that supplement the Bow River which include the Bow, Wapta and Crowfoot in the north and the Haig in the southern part of the Bow River basin.

2.2 Spatial data

Available land surface data consist of digital elevation models (DEMs), i.e. the hydrologically conditioned HydroSheds DEM that has a spatial resolution of approximately 90 m available at (https://www.mrlc.gov/downloads/sciweb1/shared/hydrosheds), and its derived products including flow direction and drainage density. Soil data was collected from a rasterized version of the Soil Landscapes of Canada (SLC) dataset (https://open.canada.ca/data/en/dataset). The dataset covers Canada at 90 m spatial resolution and is derived from original data at a scale of 1:1M. This dataset has some missing information for the Bow River Basin, for instance there is no information on the percentages of clay and sand of the first soil layer (0 – 5 cm depth). Landcover data was downloaded from the Commission for Environmental Cooperation (CEC) (http://www.cec.org/north-american-land-change-monitoring-system/) covering all of the North America at a resolution of 30 m with 19 land cover classes. The Randolph Glacier Inventory 6.0

data (https://www.glims.org/RGI/rgi60_dl.html), based on Landsat imagery from 2004–06, were used to delineate glacier coverage in the basin. The inventory was generated and manually checked in 2008 (Bolch et al., 2010).

2.3 Meteorological data

There are many sets of gridded meteorological data available for large-scale hydrological modelling. The temporal resolution of these datasets varies from hourly to six-hourly and their spatial resolution varies from approximately 4 km to 55 km. The time periods for which the data sets are available range from 15 to 100 years (Table 1).

Table 1. List of climate forcing datasets used in this study

Forcing Inputs	Full Name	Record length	Spatial / Temporal resolution
EU-WFD-CRU	European Union Integrated Project Water and Global Change (EU-WATCH) Forcing Data	1901 - 2001	0.5° / 3 and 6 hourly
WFDEI	European Union Integrated Project Water and Global Change (EU WATCH) ERA-Interim	1979 - 2016	0.5° / 3 hourly
GEM-CaPA	Global Environmental Multiscale and Canadian Precipitation Analysis	2002 - 2019	0.09-0.22° / 1 hourly
WFDEI-GEM-CaPA	Bias corrected WFDEI using GEM-CaPA	1979 - 2016	0.125° / 3 hourly
CanRCM4-r8i2p1r1	Canadian Centre for Climate Modelling and Analysis Canadian Regional Climate Model	1950 - 2100	0.125° / 1 hourly
CanRCM4-WFDEI -GEM-CaPA	Bias corrected CanRCM4 using WFDEI-GEM-CaPA	1950 - 2100	0.125° / 3 hourly
WRF	Weather Research and Forecasting	2000 - 2015	0.05° / 1 hourly

The European Union Integrated Project Water and Global Change (EU-WATCH, 2007-11, www.eu-watch.org) meteorological forcing dataset has the longest historical record of all reanalysis data sets. WATCH Forcing Data (WFD) covers the period 1901 – 2001 at a 0.5° spatial resolution (about 55 km) with a 3 hour resolution for precipitation and downward shortwave radiation; other fluxes have a 6-hour resolution (Weedon et al., 2010, 2011). It has two sources of precipitation observation for assimilation into ERA-40 that result in two versions: Global Precipitation Climatology Centre (GPCC) and Climatic Research Unit (CRU). WFD comprises rainfall and snowfall rates, air temperature at 2 m, wind speed at 10 m, specific humidity at 2 m, surface pressure, downward longwave radiation flux and downward shortwave radiation flux.

The EU WATCH ERA-Interim (WFDEI) dataset is available for the period from 1979 to 2012, and is believed to be of better quality than the WFD data set. Enhanced computing power allowed WFDEI to use 4-dimensional variational assimilation (4D-Var) rather than 3D-Var as in EU-WFD.

It also increased horizontal resolution from 1.125 degrees (~125 km) to 0.703125 (~80 km) degrees, and used the latest cycle of the atmospheric model (ERA-Interim), taking advantage of improved model physics. Moreover, experience gained on variational bias correction of satellite radiance data, and more extensive use of radiances with an improved fast radiative transfer model improved the data assimilation of ERA-Interim. The temporal resolution of the data is the same as WFD data.

The second-highest resolution (0.09 degrees, approximately 10 km) gridded climate data set is GEM-CaPA (Global Environmental Multiscale and Canadian Precipitation Analysis). Because the GEM-CaPA record contains archived operational numerical weather prediction outputs, the resolution variables from 0.22 degrees to 0.09 degrees over the course of the record. GEM is the Canadian Global Environmental Multiscale model (Côté et al., 1998a, 1998b) used for numerical weather forecasting by ECCC. This study uses the Regional Deterministic Prediction System product (RDPS) from GEM, which has a spatial resolution of approximately 10-15 km (0.09-0.1375 degrees) over Canada, begins in 2002 and provides hourly values. The GEM precipitation is replaced in the dataset by that of the Canadian Precipitation Analysis (CaPA - Mahfouf et al., 2007) which assimilates observations. CaPA has a 6-hour time step and a 10 km resolution available from 2002 to date. Unfortunately, this dataset has a much shorter historical period of record than WFD or WFDEI. GEM-CaPA provides all the required meteorological fields required to drive land surface hydrological model including incoming shortwave radiation, incoming longwave radiation, precipitation, air temperature, barometric pressure, specific humidity and wind speed. To extend the temporal coverage of the GEM-CaPA data, the WFDEI dataset was bias-corrected with GEM-CaPA for the overlapping period (2004 - 2016) producing the WFDEI-GEM-CaPA dataset (Asong et al., 2020), developed by GWF, and which combines the advantages of WFDEI (the longer period of coverage and the finer temporal resolution), with the advantages of GEM-CaPA (the higher spatial resolution and better performance over Canada).

The third dataset is the Canadian Centre for Climate Modelling and Analysis Canadian Regional Climate Model (CanRCM4) between 1951–2100 under Representative Concentration Pathway-(RCP) 8.5 over the North American Domain. CanRCM4 shares the same package of physical parameterizations with the fourth-generation Canadian atmospheric global climate model (CanAM4) and the dynamic downscaling of the CanESM2 earth system model. This project used the CanRCM4 that was bias corrected using quantile mapping against WDFEI that was bias corrected using GEM-CaPA as described in Asong et al. (2020). As mentioned in that paper, the dataset has cascades of uncertainties which are transferred from one data to another during bias correction and so must be treated with caution. The dataset is available at an approximately 10 km by 10 km spatial resolution and 3- hour time step under the RCP8.5 scenario. The dataset has also included 15 ensamples for all climate variables that are required to drive land surface model to some how address climate forcing uncertainty assessments.

The highest spatial resolution climate dataset is from a recent application of the Weather Research and Forecasting (WRF) model that provides 4 km simulation outputs for both current and future climate scenario. The model has been used to dynamically downscale from reanalysis data with perturbations from an ensemble of Regional Climate Model (RCM) projections over

western Canada. The downscaling technique is called pseudo global warming (PGW) (Li et al., 2019). The high resolution WRF regional simulation uses convention-permitting models, which explicitly represent the fine-scale weather processes critical for simulating convective precipitation. Two sets of experimental runs were conducted: one consisting of a control (CTRL) simulation and a pseudo global warming (PGW) simulation. In the CTRL (historical for 2000 - 2015) simulation WRF was driven with initial and boundary conditions from 6-hour 0.703° ERA-Interim reanalysis data (Dee et al., 2011) whereas the PGW simulation (2000 - 2015) WRF model was driven with the 6-hour ERA-Interim reanalysis data plus a climate perturbation. The climate perturbation was derived from the Coupled Model Intercomparison Project Phase 5 (CMIP5) multi-model ensemble mean (19 ensemble members) under the RCP8.5 (business as usual emission scenario) from 2071–2100 relative to 1976–2005 (Rasmussen et al., 2011, 2014). There exists a large range of variability among the CMIP5 models' projections in temperature and precipitation under the RCP8.5 scenario, which can be attributed to the hierarchy of differences among the representation and parameterization of climatic processes in the models. It has been shown that the multi-model ensemble mean performs better than individual models in reproducing the historical climate. That is the reason for using the ensemble mean instead of a single model. The final outputs of the experiment represent the PGW weather for 2085 - 2100. From a hydrological perspective, these fine resolution simulations are required to model precipitation and runoff generation mechanisms for the complex terrain in mountains. Complex terrain has a large spatial variability in forcings, particularly of precipitation, due to the large differences in surface elevation over small distances. More information on the dataset development can be found in Li et al., 2019. It is noted that the changes in large scale teleconnections such as El Niño/Southern Oscillation (ENSO) and Pacific Decadal Oscillation (PDO) are not represented in this method. However, these teleconnections have no statistical association with floods on the Bow River (Whitfield and Pomeroy, 2016).

2.4 Streamflow data

The streamflow gauged data provided by the Water Survey of Canada (accessed 27 July 2020) were used were used to calibrate and validate the model. Gauge 05BB001 (Bow River at Banff) is particularly important as the basin above it is protected and unregulated, and the gauge has the longest streamflow record in the Alberta Rocky Mountains, beginning in 1909, and the observations are of exceptionally high quality (Whitfield and Pomeroy, 2017). The gauge has been particularly useful to researchers on the effects of climate change on streamflows (Hopkinson and Young, 1998; Bash and Marshall, 2014; Whitfield and Pomeroy, 2016). This gauge is included in the Canadian Reference Hydrometric Basin Network, because of its largely pristine basin condition (as all of the basin is located within a National Park) and its long record (Zhang et al., 2001). The flows of gauge 05BJ0010 (Elbow River at Sarcee Bridge) are also unregulated, making them suitable for model calibration and validation. The four streamflow gauge stations used in this study are listed in Table 2.

There are some discrepancies between the gross drainage area and modelled drainage area, generally smaller than 4%, caused by the size of the modelling grid.

Table 2. Details of streamflow gauging stations in the Bow and Elbow River Basins below Calgary

Gauge ID	River Name	Regulation type	Record length	Lat.	Long.	Gross drainage area (km^2)	Modelled drainage area (km^2)
05BB001	Bow River at Banff	Unregulated	1909 -	51.500	-115.572	2210	2220
05BH004	Bow River at Calgary	Regulated	1911 -	51.050	-114.051	7740	7899
05BJ010	Elbow River at Sarcee Bridge	Unregulated	1979 -	50.993	-114.170	1190	1156
05BJ001	Elbow River below Glenmore Reservoir	Regulated	1908 -	51.013	-114.093	1240	1156

2.5 Dams and reservoirs

The Bow River Basin contains a diverse range of water bodies from natural lakes to managed reservoirs. There are 11 dams within the drainages of the Bow and Elbow rivers at Calgary (Table 3). These water bodies play an important role in regulating the water flow of the river. These lakes and reservoirs are used for a variety of activities such as power generation, drinking water storage, and recreation. The descriptive parameters, listed in Table 3, were taken from Canadian Dam Association (2019). The locations of the 6 largest reservoirs, which were modelled explicitly, are shown in Figure 2.

Table 3. Dams in the Bow and Elbow Rivers above Calgary.

Name of dam	Year of completion	River	Nearest city	Height (m)	Crest Length (m)	Gross reservoir capacity (dam^3 = $1000m^3$)	Spillway capacity (m^3/s)
HORSESHOE	1911	Bow	Canmore	21	133		1274
KANANASKIS	1913	Bow	Canmore	18	207		1625
GHOST	1929	Bow	Cochrane	42	1289	131983	3110
GLENMORE	1933	Elbow	Calgary	27	277	19584	2500
CASCADE, LK. MINNEWANKA	1942	Cascade	Banff	35	617	387300	173
UPPER KANANASKIS (INTER. RES.)	1943	Kananaskis	Canmore	24	472	160354	
BARRIER	1947	Kananaskis	Canmore	44	707	23203	623
SPRAY CANYON, SPRAY LK. RES.	1951	Spray	Canmore	60	195	421854	170
THREE SISTERS	1951		Canmore	21	671		
BEARSPAW	1954	Bow	Calgary	32	395		2830
POCATERRA	1955	Kananaskis	Canmore	29	594	62908	94

3. MESH Model

3.1 Model configuration

Land surface models (LSMs) are used with GCMs and RCMs (coupled or offline) to represent the lower boundary condition of the atmosphere. These models typically represent the coupled energy and water balance, including vegetation and soil exchanges of energy and mass between the land-surface and the atmosphere. In the soil, these exchanges are based on numerical solution of the Richards equation using relatively coarse horizontal and vertical discretizations. However, all land surface schemes and most hydrological models have insufficient representation of complex terrain topography and cold regions processes to accurately simulate hydrology in high mountain basins (DeBeer and Pomeroy, 2017; Dornes et al., 2008b). Problems include poor representation of cold regions physical processes such as snow redistribution, snow cover depletion, snowmelt on slopes, and glacier melt in models, and low-resolution atmospheric inputs. These problems, coupled with the reality that large grid-sizes and sub-grid variability are rarely dealt with when modelling these processes, makes their use in hydrological studies and water resource applications problematic. For the present study, significant developments are included to overcome many of these limitations.

MESH (Modélisation Environnementale Communautaire - Surface Hydrology) couples the Canadian Land Surface Scheme (CLASS) and the WATROF sub-grid land flow routing scheme for sub-surface lateral flow (interflow) and overland flow to an assumed within-grid stream network. The hydrological response model of MESH is a blend of vertical flux equations from CLASS and lateral flux equations and concepts from WATFLOOD and other models (Pietroniro et al., 2007). The vertical flux equations of CLASS are more physically based than in most hydrological models and, within MESH, other critical cold regions processes are included such as blowing snow, frozen soil infiltration, slope/aspect, glacier melt, and the water management processes of reservoirs. Manning's equation is used to calculate the flows in the assumed stream network in each grid. Within each grid, the water level is assumed to be constant and channels are assumed to be rectangular, with sloping sides for the floodplain

The MESH model of the Bow and Elbow Rivers above Calgary has had substantial development for this study. "Mountain MESH" is an improved representation of slope, aspect and topography over the original MESH model, and was set up for Bow River Basin above Calgary. Lakes and reservoir management are also now included. Two MESH configurations were created, one with 10 km by 10 km spatial modelling grid that was consistent with the spatial resolution of the GEM-CAPA forcing (Figure 2, top panel) and the other with 4 km by 4 km spatial resolution for the WRF forcing (Figure 2, bottom panel). The 10 km by 10 km spatial modeling grid was used for WFD, WFDEI and WFDEI-GEM-CaPA-RCM4 forcings as the data are available at that spatial resolution. The time step of the model was set to 30 minutes.

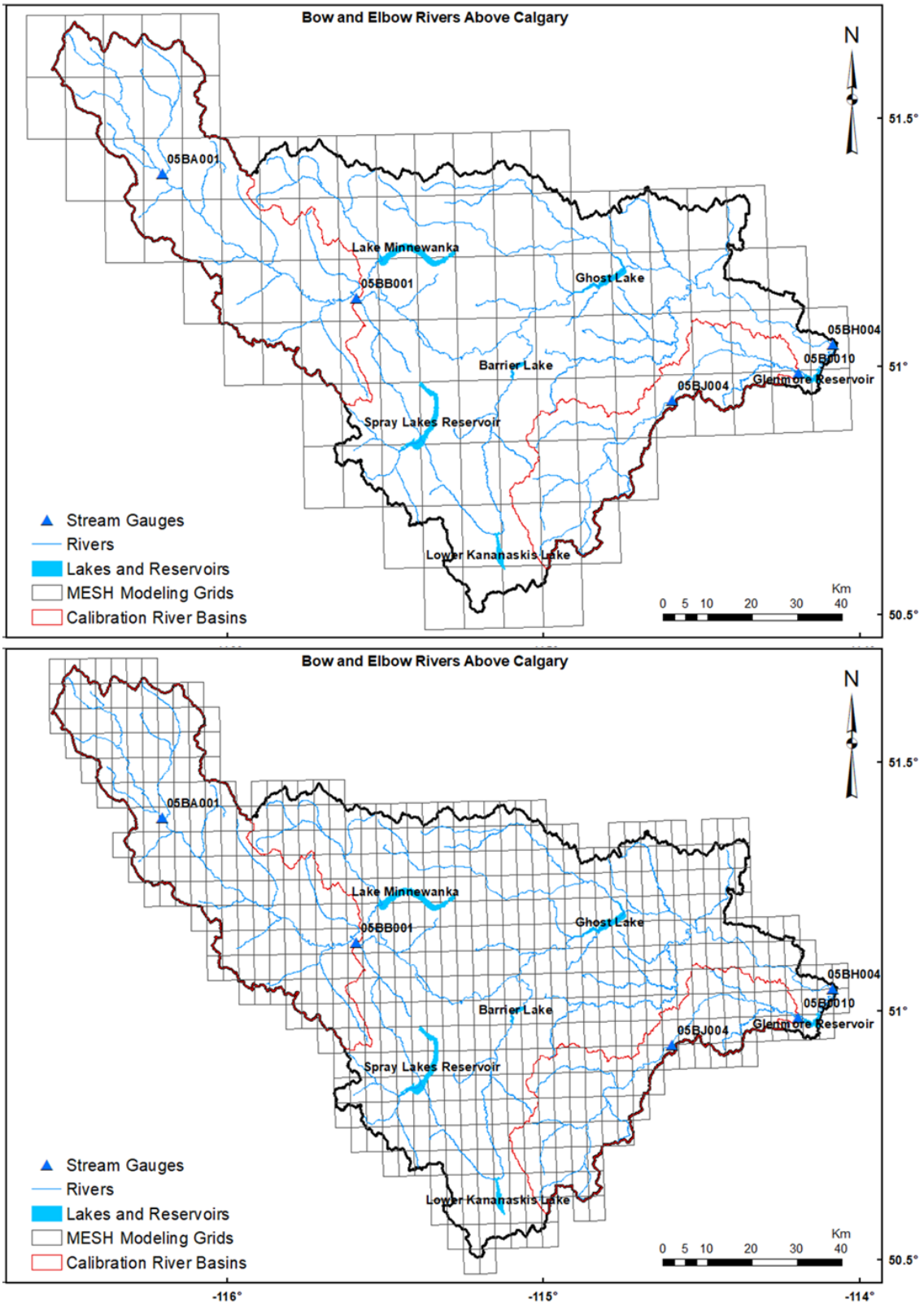

Figure 2. Bow and Elbow River basins MESH model configuration (the top is for the 10 km model grid and bottom is for the ~4 km model grid).

The original CEC 30 m by 30 m resolution Landsat landcover data has 19 classes that required regrouping to reduce the number of model computation units. Hence, similar vegetation types were combined to produce six dominant landcover types (Urban, Glacier, Barren land, Crop, Grassland, Forest and Water bodies) as shown in Figure 3. The map generated from this dataset was compared with the MODIS 2010 land cover dataset (~250 m resolution) produced by CEC for the purpose of validation. Based on the Randolph Glacier Inventory 6.0 data and including only ice bodies with areas greater than 0.05 km^2, about 105 ice bodies covering 60.52 km^2 with a mean area of 0.58 km^2 were located over Bow River Basin above Calgary. This is much smaller than the CEC landcover-based glacier area for the same basin of 165.9 km^2 and is considered to be far more accurate. Future projected deglaciation of the Bow River Basin above Calgary was estimated from a glacier dynamics model driven by a climate model (Clarke et al., 2015). Under the RCP8.5 (business as usual emission scenario) the glacier ice in Bow River Basin above Calgary at the end the century was estimated to shrink by 99% relative to 2005. This rapid deglaciation does not leave time for soil development and afforestation. Hence, it is reasonable to substitute barren land in the place of glacierised areas for simulations of future hydrology.

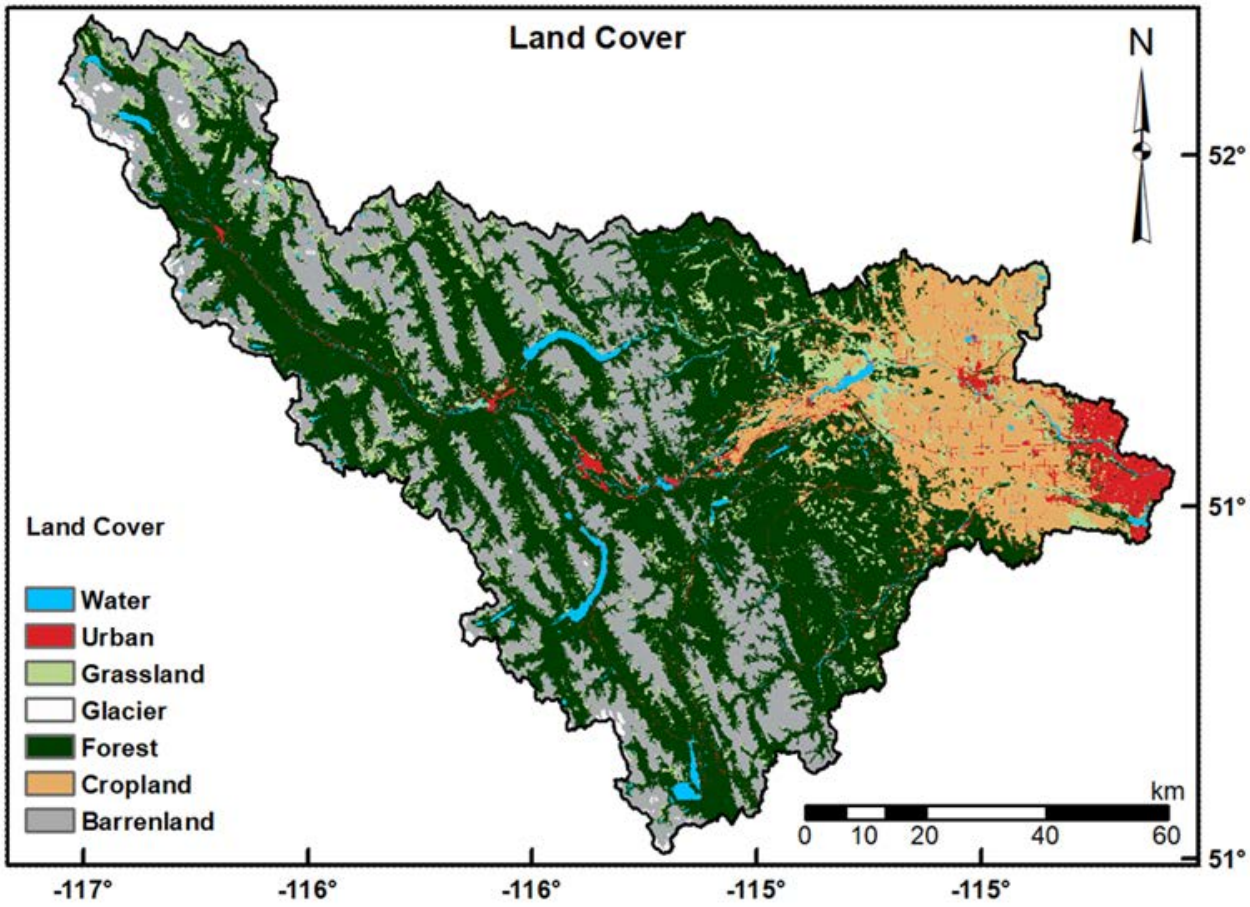

Figure 3. Re-grouped landcover map of Bow and Elbow River basins above Calgary (from CEC 30 m land cover)

To account for topographic and vegetation effects in snowcover ablation and snowmelt runoff, the GRU discretization was based on landcover types and slope and aspect categories which strongly control snow accumulation and snow energetics. Terrain was classified as flat (slope < 10°) and steep (slope > 10°). Steep slope was further classified as south-facing where the aspect was between 90 to 270° and north-facing where the aspect was outside of this range (Figure 4). Based on this classification, the Bow River at Banff is comprised of 35%, 39%, 26% and Elbow River near Sarcee Bridge is comprised of 34%, 35%, 31% North Facing, South Facing and Flat areas respectively.

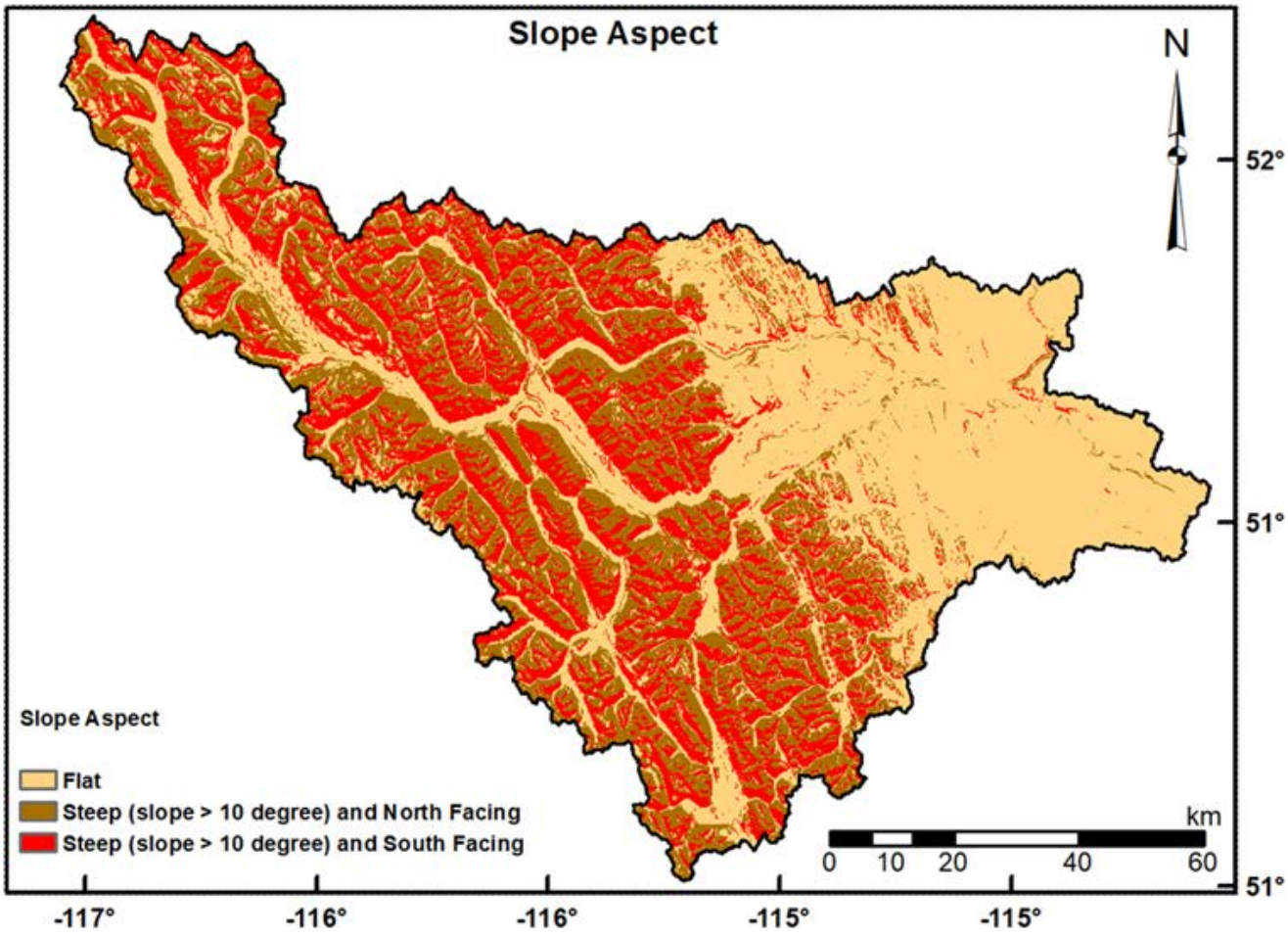

Figure 4. Slope and aspect classes of topography in the Bow and Elbow River basins above Calgary (derived from 90 m DEM)

MESH Grouped Response Units (GRUs) were created by combining the three slope-aspect classes (North-facing, South-facing and flat) with two mountain landcover classes (Barren land and Forest) and the remaining landcover classes (Urban, Glacier, Cropland, Grassland (Tundra), and Waterbodies). This created 11 GRUs - mapped in Figure 5.

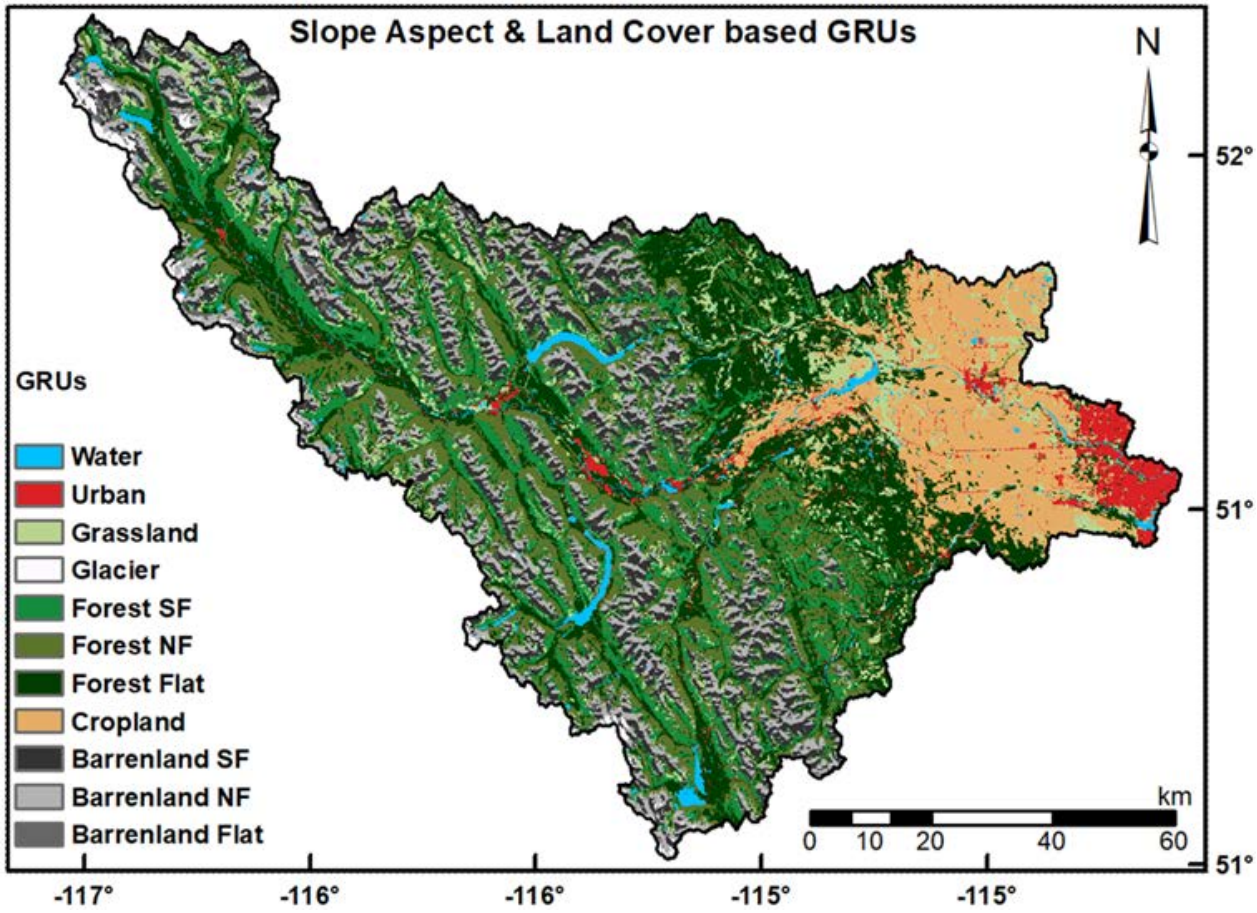

Figure 5. Grouped Response Unit discretization by combining slope aspect and landcover

The low-resolution DEM data corresponding to the WRF (4 km by 4 km), GEM, WFD, and WFDEI (10 km by 10 km) atmospheric models were resampled using bilinear sampling to a higher resolution (90 m) as shown in Figure 6 to make the spatial resolution consistent with the high-resolution DEM (i.e., the HydroShed DEM) used to build the MESH models. Then, for each GRU in the MESH model grid, the weighted-average elevation, slope, aspect and the elevation difference between the low-resolution and high-resolution elevations were calculated. These values were used to redistribute the gridded climate forcing values from a single value per grid to one value per GRU inside the model grid that considers the impact of elevation, slope, aspect and the elevation difference relative to the meteorological forcings from the atmospheric model. The three maps in Figure 6 show the low and high resolution DEMs and their differences over the Bow River Basin above Calgary as used to parameterize Mountain MESH for WRF (4km by 4 km). Figure 7 shows the same but for GEM-CaPA (10 km by 10 km) climate forcing. The same was done for the other forcing datasets.

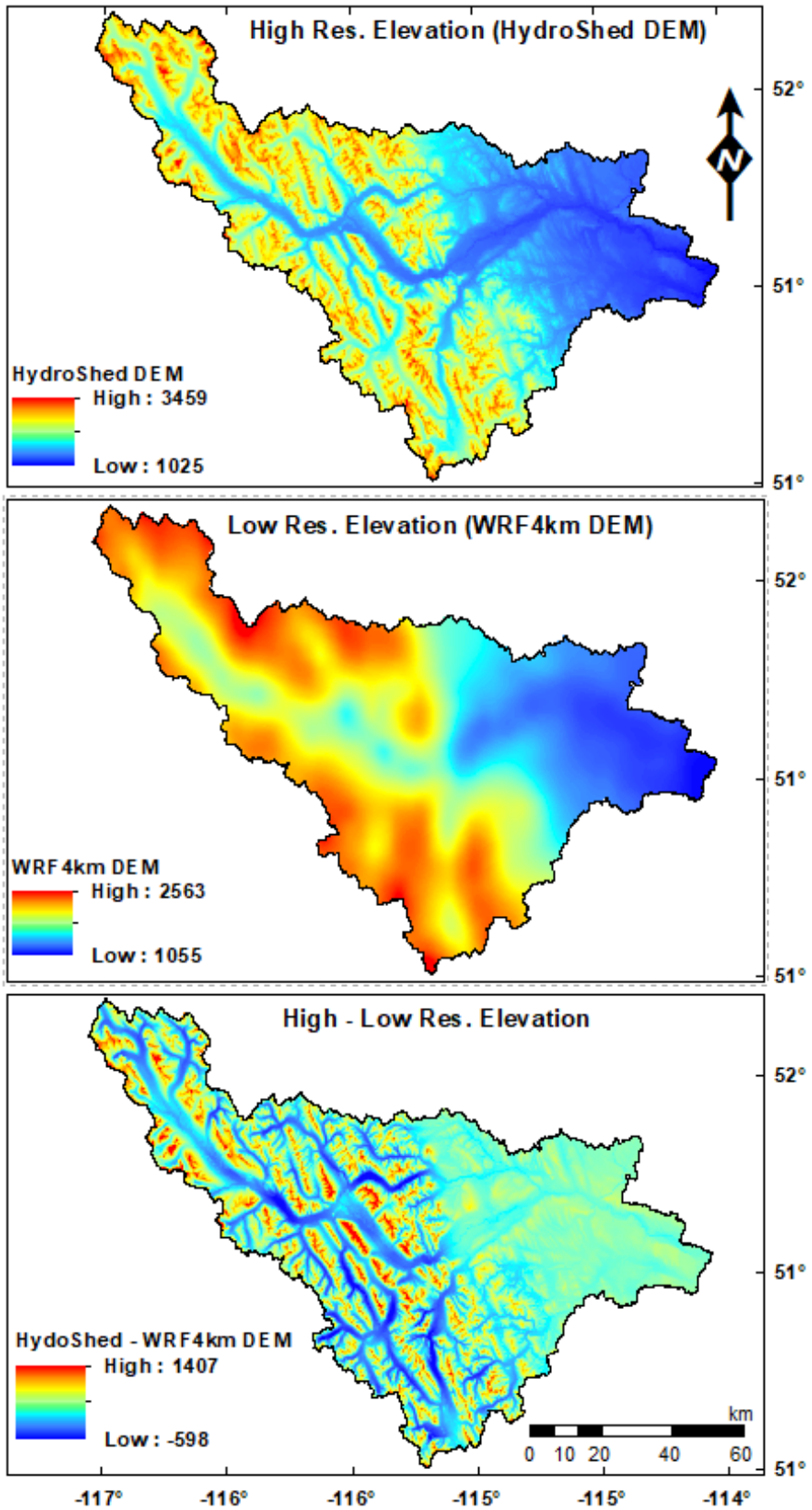

Figure 6. High resolution elevation, WRF elevation and their difference for model parameterisation

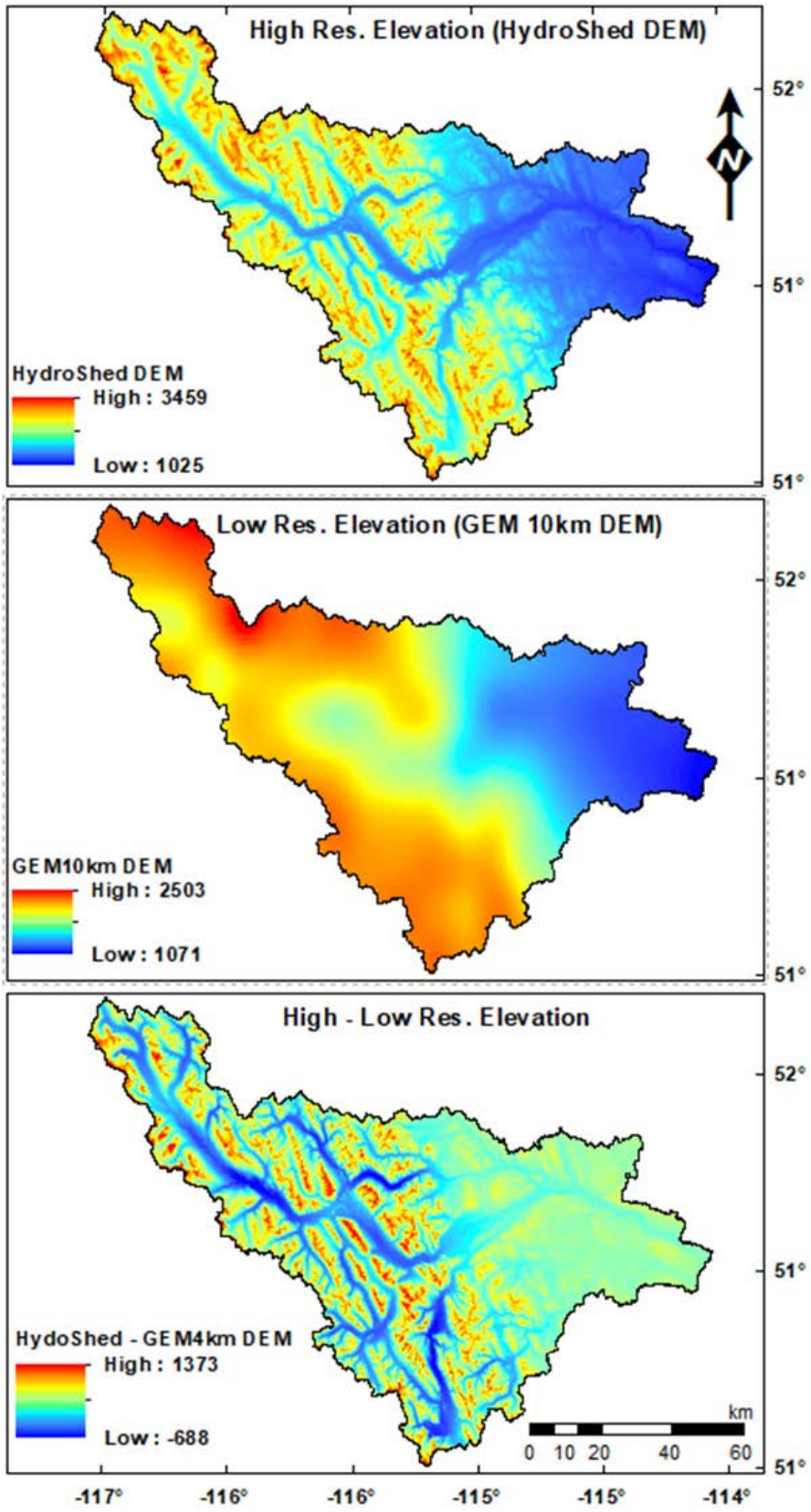

Figure 7. High resolution elevation, GEM elevation and their difference for model parameterisation

3.2 Mountain MESH module

Most global and regional climate models use the NWP-calculated shortwave irradiance to a flat plane as an upper boundary condition for land surface calculations, and do not redistribute meteorological forcings for elevation, slope, or aspect. As a result, land surface and hydrological models that use outputs directly from NWP lack any means to address the spatial variability in energetic processes that is inherent in mountains (Marsh et al., 2020). Oliphant et al. (2003) conducted sensitivity studies to separate the role of spatial variability of surface characteristics from the spatial variability in incoming solar radiative fluxes and found that slope-aspect is the most important surface characteristic. Pomeroy et al. (2003) presented observations demonstrating that slope and aspect had a defining role in all energy fluxes to melting snow on mountain slopes and that the net direction of the snowmelt energy budget depended on slope-aspect. In the Northern Hemisphere, north-facing slopes receive less direct sunlight than south-facing slopes, which results in north-facing slopes being cooler than south-facing slopes in both winter and summer. Hence, snow on north-facing slopes melts more slowly than on south-facing slopes as has been demonstrated in the Bow River Basin (Schirmer and Pomeroy, 2020). Dornes et al., (2008a, 2008b) showed that model performance can be improved by downscaling climate forcing using high resolution topography and permitting snow redistribution. The inclusion of landscape heterogeneous climate forcing can improve hydrological prediction of land surface model, as it has effects on snow cover extent (SCE) and snow water equivalent (SWE) that are affected by snow accumulation, snowmelt fluxes, and runoff contributing area. Therefore, it is necessary for LSMs to accurately present the interaction between the land surface and atmosphere over complex terrain, addressing the influences of climate change and landcover change on surface-atmosphere energy-water-mass exchanges. Low resolution forcing in mountain basins can lead to poor representation of cold regions hydrology processes and impaired hydrological predictions as these forcing inputs cannot provide sufficient heterogeneity in snowpack energetics, precipitation amount and phase to simulate snowpack dynamics and melt. The precipitation phase problem is due to inadequate resolution of near surface air temperature and humidity fields in complex terrain. As Bernier et al. (2011) suggest, a simple lapse rate correction of temperature between low to high resolution elevation could represent the freeze–thaw line better, and thus of the precipitation phase as most land surface hydrological model use temperature to distinguish between rain and snow. However, Harder and Pomeroy (2014) showed substantial errors in simple temperature-based precipitation phase models and model sensitivity to these errors that could be corrected by employing a psychrometric energy budget equation (Harder and Pomeroy, 2013).

A module that downscales and adjust climate fields from any Numerical Weather Prediction (NWP) to the GRU in MESH was therefore integrated into the MESH modelling system. The module uses the original low-resolution climate field and weighted average elevation and its derivatives: slope, aspect and difference in elevation between the NWP grid and the model grid for every GRU in modelling grid. The downscaling module is described in the following sections.

3.2.1 Temperature

Air temperature from the low-resolution NWP was lapsed using a calculated lapse rate and the difference in elevation between the NWP grid and the model GRUs as follows:

$$T_{HR} = T_{LR} - \Delta * T_{Lapse\ rate}$$

where T_{HR} is the adjusted air temperature for GRUs in the modelling grid; T_{LR} is the temperature from the low resolution NWP; Δ is the elevation difference between high-resolution GRUs in the modelling grid and the bilinear interpolated low-resolution NWP elevation grid and $T_{Lapse\ rate}$ is the hour-month lapse rate (each month has 24 lapse rate for each hour of the day) that was derived from available historical hourly temperature data collected from Environment Canada, Alberta Environment and Parks and Global Water Future for the historical period (2000 – 2015).

3.2.2 Pressure

Air pressure was adjusted from the original low-resolution fields for every GRU using the corrected temperature and other constants as follows:

$$P_{HR} = P_{LR} \exp\left(-\frac{\Delta g}{RT_{HR}}\right)$$

where P_{HR} is the high-resolution adjusted pressure, P_{LR} is low-resolution pressure, Δ is the difference in elevation as described above, g is the gravitational constant (9.807 m s^{-1}), R is the universal gas constant for dry air R equal to 287.05 J kg^{-1} K^{-1} and T_{HR} is the high resolution adjusted temperature as computed above.

3.2.3 Specific humidity

Specific humidity is a nonlinear function of elevation, and so the correction was based on actual vapour and surface pressure fields. First the low-resolution NWP grid dew-point temperature was calculated from the actual vapour pressure of the low-resolution NWP field using (Buck, 1981).

$$DT_{HR} = \begin{cases} \dfrac{272.55 \ln(VP_{LR}/611.15)}{22.452 - \ln(VP_{LR}/611.15)} & if\ T_{LR} \leq 0 \\ \dfrac{240.97 \ln(VP_{LR}/611.21)}{17.502 - \ln(VP_{LR}/611.21)} & if\ T_{LR} > 0 \end{cases}$$

The relatively linear dew-point temperature was corrected for elevation using the dew-point temperature lapse rate in the same way as the air temperature was lapsed, as described above.

$$DT_{HR} = DT_{LR} - \Delta * DT_{Lapse\ rate}$$

The actual vapour pressure was calculated for the new dew-point and air temperature as follows:

$$VP_{HR} = \begin{cases} 611.15\ exp\left(\dfrac{22.452\ DT_{HR}}{DT_{HR} + 272.55}\right) & if\ T_{HR} \leq 0 \\ 611.21\ exp\left(\dfrac{17.502\ DT_{HR}}{DT_{HR} + 240.97}\right) & if\ T_{HR} > 0 \end{cases}$$

Finally, specific humidity was corrected for changes in surface and actual vapour pressure fields as follows:

$$SH_{HR} = 0.622\left(\frac{VP_{HR}}{P_{HR} - 0.378\,VP_{HR}}\right)$$

where SH_{HR}, VP_{HR}, P_{HR} and DT_{HR} are adjusted for the high resolution NWP grid specific humidity (kg kg^{-1}), actual vapour pressure (Pa), surface pressure (Pa) and dew-point temperature (C°) respectively and VP_{LR} and DT_{LR} and $DT_{Lapse\ rate}$ are the low resolution NWP grid, actual vapour pressure (Pa), dew-point temperature (C°) and dew-point temperature lapse rate (C° km^{-1}) respectively.

3.2.4 Incoming shortwave radiation

The incoming shortwave radiation output from the NWP was used to correct the theoretical radiation on sloped surfaces for cloud cover by comparing it with the theoretical flat surface radiation estimate. $SR_{HR} = \frac{SR_{LR}}{SR_{flat}}\left(SR_{slope}\right)$

$$SR_{slope} = SR_{dir\_slope} + SR_{dif\_slope}$$

where SR_{HR} is the corrected incoming shortwave radiation over a sloped surface, SR_{LR} is the incoming shortwave radiation from the NWP, SR_{slope} is the theoretical clear sky direct and diffuse incoming shortwave radiation over a sloped surface was calculated by converting the integration into a summation following Garnier and Ohmura (1970, 1968).

3.2.5 Incoming longwave radiation

Incoming longwave radiation was corrected for elevation using lapse rates developed from the high-resolution NWP and elevation. Following Brutsaert (1975), incoming longwave radiation can be estimated as follows

$$LR_{HR} = F_{LR}\left(1.24\left(\frac{VP_{HR}}{T_{HR}}\right)^{\frac{1}{7}}\right)\sigma {T_{HR}}^{4}$$

where, LR_{HR} , F_{LR}, VP_{HR}, T_{HR}, and σ represent the incoming longwave radiation at each GRU, the lower resolution NWP modelled increase in the sky emissivity due to cloud emissions, the vapour pressure for GRU (mb), air temperature for GRU (K) and the Stefan–Boltzmann constant (5.67×10^{-8}) respectively.

The low-resolution NWP modelled increase in the sky emissivity due to cloud emissions can be back-calculated from the respective low-resolution NWP modelled incoming longwave radiation, temperature and vapour pressure as follows.

$$F_{LR} = \frac{LR_{LR}}{\left(1.24\left(\frac{VP_{LR}}{T_{LR}}\right)^{\frac{1}{7}}\right)\sigma {T_{LR}}^{4}}$$

3.2.6 Precipitation and phase change

Precipitation depth and phase were corrected for elevation differences between high resolution GRUs and low-resolution NWP grids using the Zhang et al., 2018, Tesfu et. al., 2020 Elevation Range with Maximum elevation Method (ERMM) to downscale the precipitation from low-resolution NWP model to the MESH GRUs as follows:

$$P_{HR} = P_{LR} + \Delta P$$

where P_{HR} represents the precipitation value at each GRU, P_{LR} is grid level precipitation calculated by the NWP model, and ΔP refers to the deviation of the GRU's precipitation from the grid level precipitation of the NWP model and is calculated as follows:

$$\Delta P = P_{LR}\left(\frac{E_{HR} - E_{LR}}{E_{HR\_max}}\right)$$

where E_{HR}, E_{LR} and E_{HR_max} are the GRU elevation, the modelling grid level elevation and the maximum grouped response unit level elevation value within the modelling grid, respectively.

Precipitation phase change was corrected using the hydrometeor temperature which can be accurately estimated as a function of the psychrometric energy balance (Harder and Pomeroy, 2013). Using the psychrometric approach gives snowfall a temperature near the wet bulb temperature, which is lower than the air temperature when relative humidity is less than 100% (Harder and Pomeroy, 2013). A given GRU in the mountains may find itself below (or above) the freeze–thaw line and receive rain (snow) instead of snow (rain), therefore the distinctive hydrology of valleys and mountain tops become better resolved.

3.2.7 Wind speed

Wind speed was corrected for topography following the simple formulations of Liston and Sturm (1998) and Liston and Elder (2006) as follows:

$$W_{HR} = W_{LR}[1 + \lambda_c \Omega_c + \lambda_s \beta \cos(Wdir_{LR} - A)]$$

where W_{HR}, $W_{LR,}$ and $Wdir_{LR}$ are the high-resolution NWP grid wind speeds, low resolution NWP grid wind speeds and direction. Ω_c, β, A, λ_c and λ_s are the curvature, slope (in radian), azimuth with north having zero azimuth, the slope weight and curvature weight respectively. The λ_c and λ_s values (between 0 and 1) constrain the total wind weight to between 0.5 and 1.5. The curvature is calculated from the high-resolution digital elevation model as follows:

$$\Omega_c = 0.25\left[\frac{2E - 0.5(E_N + E_E + E_S + E_W)}{2\eta} + \frac{2E - 0.5(E_{NE} + E_{NW} + E_{SE} + E_{SW})}{\eta 2\sqrt{2}}\right]$$

where E, E_N, E_E, E_S, E_W, E_{NE}, E_{NW}, E_{SE}, E_{SW} and η are the elevation of the processing, the elevation of its north, east, south, west, north east, north west, south east, south west and the resolution the elevation data respectively. The calculated curvature value is then scaled to fall between -0.5 and 0.5 over the low-resolution NWP grid. This method was used because it was

available and computationally simple, despite concerns about its performance at high resolution in the Canadian Rockies (Musselman et al., 2015). A new, higher fidelity method has been developed using the WindNinja software (Vionnet et al., 2020) that we will employ in the future.

3.3 Glacier modeling in MESH

MESH includes a glacier module that simulates the mass balance of snow/ice melt, ponding, runoff, and conversion of snow to ice. These processes are important for capturing the energetics of a glacier as well as the contribution of melt water from glaciers. Conversion of snow to ice is calculated based on either one of the two thresholds: snow water equivalent (SWE) or snow density. The original version of MESH that was examined (before version r1693) used hardcoded default SWE thresholds greater than 100 kg m^{-2} and a density greater than 900 kg m^{-2} for snow to be converted into ice, based on observations for continental ice sheets applicable for RCM and GCM scales. The low SWE thresholds resulted in multiple snow to ice conversion episodes during winter and the snow density never reached the density threshold at 900 kg m^{-2}. The low SWE conversion threshold also had a direct impact on glacier ice exposure to radiative fluxes and led to faster melt than would be expected in spring due to conversion of the winter snowfall to glacier ice - particularly for lower elevation glaciers. As glacier ice has a lower albedo than seasonal snowpacks, the net shortwave radiation of a melting glacier can be two to three times that of a melting snowpack. These original hardcoded parameters led to calculations that were erroneous and inconsistent with known glacier energetics and snow to ice conversion when the model was applied to the watershed scale. This version of the glacier module also used large hardcoded ice albedo values, again based on literature for continental ice sheets: visible and near-infrared values (0.95 / 0.73) that are inconsistent with observed mountain glacier albedos and produce little icemelt. The other issue with the module was that all the converted snow/ice volume was added to an internal runoff variable for bookkeeping, and that the model does not otherwise keep track of the glacial ice volume. The hardcoded parameterization of these values caused erroneous winter streamflows. In general, with the original MESH version (before version r1693), which used hardcoded glacier model parameters, we figured it was impossible to parameterise the model in a way that was consistent with available experimental observations for mountain glaciers.

A more recent version of this code (MESH.r1693) produced in July 2020, made many hardcoded parameters relevant for glacier dynamics available for calibration or parameterisation outside of the code, making it more flexible for users. These parameters include glacier albedo, snow depth conversion threshold, and snow density conversion threshold. The modified thresholds were set for this study to a SWE of 2500 mm and a snow density of 650 kg m^{-2}. The broadband ice albedo was set to 0.3 which is consistent with Centre for Hydrology measurements of the Athabasca Glacier.

The performance of the revised glacier module parameterisation was assessed by comparing the annual mass balance from MESH.r1693, parameterised as above, with the observed annual mass balance of Peyto Glacier - the nearest research glacier to the study area. The observed annual mass balance data for Peyto Glacier was obtained from values calculated by NRCan scientists and reported to the World Glacier Monitoring Service (WGMS). Comparing the annual glacier mass balance of a hydrological land surface model to observations has not been done before to

the best knowledge of the authors. Such analysis provides critical insights into the quality of the meteorological data and model configuration as the glacier module parameters were set from observed values from field studies rather than calibration.

3.4 Implementation of reservoir operations in the MESH model

Six reservoirs were included in the model configurations. The relationships between reservoir storage and discharge for the simulated reservoirs were analyzed using hourly water level elevation and discharge data provided by Alberta Environment and Parks (https://rivers.alberta.ca/) and collected by ECCC's Water Survey of Canada and TransAlta Utilities. The data covered the period from 2000 to 2015 except for Lower Kananaskis Lake and Ghost Lake which were reported until 2012. Like other similar climate change impact studies, we assume the empirical stage-discharge relationships derived from historical data will hold as the reservoir operating rules in the future. Elevation-storage rating curves were developed to convert the water surface elevation data into storage. The relationship between all the quantile releases against quantile storage is given in Figure 8. However, to develop the empirical statistical relationships only the quantiles of 5 to 95% were used, as shown in Figure 9.

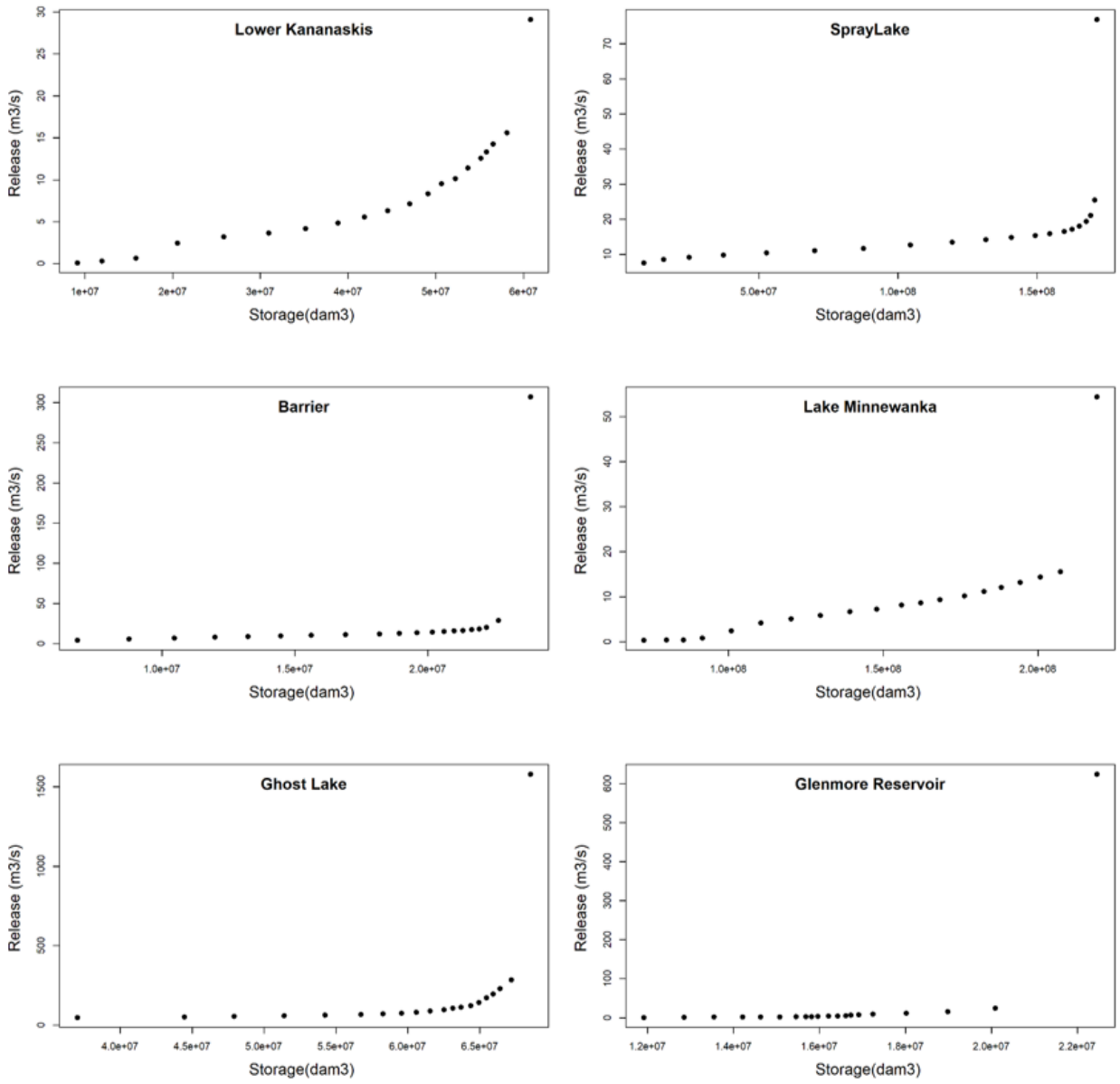

Figure 8. Plots of all quantiles of storage versus quantiles of release for the six reservoirs of the study area.

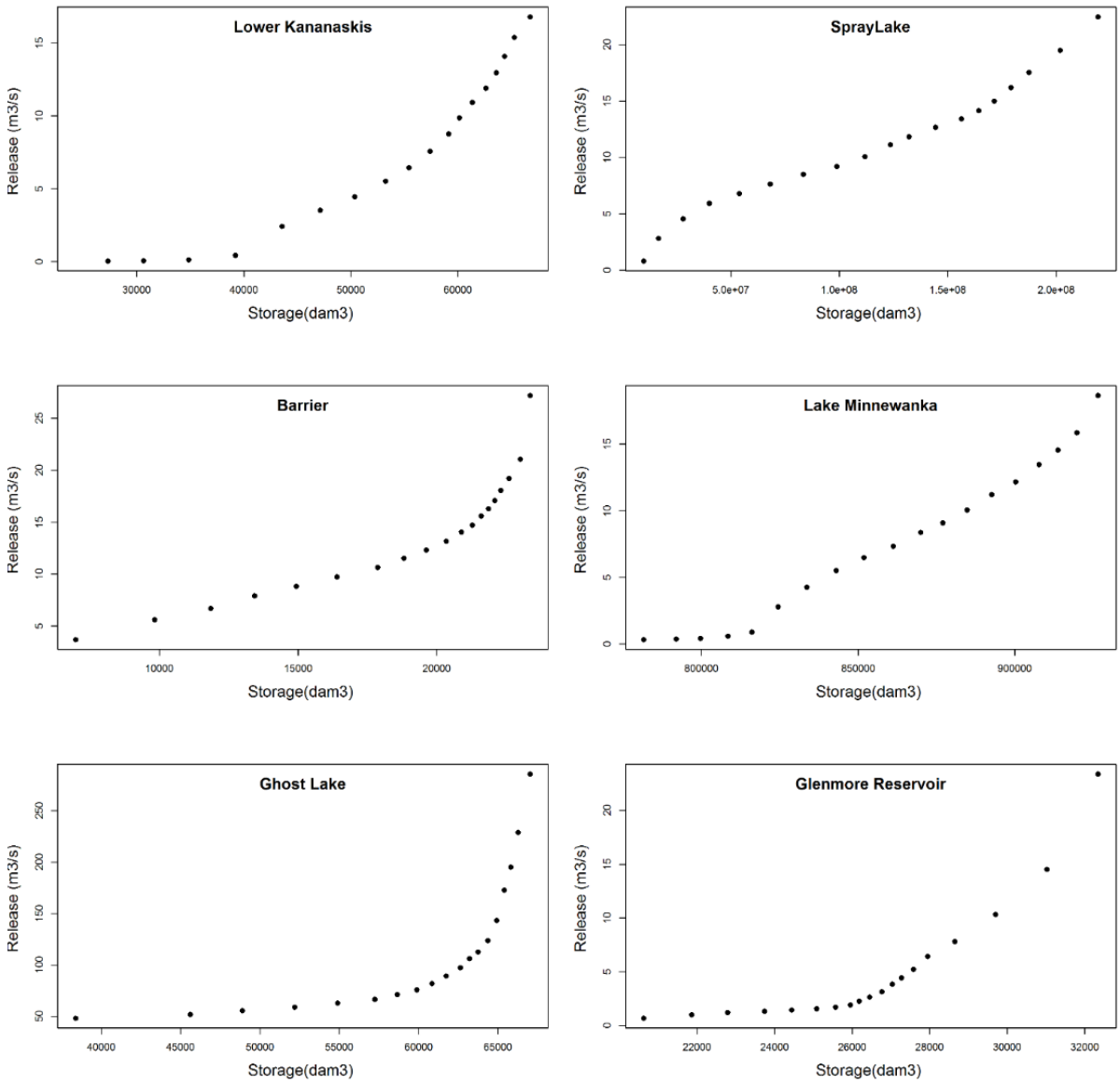

Figure 9. Plots of quantiles (5 – 95%) of storage versus quantiles of release for the six reservoirs of the study area

Quantiles of storages and outflows were determined and were fitted with monotonically increasing fourth (or smaller) degree polynomials, as shown in the equation below, to model the relationship between the discharges and storage (Figure 9), and which can easily be implemented in MESH. The values of coefficients of the fitted curves for the six reservoirs are listed in Table 4.

$Q_R = aS^4 + bS^3 + cS^2 + dS^1$,

where
Q_R = quantile of daily Discharge (m^3/s),
S = quantile of storage (m^3),
a, b, c, d= fitted constants

Table 4. Fitted constants for the developed statistical reservoir operation rule model

Reservoirs	a	b	c	d	R^2
Lower Kananaskis.	2.01E-29	-2.07E-21	6.78E-14	-5.65E-07	0.95
Spray Lake	2.06E-23	-5.49E-15	4.64E-07	0.00E+00	0.84
Barrier Lake	1.11E-27	-4.71E-20	6.34E-13	-1.99E-06	0.93
Minnewanka	5.93E-32	-2.77E-23	4.60E-15	-2.16E-07	0.98
Ghost Lake	1.47E-27	-2.36E-19	1.25E-11	-2.20E-04	0.96
Glenmore	2.45E-20	-6.52E-13	4.41E-06	0.00E+00	0.98

3.5 Model calibration

The full MESH parameterisation includes parameter selection, calibration, and selection of process options. Limited calibration on only a few parameters related to evapotranspiration, soil, and routing was carried out for this study. The parameters chosen for calibration were based on previous MESH modelling studies that had identified them as being highly uncertain and sensitive parameters (Haghnegahdar et al., 2017). Although there were 11 GRUs in upper Bow River Basin above Calgary, only parameters for the two largest GRUs (Forest and Barren land) were calibrated. As well as these GRU specific parameters, two basin-level routing and baseflow parameters were also calibrated (Table 5).

Table 5. Calibrated model parameters and their corresponding ranges for calibration

Parameter	Description of parameters	Range
ROOT	Annual maximum rooting depth of vegetation	1.0 – 2.0
RSMN	Minimum stomatal resistance (s m^{-1})	150 - 250
ZSNL	Limiting snow depth below which coverage is <100% (m)	0.02 - 0.2
ZPLS	Maximum water ponding depth for snow-covered areas (m)	0.02 - 0.5
ZPLG	Maximum water ponding depth for snow-free areas (m)	0.02 - 0.7
SDEP	Permeable depth of the soil column (m)	0.1 - 4
KSAT	Saturated surface soil conductivity (m s^{-1})	10^{-7} - 10^{-3}
DDEN	Estimated drainage density of the GRU (km km^{-2})	2 - 100
PWR	Exponent of the lower zone storage in the lower zone function (dimensionless)	1 - 4
FLZ	Lower zone function (dimensionless)	10^{-7} - 10^{-3}
R2N	Channel Manning's n (dimensionless)	0.01 - 0.16
R1N	Overbank Manning's n (dimensionless)	0.01 - 0.20

Some of these parameters have physical meaning but some do not (i.e. parameters related to fitting behaviour, such as PWR and FLZ). The average near-infrared albedo when fully leafed is the component of the total albedo of the vegetated surface. The minimum stomatal resistance is the resistance to transport of water and gases to and from leaves. The drainage density is of the rivers/stream networks per unit area. The Manning coefficients of the main river and the flood plain represents the roughness or friction applied to the flow by the channel or the flood plain/bank.

Given the focus on flood response, the model performance was primarily evaluated by the Nash–Sutcliffe Efficiency (NSE) using a parallel implementation of the Dynamically Dimensioned Search (DDS) algorithm (Tolson and Shoemaker, 2007) by OSTRICH v17.12.19 (Matott, 2017). About 500 realizations were used with the DDS algorithm in Ostrich, and the objective function was the mean NSE of streamflow at the sub-basin outlets of the Bow River at Banff and the Elbow River at Sarcee.

A series of model calibrations was conducted for the various meteorological forcings described above, using the observed streamflows of the Bow River at Banff and the Elbow River at Sarcee Bridge to produce a single parameter set for the entire basin with a one-year spin up period. Calibration was performed using the Parallel Dynamically Dimensioned Search (PDDS) optimization algorithm (Tolson and Shoemaker, 2007; Matott, 2017) with a budget of 1000 iterations allocated (but not necessarily used). A pseudo multi-objective approach was used to combine NSE values of the two gauging stations, based on mean annual runoff coefficients as weight. Twenty parameters were used to minimize the negative of the weighted average NSE of Bow River at Banff and Elbow River at Sarcee Bridge.

The period from October 2005 to September 2015 was used as a calibration period for all forcing data except the WFD where the period from October 1985 to September 1995 was used. The period October 2000 to September 2005 was used as the validation period for all forcing other than the GEM-CaPA where October 2002 – September 2005 was used and EU-WFD-CRU where the period from October 1995 to September 2001 was used.

3.6 Centre of mass of flow

The center of mass of flow help to explain the importance of seasonality for hydrological processes and water resources. It can be a very useful metric for demonstrating the impact of climate warming on the timing of streamflows from cold regions basins where seasonal melt dominates the hydrograph. The timing of Centre of Mass of flow (CT, days) was calculated as shown below:

$$CT = \frac{\sum q_i t_i}{\sum q_i},$$

where

t_i = time in days from the beginning of the water year (October 1 – September 30),
q_i = the corresponding streamflow for the i^{th} day.

The change in the mean CT at the end of the 21st century relative to 2001 – 2015 was computed for all MESH grid outlets within Bow River Basins above Calgary.

3.7 Change in runoff generation mechanism

The changes in the annual frequency of Rain-on-Snow (R-O-S), Snowmelt Runoff (S-M-R) and Rainfall-Runoff (R-R) events were calculated as follows. Event were considered as R-O-S if there was rainfall of at least 10 mm d^{-1} falling on a snowpack with at least 10 mm SWE following the designation of Freudiger et al., (2014) and Musselman et al., (2018). Events were considered as S-M-R if they consisted of daily snowmelt of at least 10 mm d^{-1}, there was a snowpack with a daily SWE of at least 10 mm d^{-1} and the daily rainfall is less than 10 mm d^{-1}. Rainfall-runoff occurred when the daily rainfall of at least 10 mm d^{-1} fell over a non-snowcovered GRU. Otherwise, runoff events were considered to be mixed events.

3.8 Streamflow bias correction

Simulated streamflows were corrected by a quantile-quantile mapping (QM) method using the three gauging stations. This bias correction used the observed daily streamflow data and historical simulated MESH-WRF streamflow for a historical calibration period (2006 – 2015), then validated for 2000 – 2006, and used to correct both the historical and future MESH-WRF simulated streamflows. Retaining this known bias history for estimating future streamflows is a necessary assumptions, despite methodological limitations.

The QM method adjusts the distribution of daily MESH-WRF simulated streamflow (*Qs*) with the distribution of daily observed streamflow (*Qo*) using a transfer function T as shown below:

$Q_S = T\,(Q_o)$.

If the variable of interest has a known (i.e. fitted) distribution, the transformation is defined as:

$Q_s = F^{-1}(F_s(Q_o))$,

where
F_s = the Cumulative Distribution Function (CDF) of Q_s, *and*
F^{-1} = the inverse CDF of Q_o.

Following the recommendation of Gudmundsson et al. (2012) that nonparametric transformations not only have the best skill in reducing biases from climate data through the entire range of the distribution but also can be applied without specific assumptions about the distribution of the data, the nonparametric Empirical Cumulative Distribution Functions (ECDF) were used. The R package qmap - Statistical Transformations for Post-processing Climate Model (Gudmundsson et al., 2012) was used to bias-correct the simulated streamflow. The process is demonstrated by the schematic plot in Figure 10.

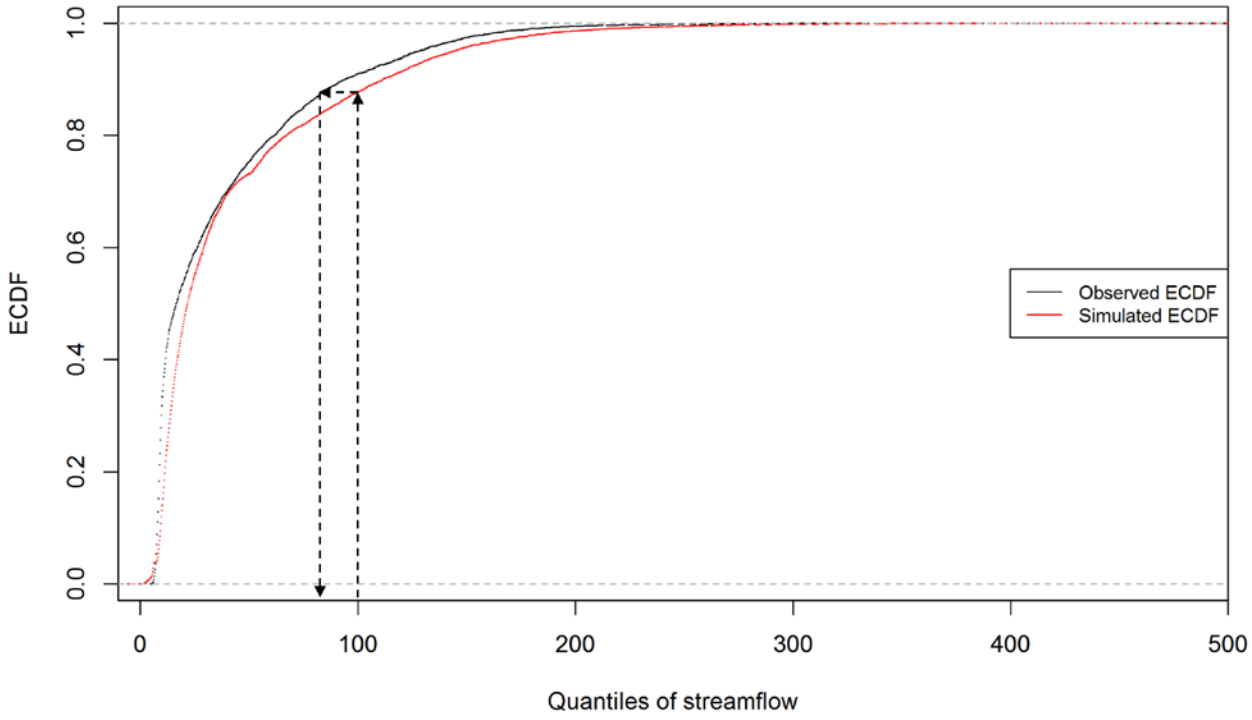

Figure 10. A schematic of the quantile mapping (QM) method for Bow River Basin at Banff.

4. Results and discussion

4.1 Model calibration and validation

The model calibration and validation results for the Bow and Elbow River basins above Calgary for the various meteorological forcing datasets are discussed in this section in the following order: EU-WFD-CRU, WFDEI, GEM-CaPA, WFDEI-GEM-CaPA, CanRCM4, CanRCM4-WFDEI-GEM-CaPA and WRF. Table 1 gives the full names and descriptions of these forcing datasets. The model performance varied with the climate forcing data, with the best performances for the Bow River at Banff and the worst performances for the Elbow River near Sarcee Bridge for most forcing data.

EU-WFD-CRU- MESH calibration and validation

The streamflow hydrographs for Bow River at Banff and Elbow River near Sarcee Bridge for the calibration and validation periods are shown in Figure 11 and Figure 12 respectively. These illustrate the model performance in all aspects of the simulation (low flow, high flow, timing, and volume), noting that the model calibration was based on the NSE criterion, which emphasizes high flows. The calibration performance of the Bow River at Banff (05BB001) can be considered good (NSE = 0.78) and NSE was improved for the validation data set (NSE = 0.86), with a smaller bias (-2%) during validation than in calibration. In most cases, the model does an excellent job of capturing the hydrograph timing and baseflow. The bias of Elbow River near Sarcee Bridge (05BJ010) is generally satisfactory with less bias (9%), but the model underestimated most of the peak flows. As the MESH model has reasonable process representations for the basins, it is believed that the model performance limitations, associated with peak flows for Elbow River near Sarcee Bridge, are most likely due to limitations in the driving precipitation data and the flashy nature of streamflow generation in the Elbow River Basin.

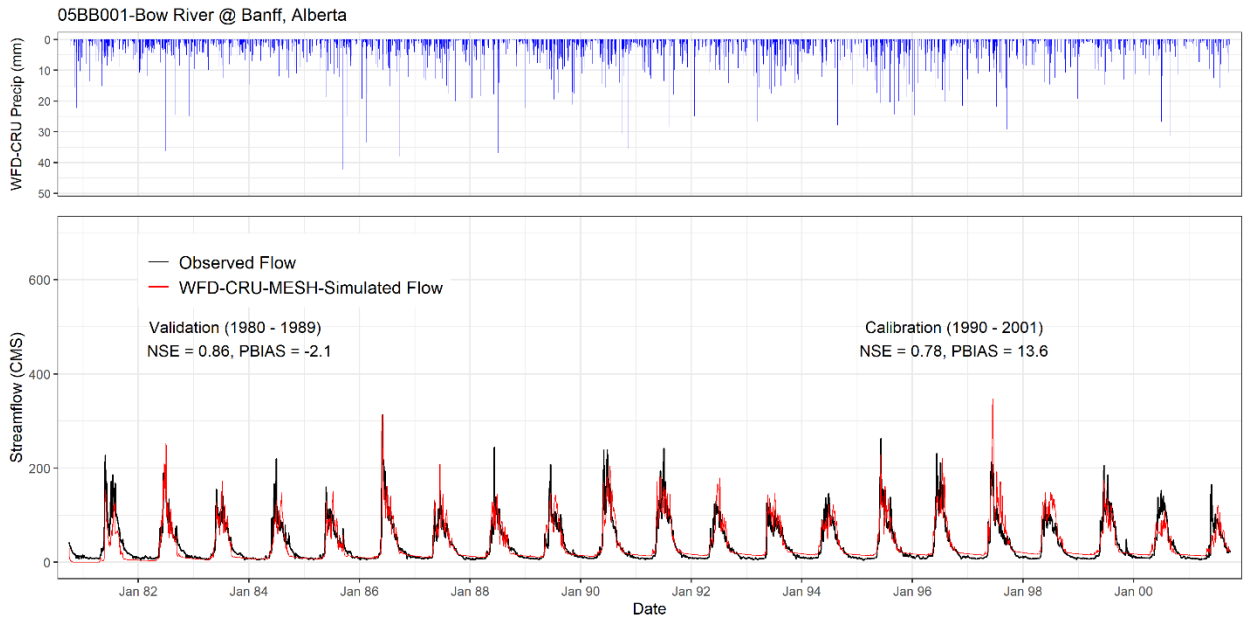

Figure 11. Calibration and validation performances for the Bow River at Banff using EU-WFD-CRU forcing data

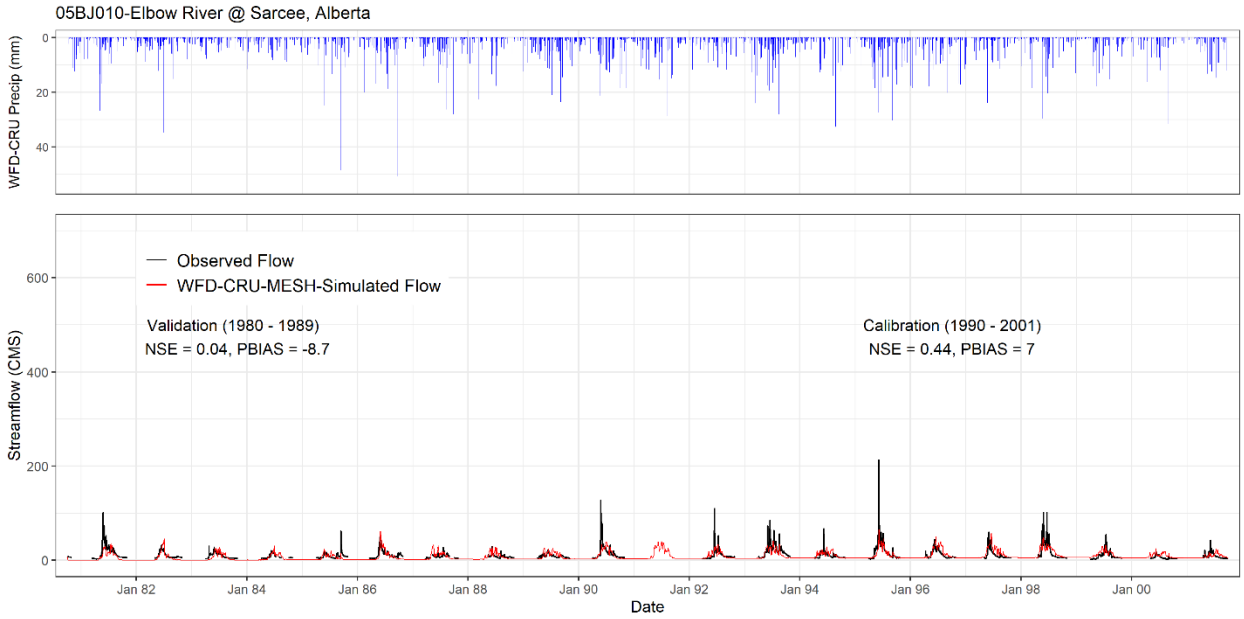

Figure 12. Calibration and validation performances for the Elbow River near Sarcee Bridge using EU-WFD-CRU forcing data

WFDEI-MESH calibration and validation

The hydrographs, calibration and validation statistics for the entire calibration and validation period, for both Bow River at Banff and Elbow River at Sarcee Bridge, are shown in Figure 13 and Figure 14. The performance model varied by basin and calibration and validation period, with the best performance of NSE=0.78 for the Bow River at Banff, and the worst performance of NSE=0.16 for Elbow River at Sarcee Bridge. In most cases, the model does an excellent job of capturing the hydrograph and timing. Both rainfall runoff and snowmelt runoff peak events are normally captured for Bow River at Banff, but the flood peaks are often underestimated for the Elbow River at Sarcee Bridge. Further efforts to improve the calibrations are unlikely to lead to improvements in performance as the quality of the driving data imposed a significant limitations. For the two years (2005 and 2013) with a known flooding event, the rainfall-runoff plot shows very small precipitation that caused the large underestimation for the peak flow for Elbow River at Sarcee Bridge while the Bow River at Banff captured that peak flow as the precipitation was large enough to produce it.

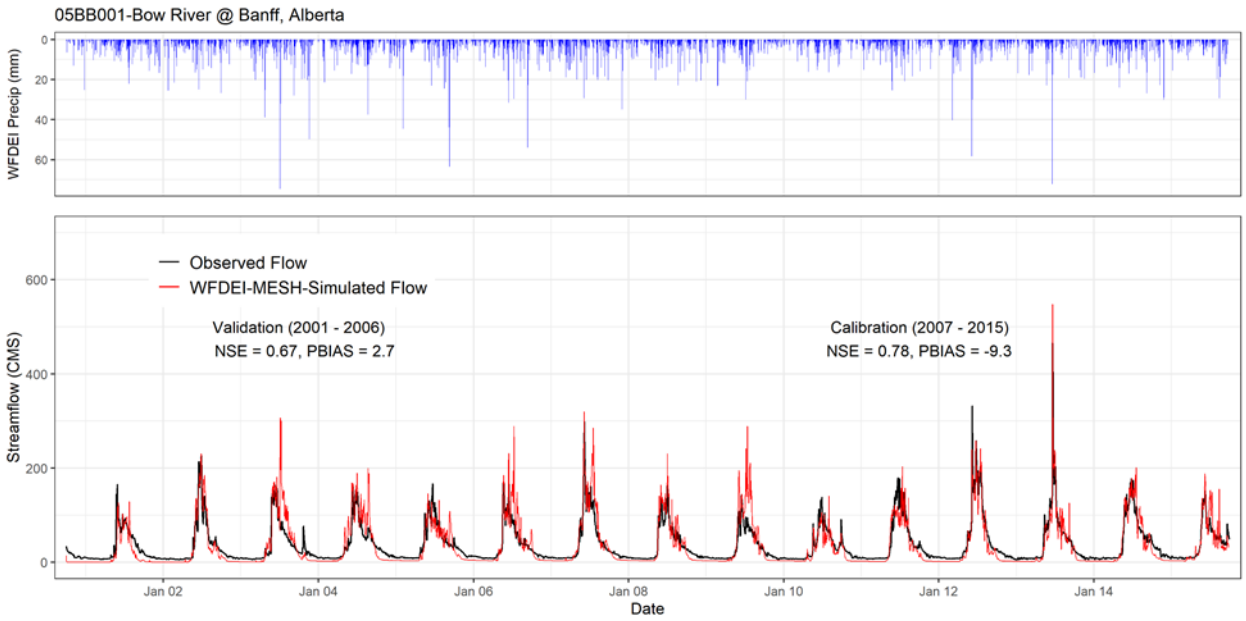

Figure 13. Calibration and validation performances for the Bow River at Banff using WFDEI forcing data

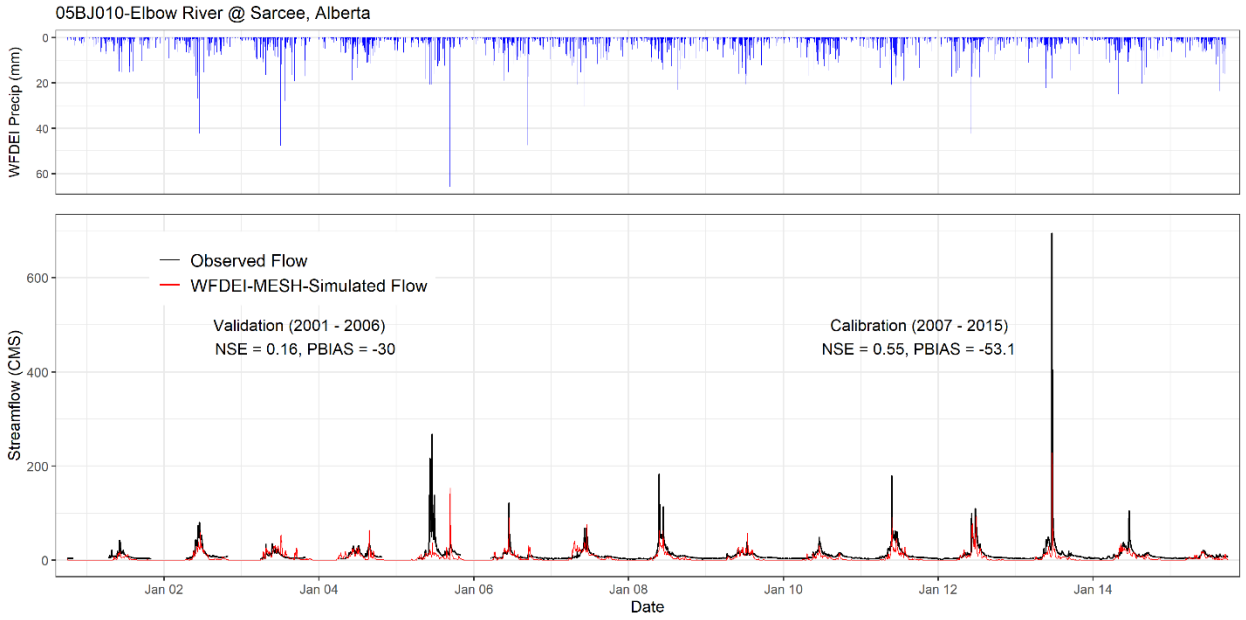

Figure 14. Calibration and validation performances for the Elbow River near Sarcee Bridge using WFDEI forcing data

GEM-CaPA-MESH calibration and validation

The observed and simulated flows for both Bow River at Banff and Elbow River at Sarcee Bridge are shown in Figure 15 and Figure 16. For the Elbow River basin near Sarcee Bridge, the calibration performance was stronger (NSE = 0.8) than for the Bow River basin at Banff (NSE = 0.77) but was highly degraded in its validation period (0.54) compared to the Bow River at Banff (0.73). Errors in low flow simulation are likely due to calibration focussing on high flows. Unlike higher resolution forcing, GEM-CaPA cannot capture convective storms and orographic

precipitation as it is a low resolution model with parameterized convection, however it can simulate long-term changes in climate over many decades, which the WRF-PGW cannot do. The model captured most of the historical peak flows but greatly underestimated important peaks such as the 2013 flood.

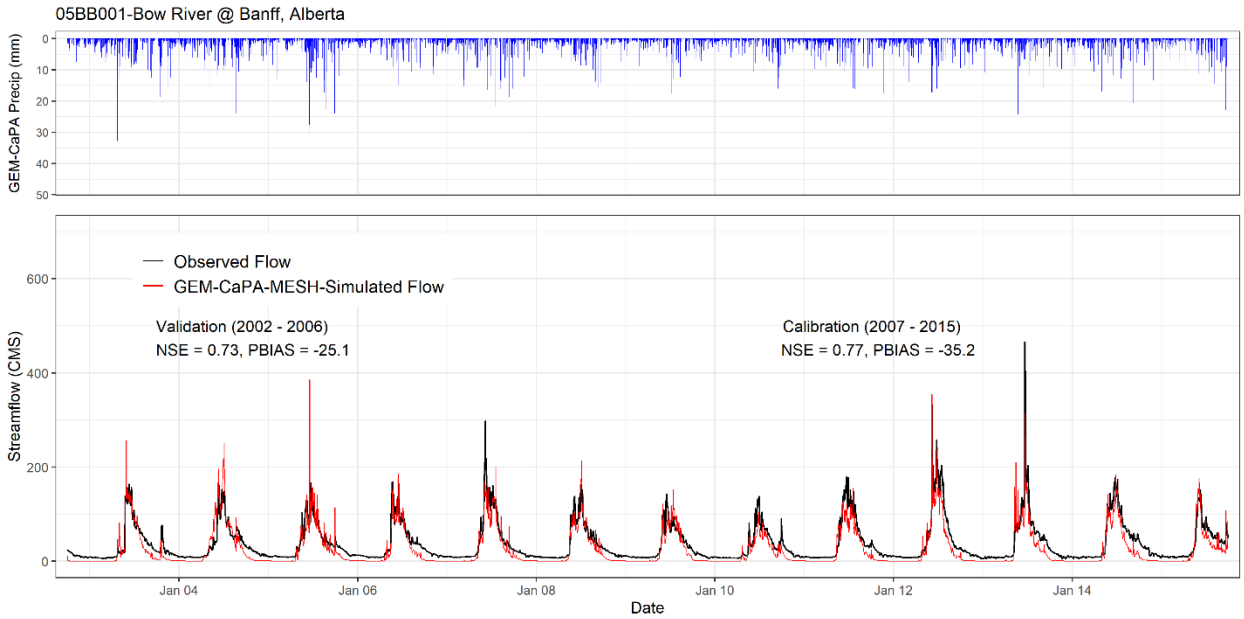

Figure 15. Calibration and validation performances for the Bow River at Banff using GEM-CaPA forcing data

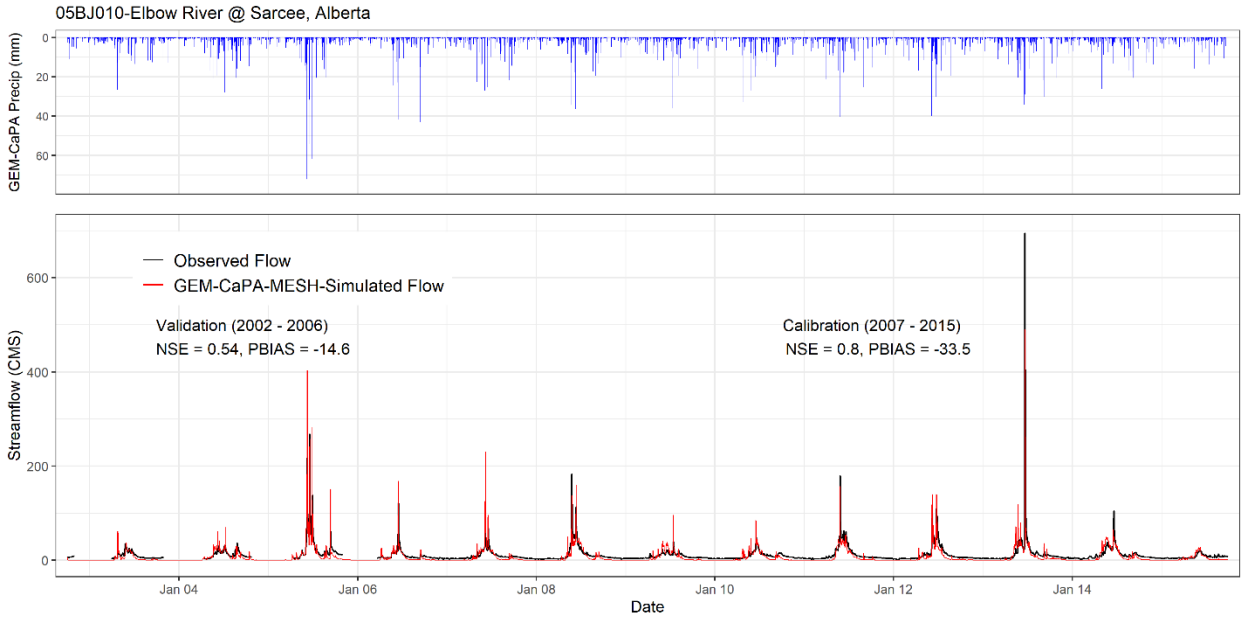

Figure 16. Calibration and validation performances for the Elbow River near Sarcee Bridge using GEM-CaPA forcing data

WFDEI-GEM-CaPA MESH calibration and validation

The model validation results of the climate forcing datasets for the Bow and Elbow River basins are given in Figure 17 and Figure 18. The model performed quite well (NSE = 0.76) during calibration while its performance degraded (NSE = 0.6) during validation. Similarly, for the Elbow River basin near Sarcee Bridge, the model performed well during calibration (NSE = 0.79) but degraded during validation (NSE = 0.23).

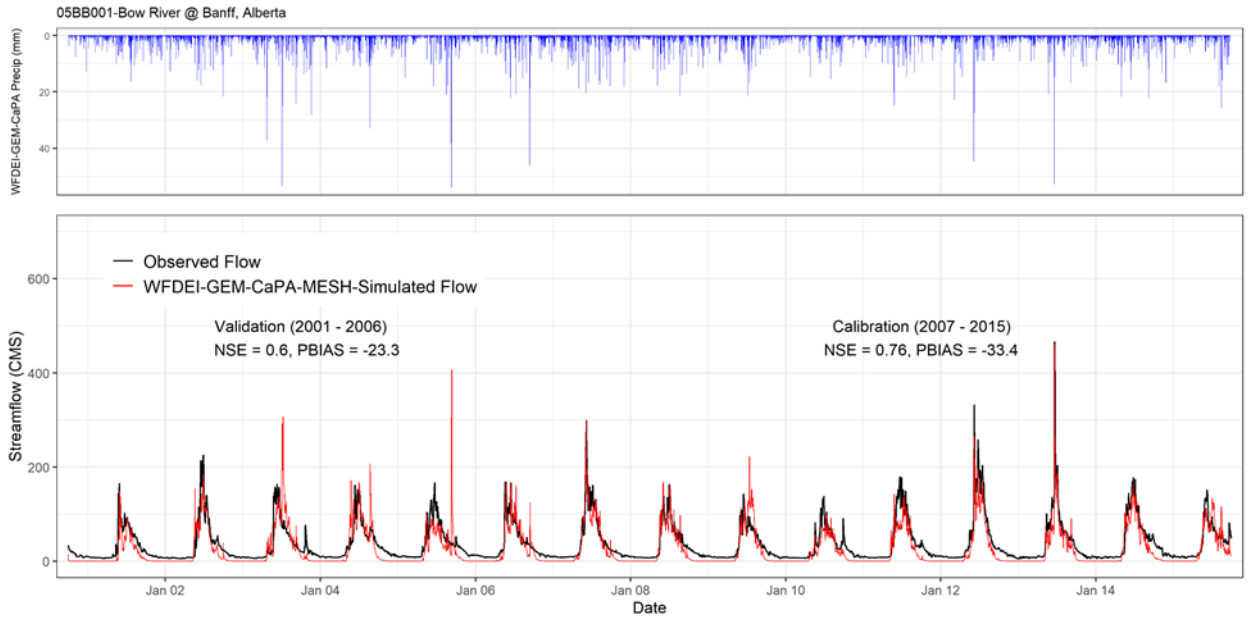

Figure 17. Calibration and validation performances for the Bow River at Banff using WFDEI-GEM-CaPA forcing data

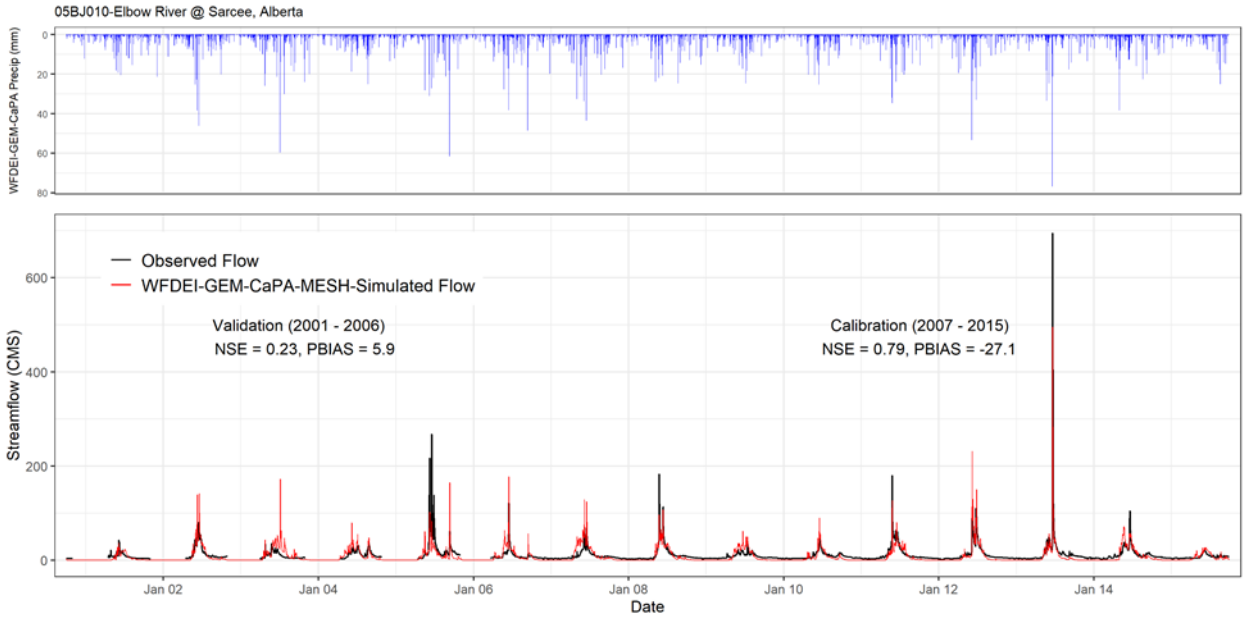

Figure 18. Calibration and validation performances for the Elbow River near Sarcee Bridge using WFDEI-GEM-CaPA forcing

CanRCM4-MESH calibration and validation

The hydrographs, calibration and validation statistics for Bow and Elbow Rivers for the entire calibration and validation period are given in Figure 19 and Figure 20 respectively. The model underestimated some of the peaks for Bow River at Banff and most of the peak flows for Elbow River near Sarcee Bridge. Given that the raw CanRCM4 forcings are a fictitious time series that can only really be compared in a climatological sense, the performance for Bow River at Banff is remarkable and is due to the seasonal snowmelt dominance of hydrograph generation.

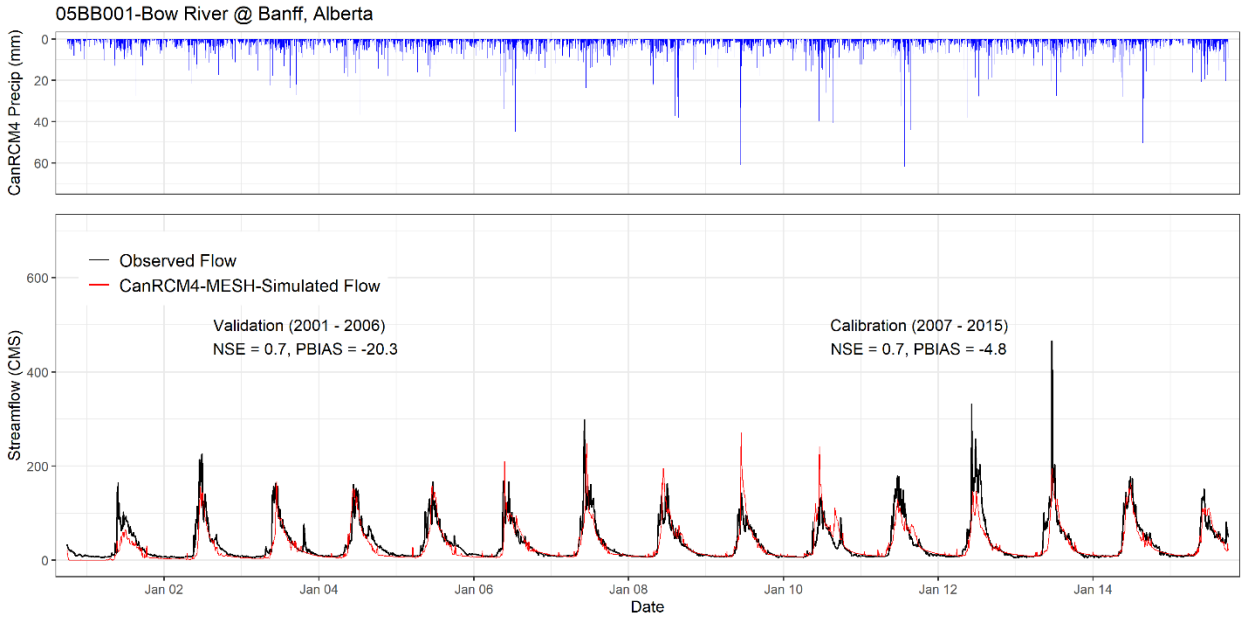

Figure 19. Calibration and validation performances for the Bow River at Banff using CanRCM4 forcing data

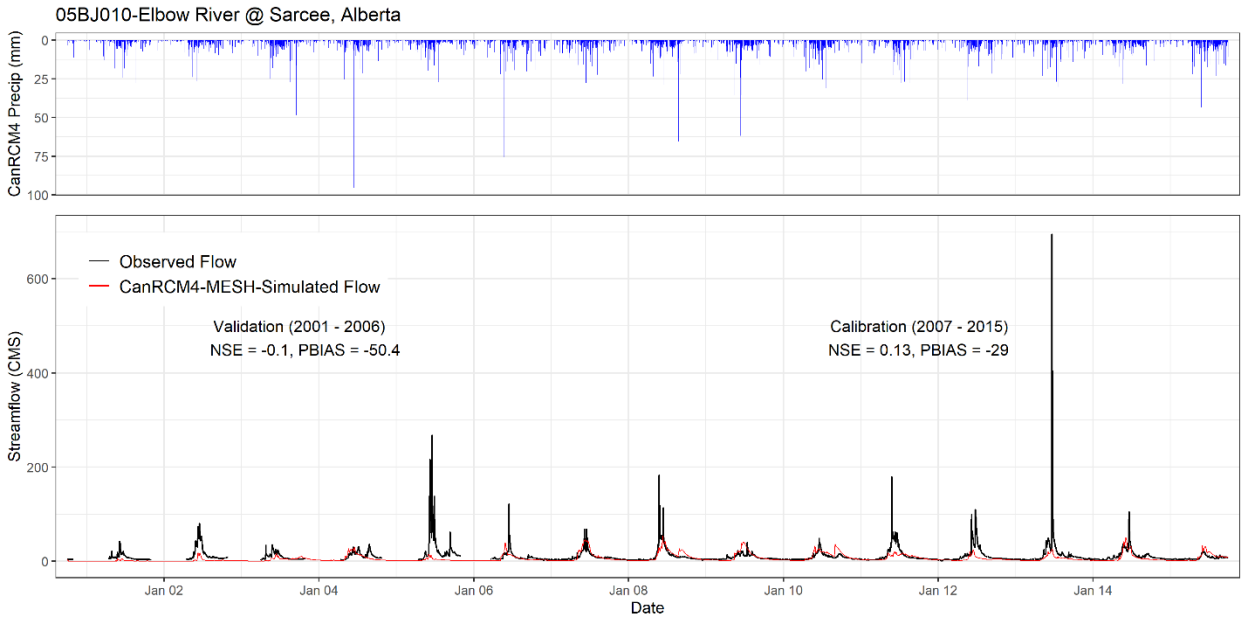

Figure 20. Calibration and validation performances for the Elbow River near Sarcee Bridge using CanRCM4 forcing data

CanRCM4-WFDEI-GEM-CaPA calibration and validation

The model simulated the historical daily streamflow of the Bow River at Banff quite well with a Nash-Sutcliffe efficiency of 0.72 in calibration and 0.66 in validation, while poor model performances were observed for the Elbow River basin near Sarcee Bridge. Further effort on improving the calibrations would only lead to modest improvements in performance and do not make sense when dealing with a partially synthetic time series generated from a climate model without assimilation. This is because, as noted above, the most significant limitation is the quality of the driving data, where precipitation and wind speed are likely to be underestimated in mountains. These driving data issues cannot readily be corrected by model calibration.

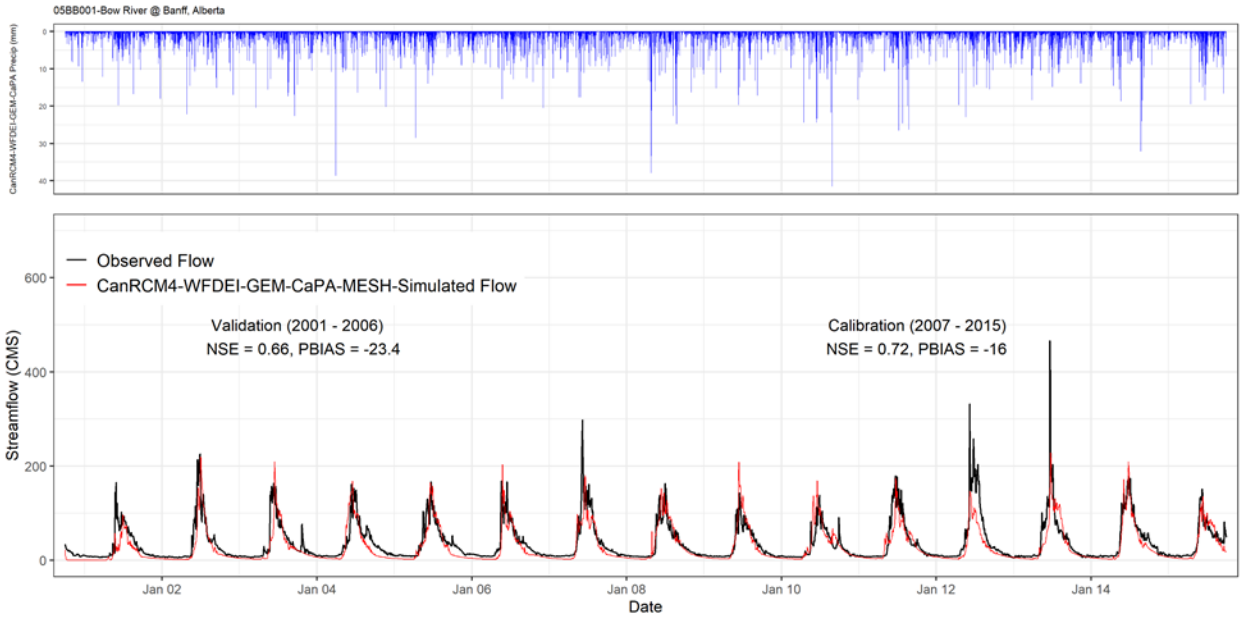

Figure 21. Calibration and validation performances for the Bow River at Banff using CanRCM4-WFDEI-GEM-CaPA forcing data

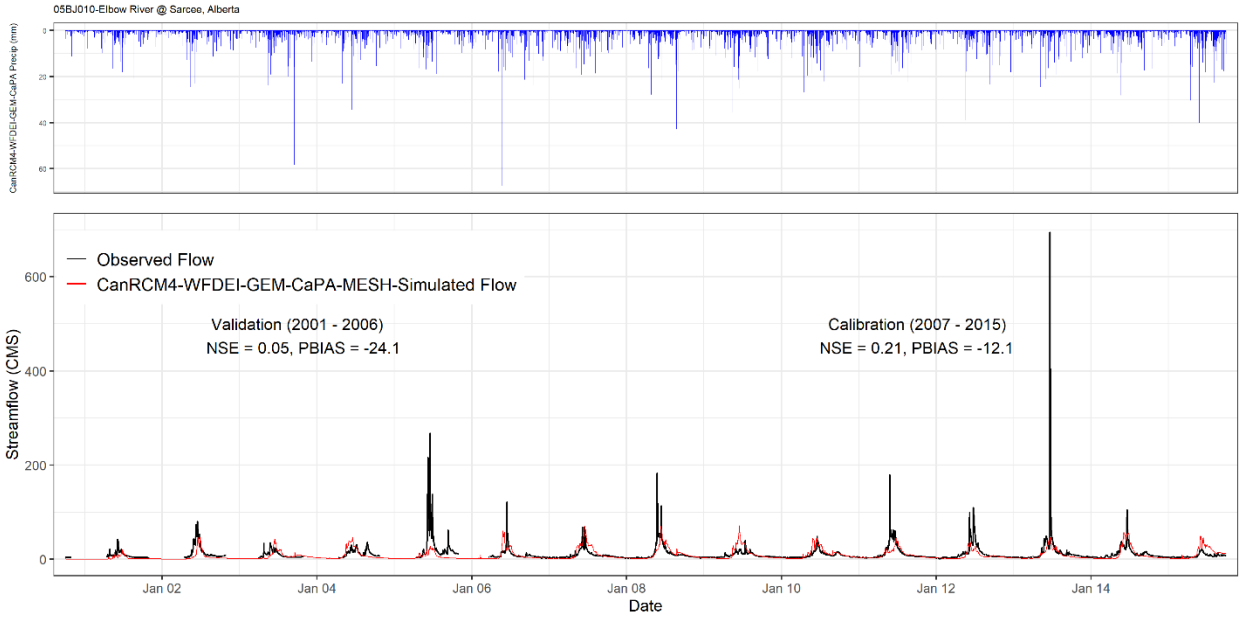

Figure 22. Calibration and validation performances for the Elbow River near Sarcee Bridge using CanRCM4-WFDEI-GEM-CaPA forcing data

WRF-MESH calibration and validation

The hydrographs and the calibration and validation statistics for the entire period (2002 – 2015), for the Bow River Basin at Banff and the Elbow River Basin near Sarcee Bridge, are plotted in Figure 23 and Figure 24 respectively. When calibrated was driven by WRF climate forcing, the model showed best performance, in calibration (NSE = 0.80) and in validation (NSE = 0.83), with low PBIAS for the Bow River at Banff. The model did a particularly good job in capturing most of the peak flows, including the 2013 peak flow for the Bow River at Banff. The model captured the

hydrograph and timing of flows, both rainfall-runoff and snowmelt-runoff events, but in a few cases the flood peaks are underestimated. The performance of the Elbow River near Sarcee Bridge is generally satisfactory (NSE > 0.63) but drops in the validation. The model underestimates most of the peak flows of the Elbow River near Sarcee Bridge. Further effort to improve the calibrations would likely lead only to modest or no improvements in performance because the greatest limitation is the quality of the driving meteorology data, mostly due to precipitation that is likely to be underestimated in the mountains and cannot readily be corrected by model calibration. In 2013 the Elbow River near Sarcee Bridge model failed to predict the peak flows as the precipitation that needed to generate the observed flow is smaller than reported for that time.

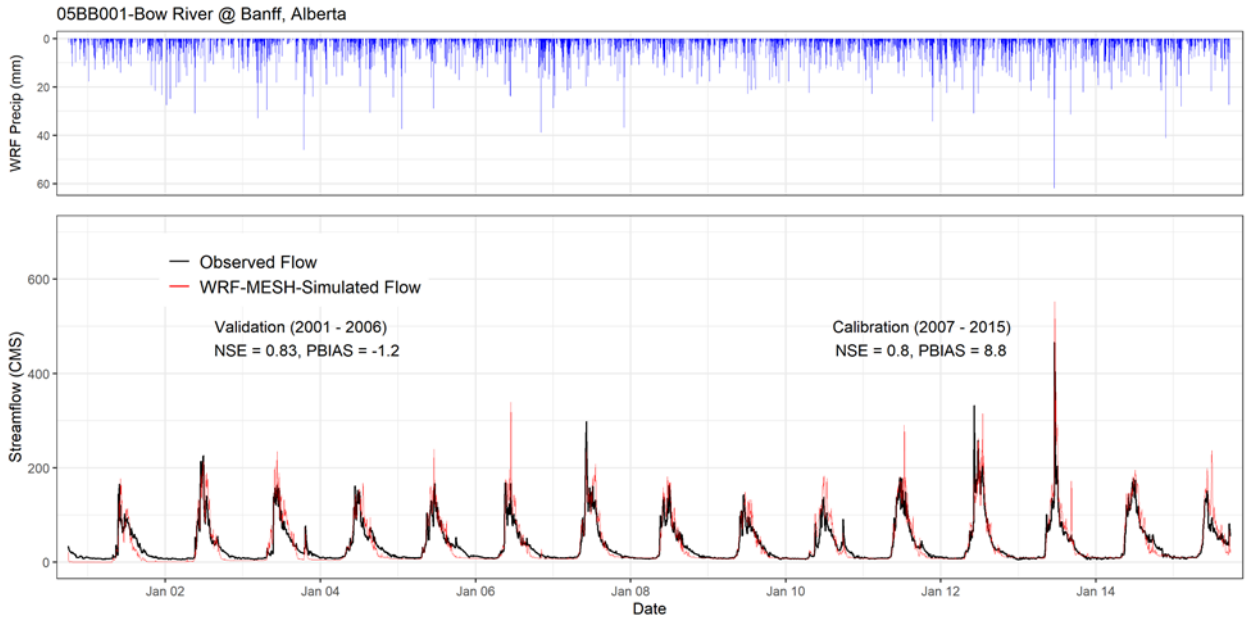

Figure 23. Calibration and validation performances for the Bow River at Banff using WRF forcing data

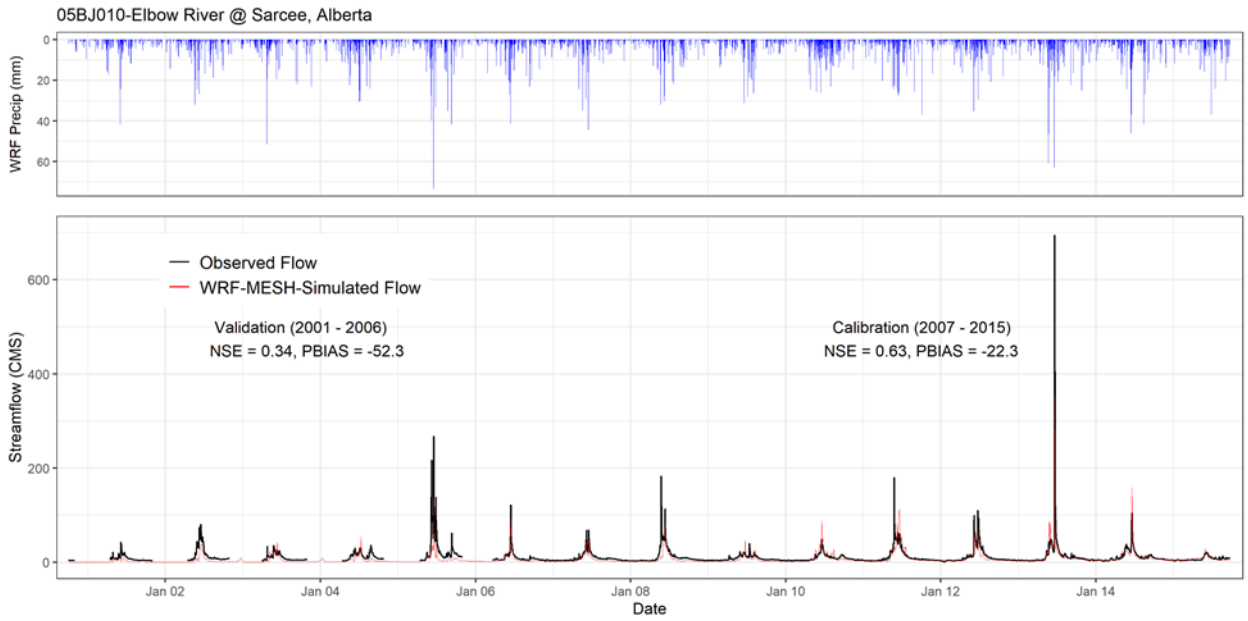

Figure 24. Calibration and validation performances for the Elbow River at Sarcee Bridge using WRF forcing data

The calibrated model parameters were used to test the reservoir model. The reservoir models were tested for the Bow River at Calgary by comparing WRF-MESH run with and without the reservoir model as shown in Figure 25. The model overestimated nearly all peak flows when the model did not include the reservoir model. The model performance increased from NSE = 0.17 (Figure 25), to a satisfactory NSE = 0.63 (Figure 26), when the statistical reservoir model was included. The model was not recalibrated after reservoir insertion. Using the NSE statistic for calibration caused the model to fail to simulate low flows well.

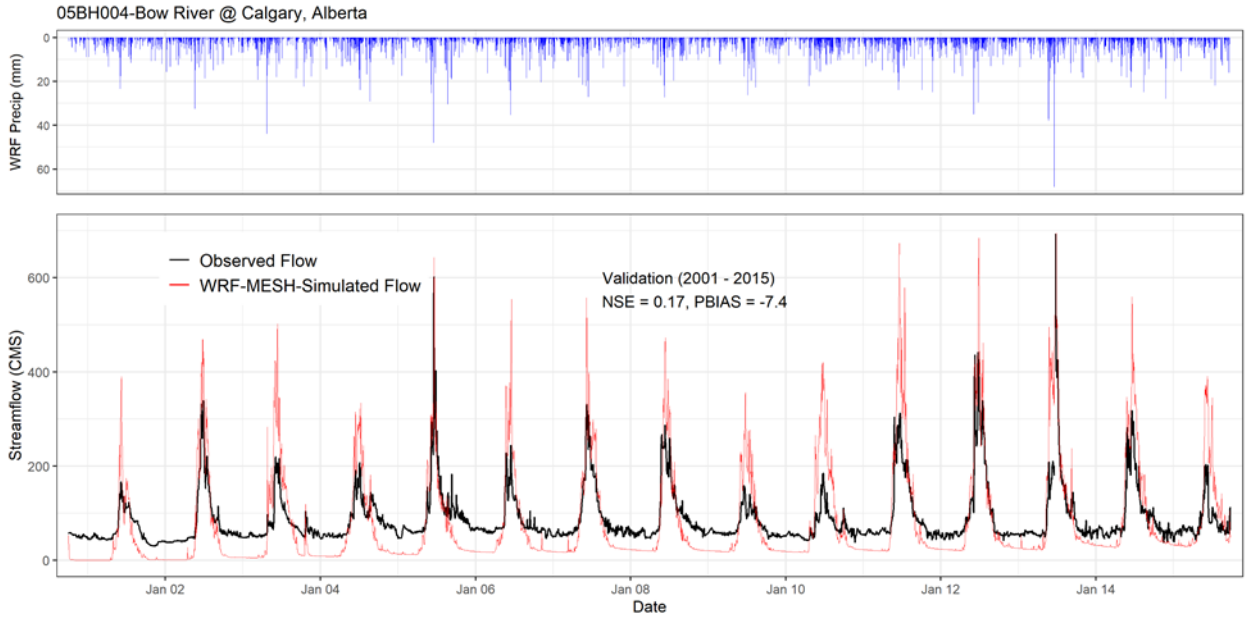

Figure 25. Validation performances for the Bow River at Calgary without Reservoir using WRF forcing data

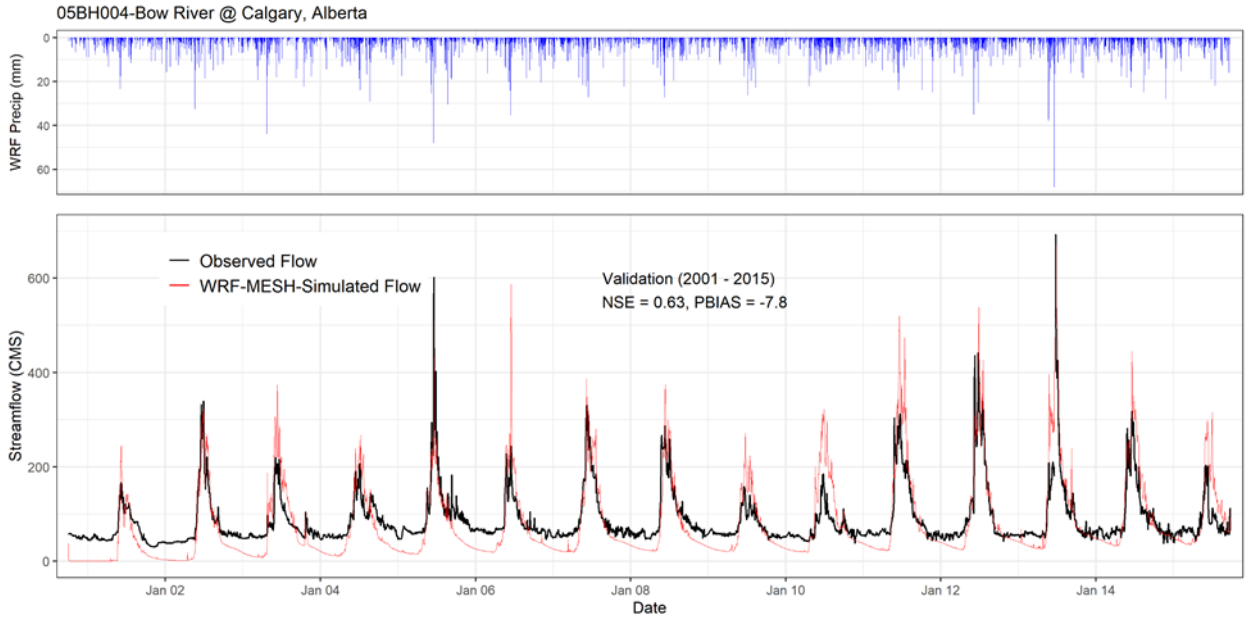

Figure 26. Validation performances for the Bow River at Calgary with Reservoir using WRF forcing data

Figure 27 and Figure 28 compare the range and the mean of the mean daily observed flow and simulated from WRF-MESH for the study basins. The simulated range captured most of the observed range and seasonal patter of events.

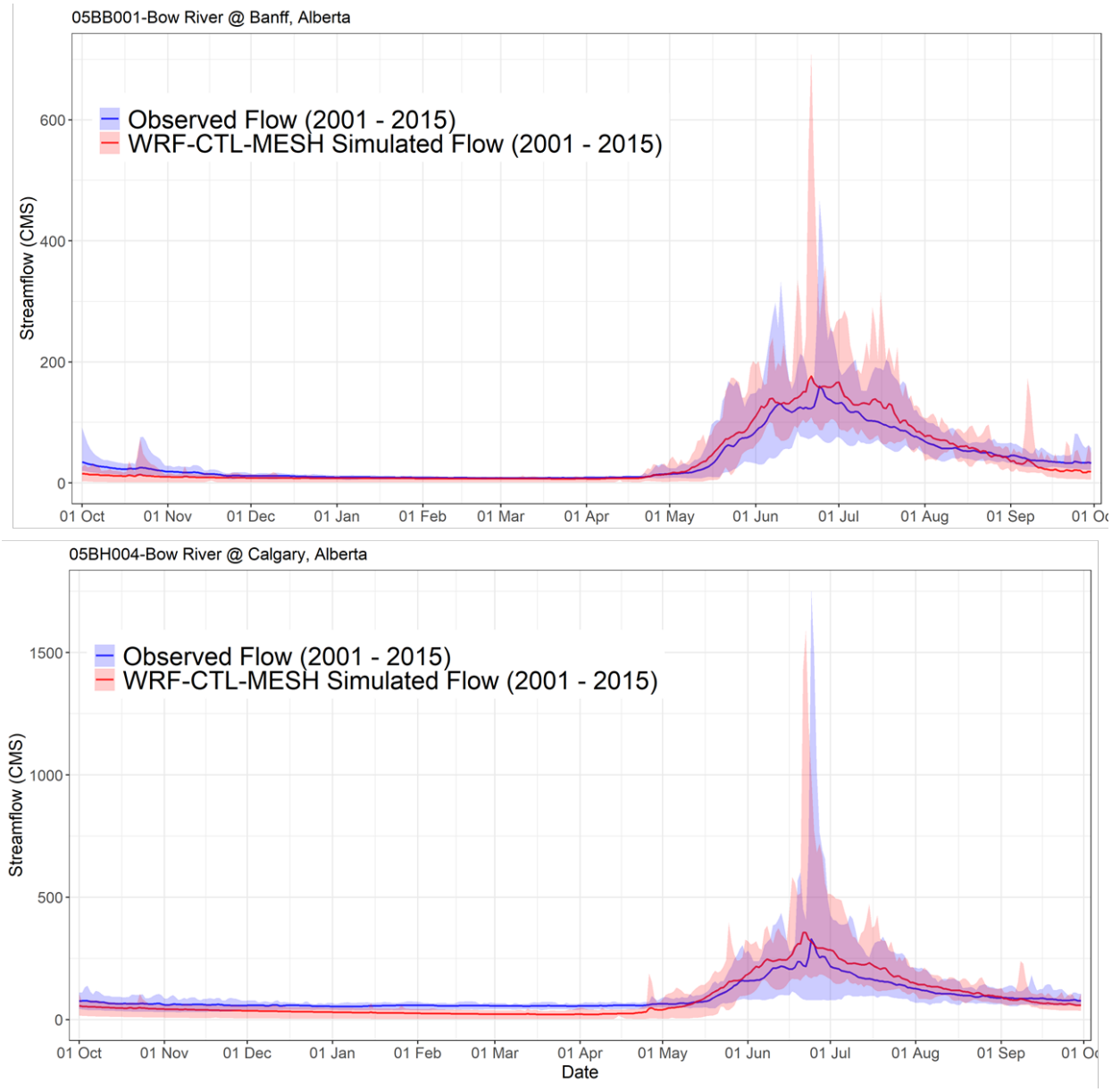

Figure 27. Minimum, mean and maximum daily observed and WRF-CTL-MESH simulated streamflow for Bow River at Banff and Bow River at Calgary.

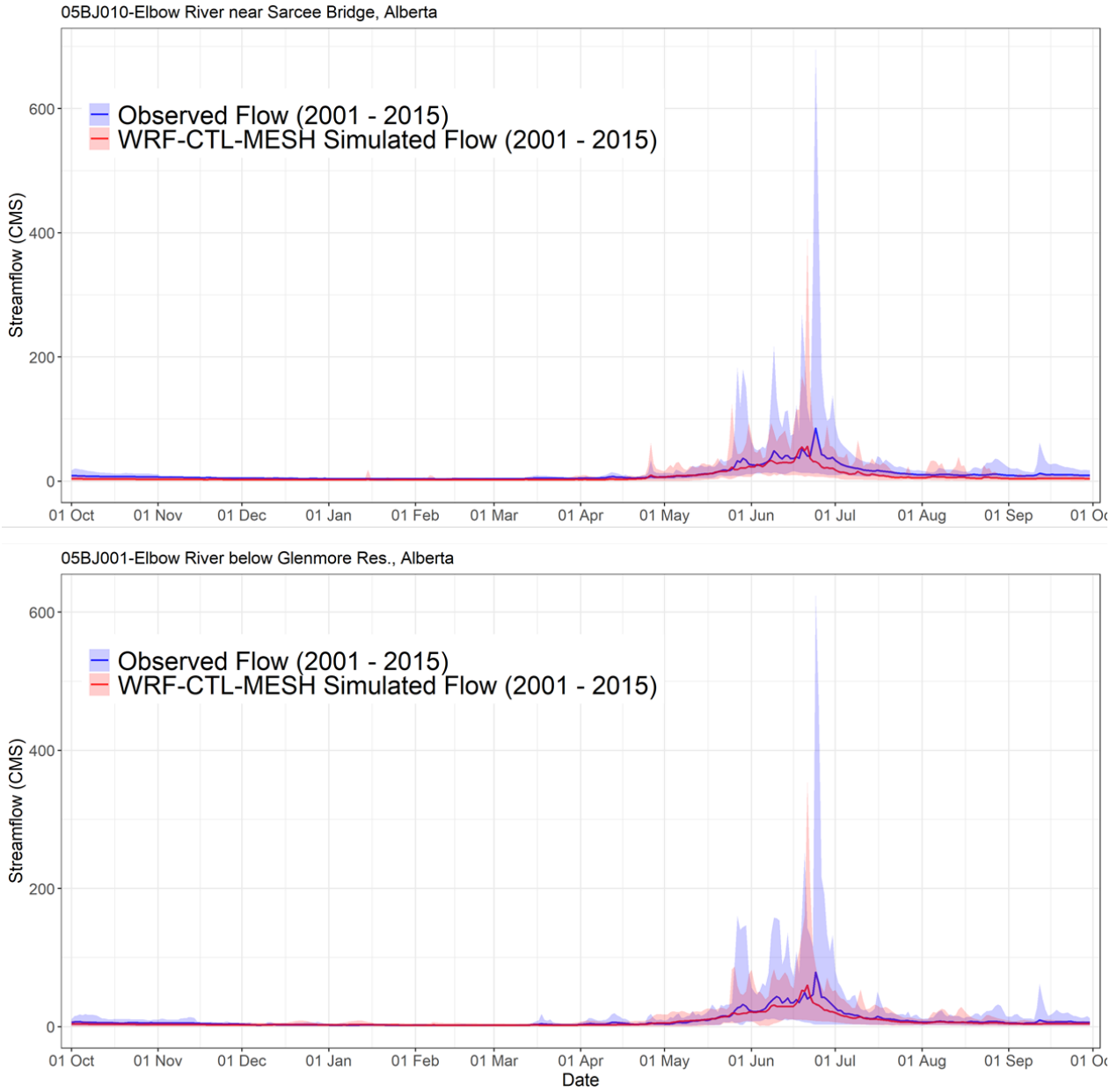

Figure 28. Minimum, mean and maximum daily observed and WRF-CTL-MESH simulated streamflow for Elbow River near Sarcee Bridge and below Glenmore reservoir

Based on the modeling assessment on the various climate forcing, WRF forcing data was found the best to simulate the historical flood flow. The rest of the study is therefore based on this data and for comparison purpose, CanRCM4 will also be used.

4.2 **Glacier model evaluation**

Figure 29 presents, for the different forcing datasets, the annual mass-balance time series for the nearest MESH glacier GRU to Peyto Glacier, which has carefully observed mass balance measurements from 1965 thanks to studies by the National Glaciological Programme of Environment Canada, Natural Resources Canada and their predecessor departments. The annual mass balance as simulated by MESH was compared with the observed annual mass

balance of Peyto Glacier for the historical period for various climate data and two model configurations. Mountain MESH performed better in simulating the annual mass balance compared with original MESH because it corrected most of the forcing variables for topography and solar radiation for slope and aspect. Amongst the forcing datasets used, GEM-CaPA and WRF with Mountain MESH were able to produce mass balances that were closest to the observations at Peyto Glacier (Figure 29). The model could capture the interannual variability of the mass balance well, which makes the model credible in simulating runoff from glacier.

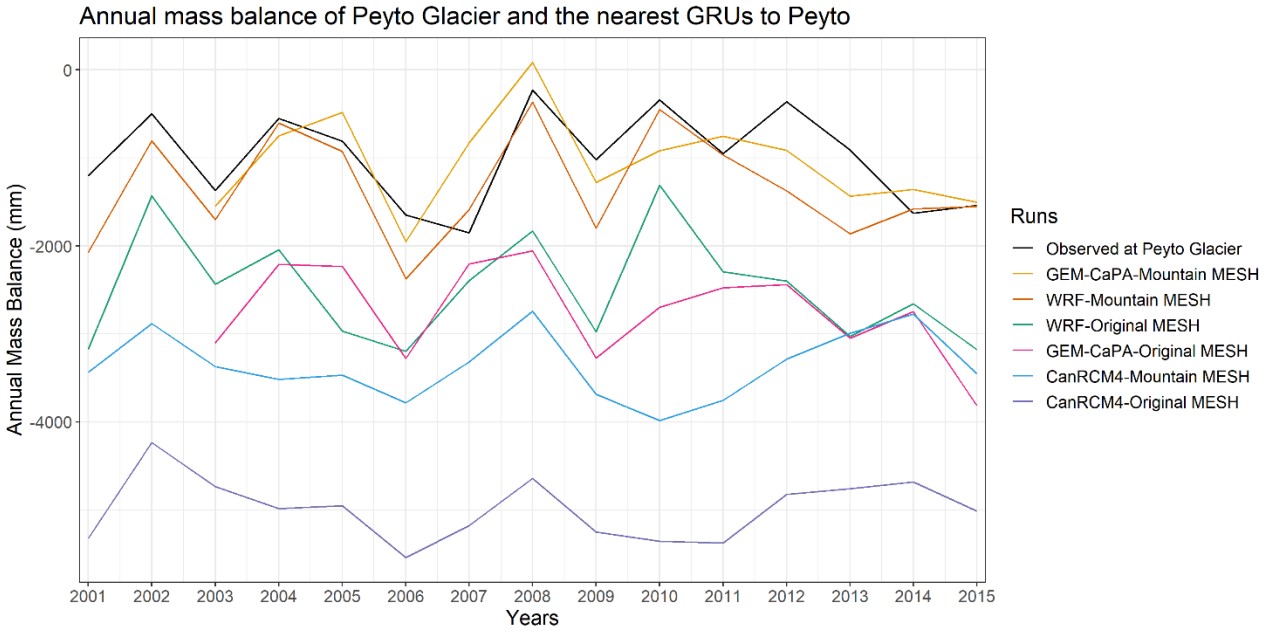

Figure 29. Comparison of annual mass balance for nearest MESH GRUs for different atmospheric forcing and MESH model configurations.

The mean annual contribution of glacier ice wastage to the total streamflow at basin outlet is given in Table 6 by examining the runoff volume output of the glacier module and subtracting it from streamflow simulations. WRF-Mountain MESH simulated annual ice wastage contributions of 2.4% for Bow River at Banff - this is comparable with previous studies Comeau et al., 2009 (2.2%), Demuth et al., 2008 (2.8%) and Hopkinson and Young 1998 (1.8%). Higher annual contributions from ice wastage were simulated when MESH driven with CanRCM4 or with original MESH showing the effect of forcing data, addressing sub-grid variation in precipitation, snow and melt energetics and model resolution on glacier hydrology calculations in mountain basins.

Table 6. Percentage of mean annual (2001-2015) glacier ice wastage contribution to the total runoff at the outlet of the basin

Basins	Simulation Runs	Glacier Ice Wastage Contribution (%)	
		Mountain MESH	Original MESH
Bow River at Banff	GEM-CaPA-MESH *	6.9	17.8
	WRF-MESH	2.4	10.8
	CanRCM4-MESH	13.6	23.0
Bow River at Calgary	GEM-CaPA-MESH *	4.4	10
	WRF-MESH	1.8	7.2
	CanRCM4-MESH	9.5	15

4.3 Future Changes in Precipitation and Temperature

Monthly outputs from CanRCM4 and WRF simulations for all basins over the periods 2001–2015 and 2086–2100 are shown in Figure 30 and Figure 31. Based on the CanRCM4 future climate, the median precipitation of Bow River at Banff and Calgary is projected to increase in all months except July, August and September which is mostly consistent with the WRF future climate. Both CanRCM4 and WRF future precipitation vary considerably from month to month. The greatest increases in median monthly precipitation for CanRCM4 RCP 8.5 climate compared with the historical period (in June) are by 56 mm for Bow River at Banff, 60 mm for Bow River at Calgary and 30 mm for Elbow River near Sarcee Bridge whilst the largest decreases (in August) are by 35, 38 and 36 mm for Bow River at Banff, Bow River at Calgary and Elbow River near Sarcee Bridge, respectively. Precipitation in the WRF PGW climate increased from current conditions in March by 26 mm for Bow River at Banff, in May by 20 mm for Bow River at Calgary and in August by 19 mm for Elbow River at Sarcee Bridge whereas the largest decreases are in August by 12 mm for Bow River at Banff, in July by 11 mm for Bow River at Calgary and in June by 16 mm for Elbow River near Sarcee Bridge.

The lower panels of Figure 30, Figure 31, and Figure 32 show boxplots of the historical and future monthly temperatures for the three study basins. Both CanRCM4 and WRF-PGW consistently simulated increases in future median monthly temperature for all three basins. The mean monthly temperature of the Bow River basin at Banff is projected to increase by 4.2 °C in January and 5.3 °C in June by the end of the century in the WRF-PGW scenarios. Similarly, the greatest increases in the mean monthly temperature for Bow River at Calgary and Elbow River near Sarcee Bridge were in May, where it increased by about 4.9 and 5.1 ºC respectively while the smallest increases were in July by about 3.8 and 4 °C respectively.

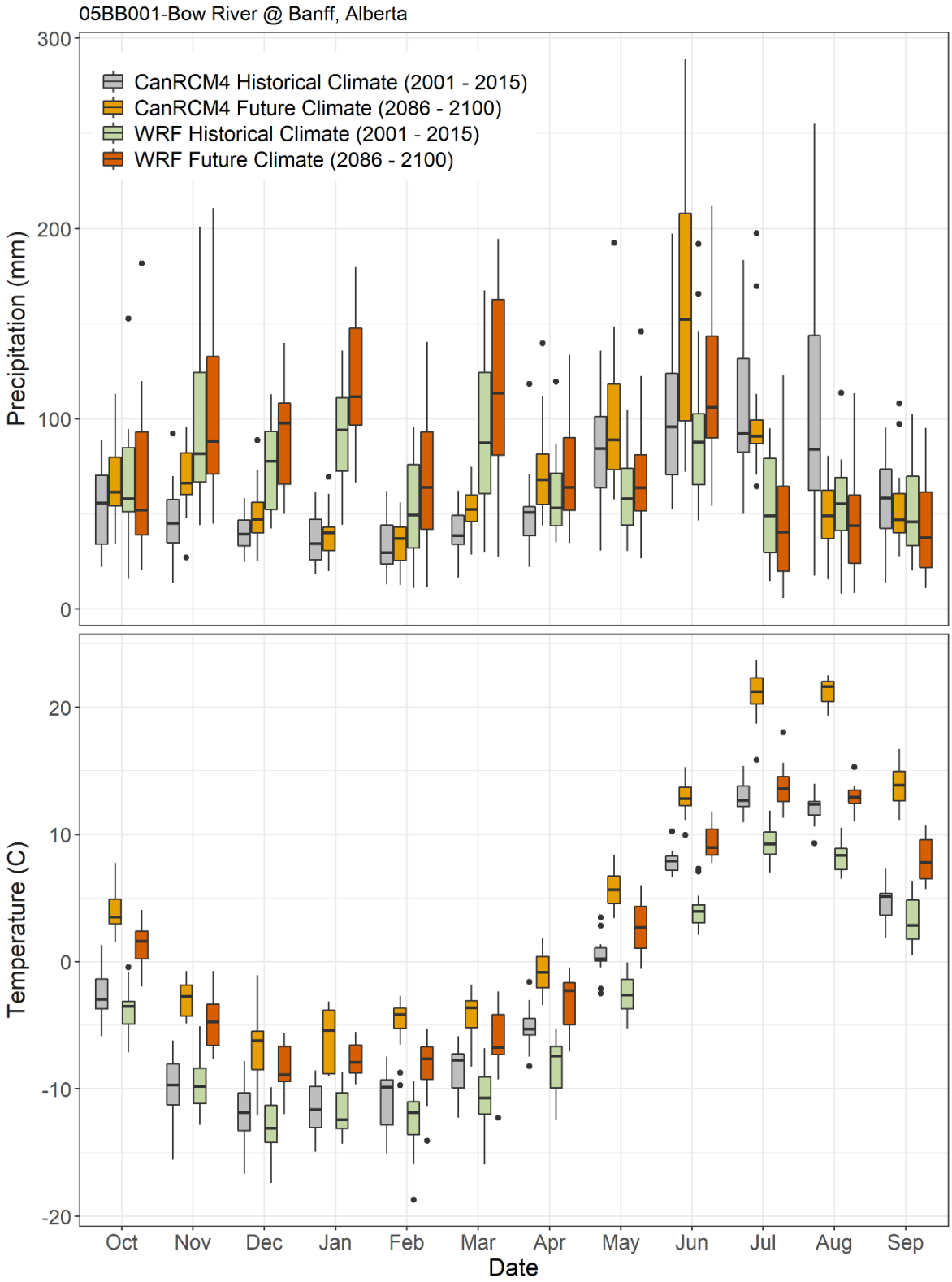

Figure 30. Comparison of historical and future monthly precipitation and temperature between CanRCM4 and WRF climate simulations for Bow River basin at Banff. The band near the middle of each box shows the median and the bottom and top of each box spans the lower and upper quartiles. Whiskers above and below the box show the maximum and minimum values.

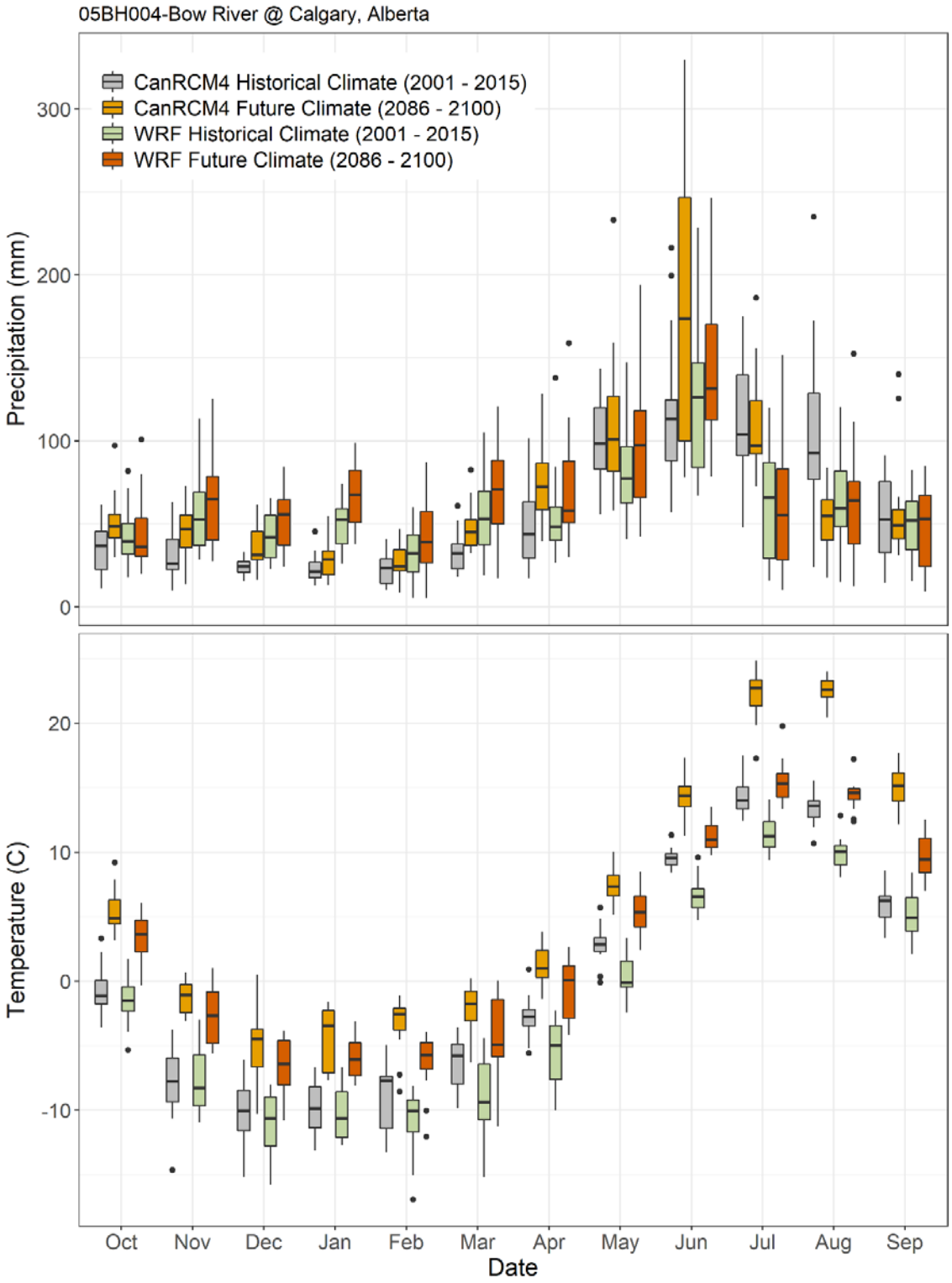

Figure 31. Comparison of historical and future precipitation and temperature between CanRCM4 and WRF climate simulations for Bow River basin at Calgary. The band near the middle of each box shows the median and the bottom and top of each box spans the lower and upper quartiles. Whiskers above and below the box show the maximum and minimum values.

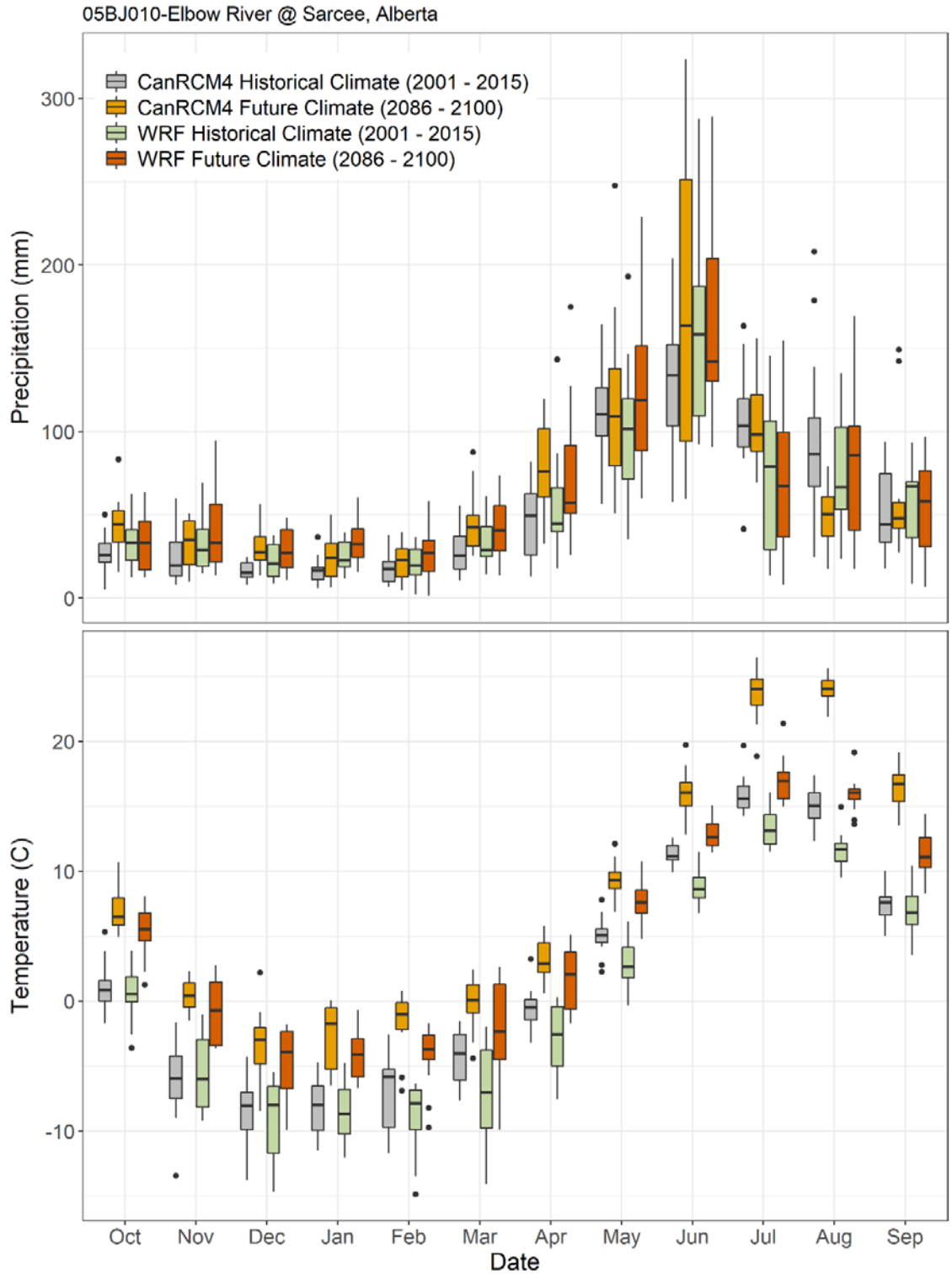

Figure 32. Comparison of historical and future precipitation and temperature between CanRCM4 and WRF climate simulations for Elbow River basin near Sarcee Bridge. The band near the middle of each box shows the median and the bottom and top of each box spans the lower and upper quartiles. Whiskers above and below the box show the maximum and minimum values.

Figure 33 maps the WRF projected changes in mean annual precipitation and temperature between the historical climate (represented by the 2001-2015 means) and the PGW (RCP8.5 scenario) climate at the end of the century (2086-2100). Precipitation in the Bow and Elbow River basins is expected to have increased by up to 200 mm per year by the end of 21st century. The precipitation increases are projected to be greater in the higher elevation mountains and foothills and smaller in the lower elevations, down basin. Future WRF-PGW annual average temperatures are projected to increase by up to 5 ºC (likely range 4–5 ºC) with greater warming at higher elevations.

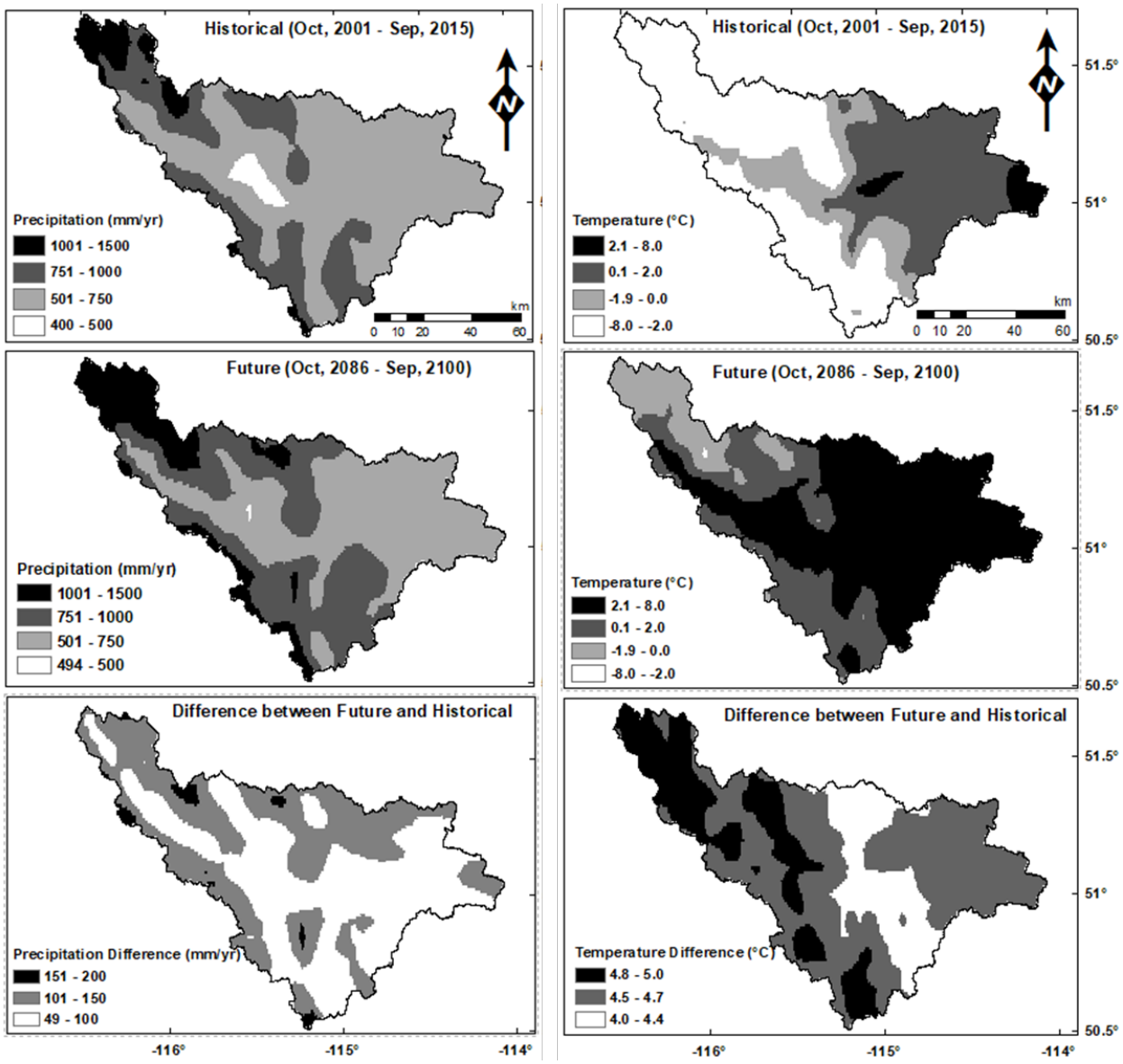

Figure 33. The spatial distribution of change in mean annual precipitation and temperature between historical and future WRF-PGW climate

With warmer air temperatures, snowfall events will become less frequent as the precipitation phase shifts from snowfall to rainfall in transitional seasons and elevations (Figure 34). The annual rainfall to precipitation ratio (R/P or rainfall ratio) increases in all parts of the basins by between

0.1 and 0.23 under the future WRF-PGW climate. The mean annual rainfall rises to 454 mm of the annual total precipitation of 966 mm (R/P = 0.47) in the Bow River basin at Banff whereas in the Bow River basin at Calgary it increases to 514 mm of the mean annual precipitation of 830 mm (R/P = 0.62). The Bow River basin at Banff continues to contain snowfall-dominated regions whereas the Bow River basin above Calgary is projected to become rainfall-dominated under the warmer future WRF climate.

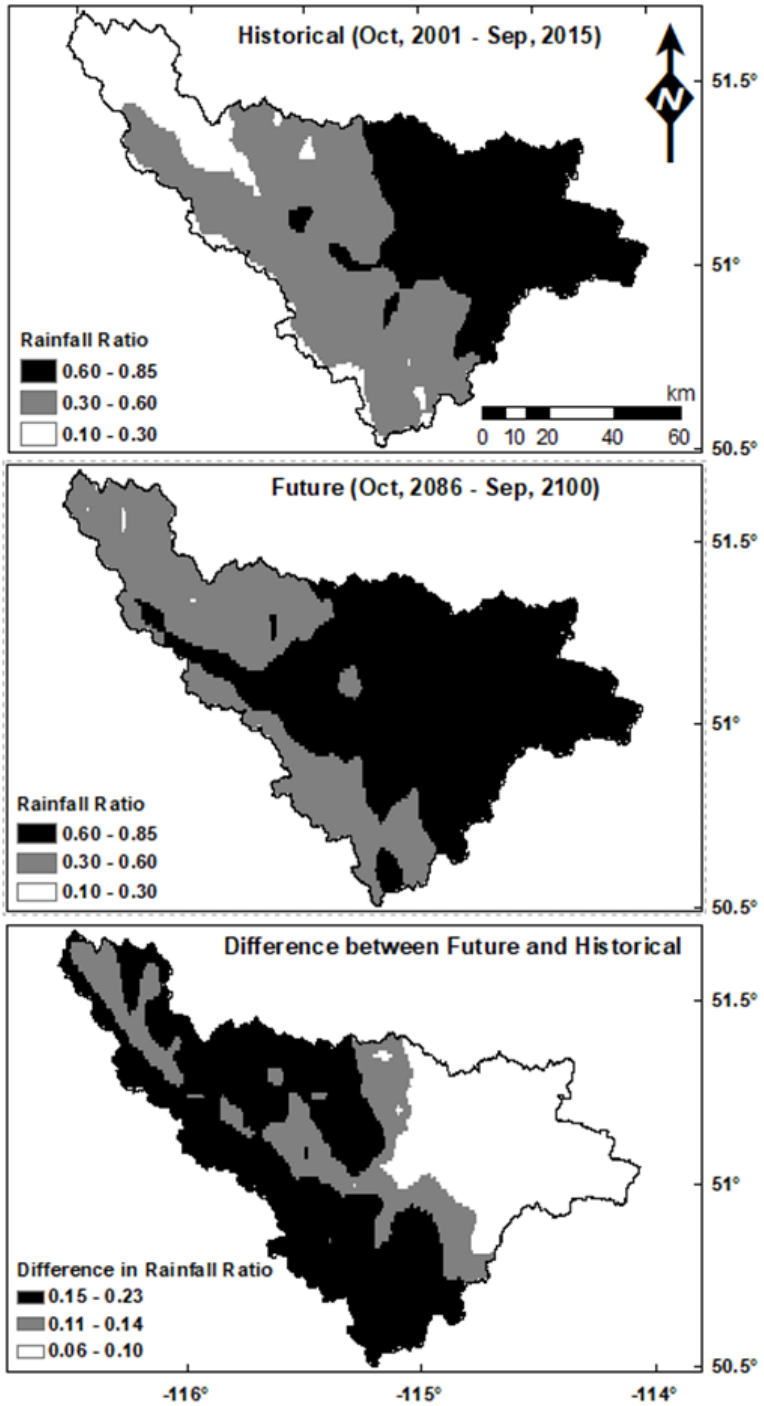

Figure 34. Mean annual rainfall to total precipitation ratios (rainfall ratios) under WRF historical and future climate

4.4 Impact of Future Climate Change on Streamflow

4.4.1 Simulated Future Streamflow

The impacts of future climate change of the streamflow of Bow River Basin above Calgary have been assessed using WRF with and without pseudo global warming (PGW) and using one representative ensemble members of CanRCM4: CanRCM4-r8i2p1r1 (the average this specific member found to be close to the ensample average). The observed and modelled flow duration curves (exceedance probabilities) of the current WRF climate and the WRF-PGW future climate are presented followed by the results from CanRCM4-r8i2p1r1 future climate in Figure 35 and Figure 36 respectively for the same period 2001-2015 and 2086-2100. All the results shown below assume that glacier coverage is held constant from the historical period and include the simple empirical reservoir model developed for this project that was described in Section 3.4. Similarly, the reservoir rules were held constant for these simulations as it is difficult to predict future water management and operation rules. Table 8 shows these results for selected quantiles of streamflow and provides the percentage increase or **decrease** (i.e. in bold) in flows with climate change.

The model results show an increase in flow for all rivers of up to 133% for low to medium flows and decreases of up to 13% for the highest flows. The increases in low to medium flows are due to the wetter future climate and also to accelerated glacier ice melt for the Bow River. Holding glacier coverage constant is not a realistic scenario but is instructive to see the water that would be available if Bow River Basin glaciers were not being depleted over this century. The decreases in the larger flows are due to reduced snowmelt contributions to ROS and SMR driven high flows and possibly to drier and less frequently frozen soils due to increased evapotranspiration rates and a shorter snowcovered season. This is a result of shallower and more ephemeral spring snowpacks and the loss of springtime low elevation snowpacks. The differences between observed and modelled exceedance probabilities suggest that some bias correction is needed before the modelled flow duration curves can be used with confidence for design or flood estimation purposes.

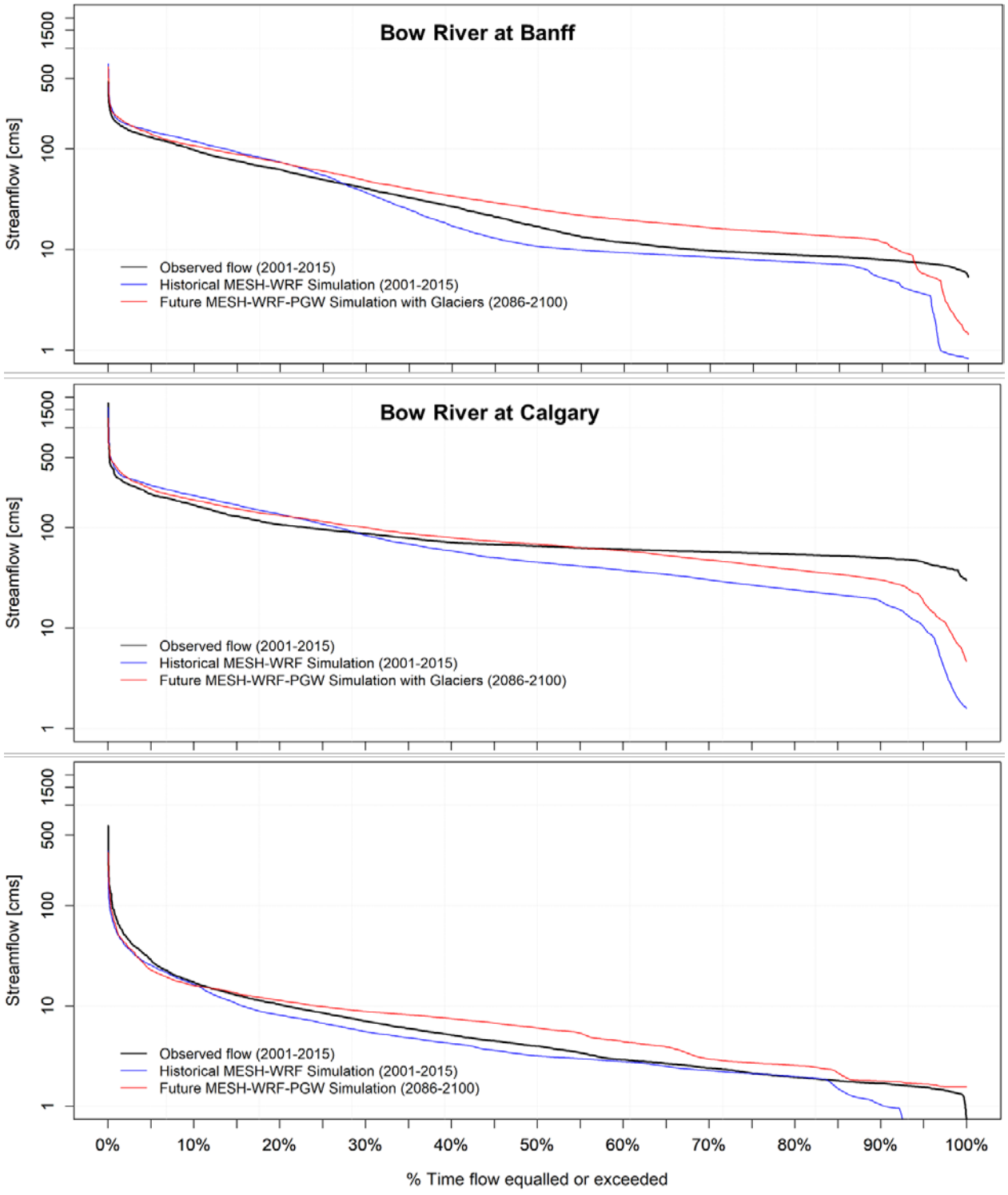

Figure 35. The observed and MESH-modelled flow duration curves for current and future WRF climate with unchanged glacier coverage for the Bow River at Banff (top), Bow River at Calgary (middle) and Elbow River below Glenmore Reservoir (bottom).

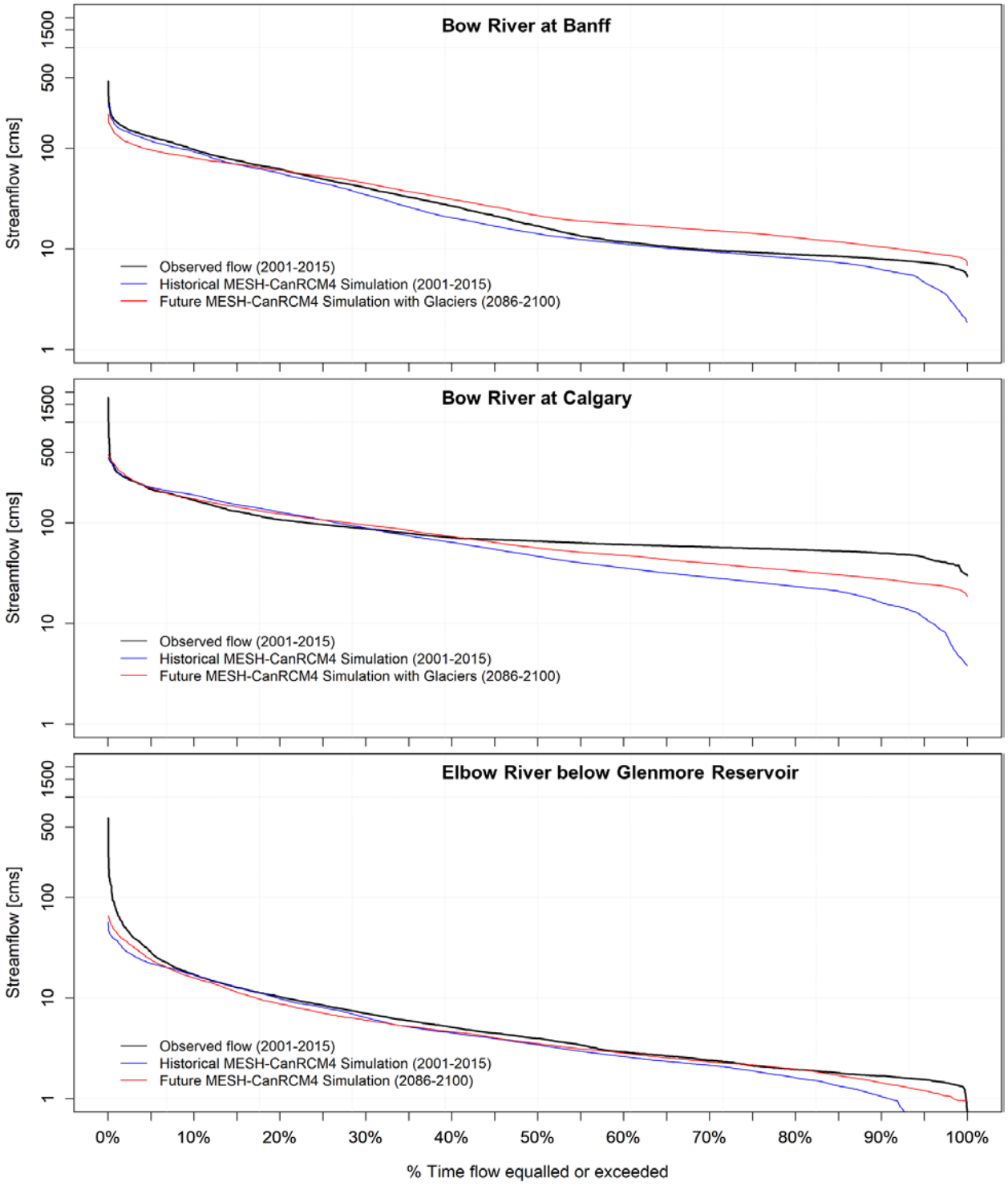

Figure 36. The observed and MESH-modelled flow duration curves for current and future CanRCM4 climate with unchanged glacier coverage for the Bow River at Banff (top), Bow River at Calgary (middle) and Elbow River below Glenmore Reservoir (bottom).

Table 7. Selected quantiles of observed and simulated streamflow from WRF and CanRCM4 climate change while historical glacier coverage is held constant. Negative percentage change values are in bold.

% Time Flow Equalled / Exceeded	QObs	WRF-MESH QS_{Hist}	WRF-MESH QS_{Futu}	% Change	CanRCM4-MESH QS_{Hist}	CanRCM4-MESH QS_{Futu}	% Change
Bow River at Banff							
10	97.6	119.4	107.9	**-9.7**	92.7	80.4	**-13.3**
20	62.5	73.9	73.3	**-0.7**	56.7	60.7	7.0
30	40.3	37.0	48.5	31.0	34.7	45.2	30.2
40	26.7	17.2	34.0	97.5	20.4	31.2	52.6
50	17.0	10.8	25.1	133.3	14.2	21.6	52.2
60	11.8	9.3	19.8	112.0	11.3	17.7	57.2
70	9.8	8.4	16.5	96.7	9.4	15.4	62.9
80	8.8	7.6	14.4	90.2	8.1	13.0	60.9
90	7.9	5.2	11.8	127.3	6.2	10.5	67.7
Bow River above Calgary							
10	167.9	210.2	189.8	**-9.7**	189.9	172.6	**-9.1**
20	107.6	137.3	133.3	**-2.9**	127.7	123.6	**-3.2**
30	87.6	84.3	100.5	19.3	88.9	95.5	7.4
40	71.2	59.0	79.7	35.0	64.3	73.4	14.2
50	65.8	45.4	69.0	51.8	46.5	56.6	21.7
60	61.0	37.8	59.1	56.0	35.8	47.6	32.9
70	57.6	30.4	47.8	57.3	28.7	39.8	38.6
80	54.2	24.1	38.3	58.9	23.4	33.4	42.8
90	50.0	18.5	30.3	63.8	16.2	27.8	71.0
Elbow River below Glenmore Reservoir							
10	17.3	16.4	15.0	**-8.2**	16.9	15.9	**-6.2**
20	10.3	8.1	9.0	10.5	9.9	8.8	**-11.2**
30	7.1	5.5	7.1	27.6	6.4	6.1	**-5.9**
40	5.1	4.2	5.9	38.9	4.5	4.6	2.4
50	4.0	3.2	4.9	53.0	3.4	3.5	2.4
60	2.9	2.8	3.6	27.9	2.6	2.8	8.3
70	2.4	2.3	2.8	24.6	2.2	2.3	8.2
80	2.0	2.0	2.4	20.0	1.6	2.0	21.5
90	1.7	1.0	1.4	39.2	1.1	1.4	36.3

Figure 37 below shows the MESH-projected mean annual local runoff for the WRF-PGW future climate. Increases in local runoff are expected all over the basins following similar spatial patterns to the precipitation, with the greatest increases in the mountains. Local runoff is projected to increase by up to 250 mm per year in much of the basin. Mountain runoff is projected to increase by up to 2000 mm per year, with much of this coming from rising glacier ice wastage as the scenario held glacier coverage constant (Figure 37).

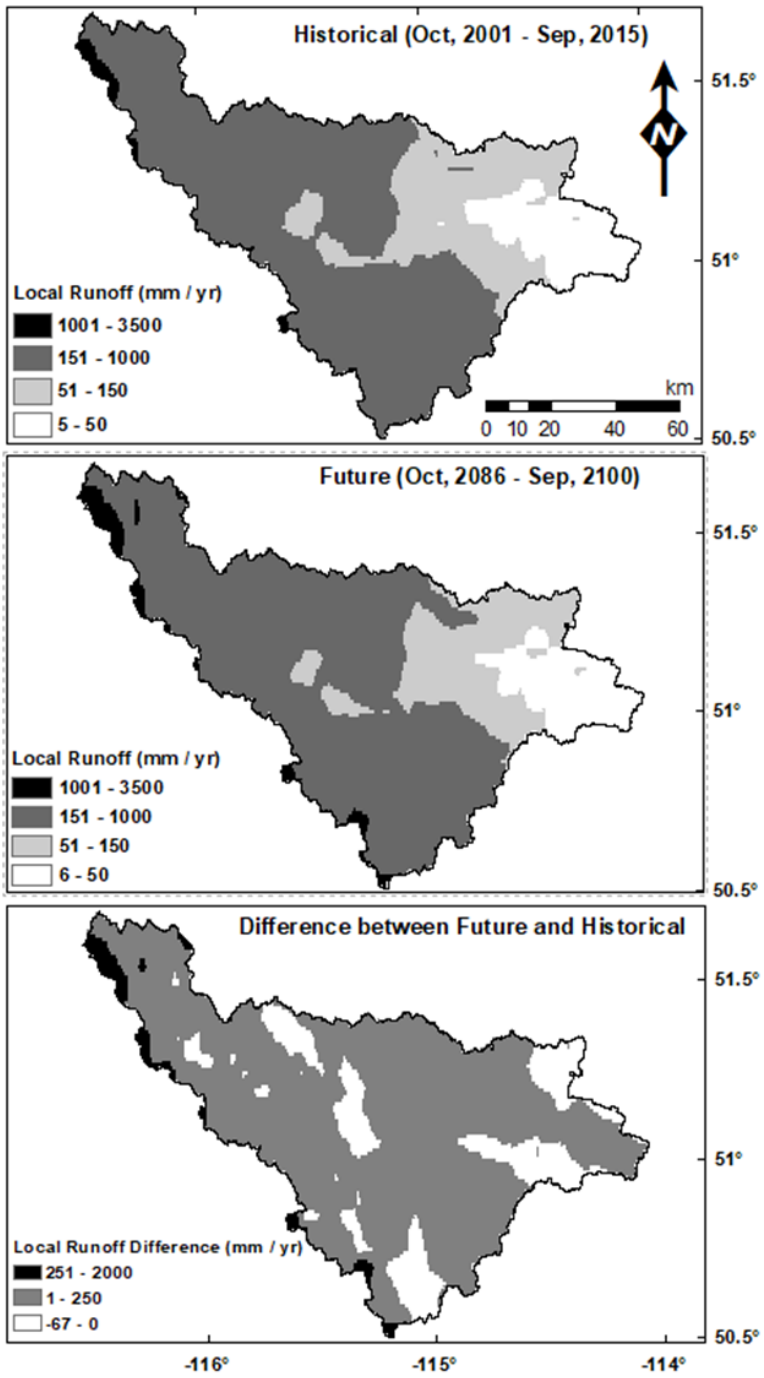

Figure 37. Change in mean annual local runoff under WRF future climate situation and historical glacier coverage.

4.4.2 Future Change in the River Regime and Centre of Streamflow Mass

Comparisons between the historical and future WRF-MESH and CanRCM4-MESH simulated mean daily streamflow and its range are shown in Figure 38, Figure 39, Figure 40 and Figure 42for the Bow River at Banff, Bow River at Calgary and Elbow River near Sarcee Bridge and Elbow River below Glenmore Reservoir respectively. Future climate warming is projected to accelerate the timing of snowmelt, leading to earlier spring freshets. Streamflow peaks will occur from a few days to a month earlier with greater changes predicted by the CanRCM4-driven models and for the Bow River at Banff.

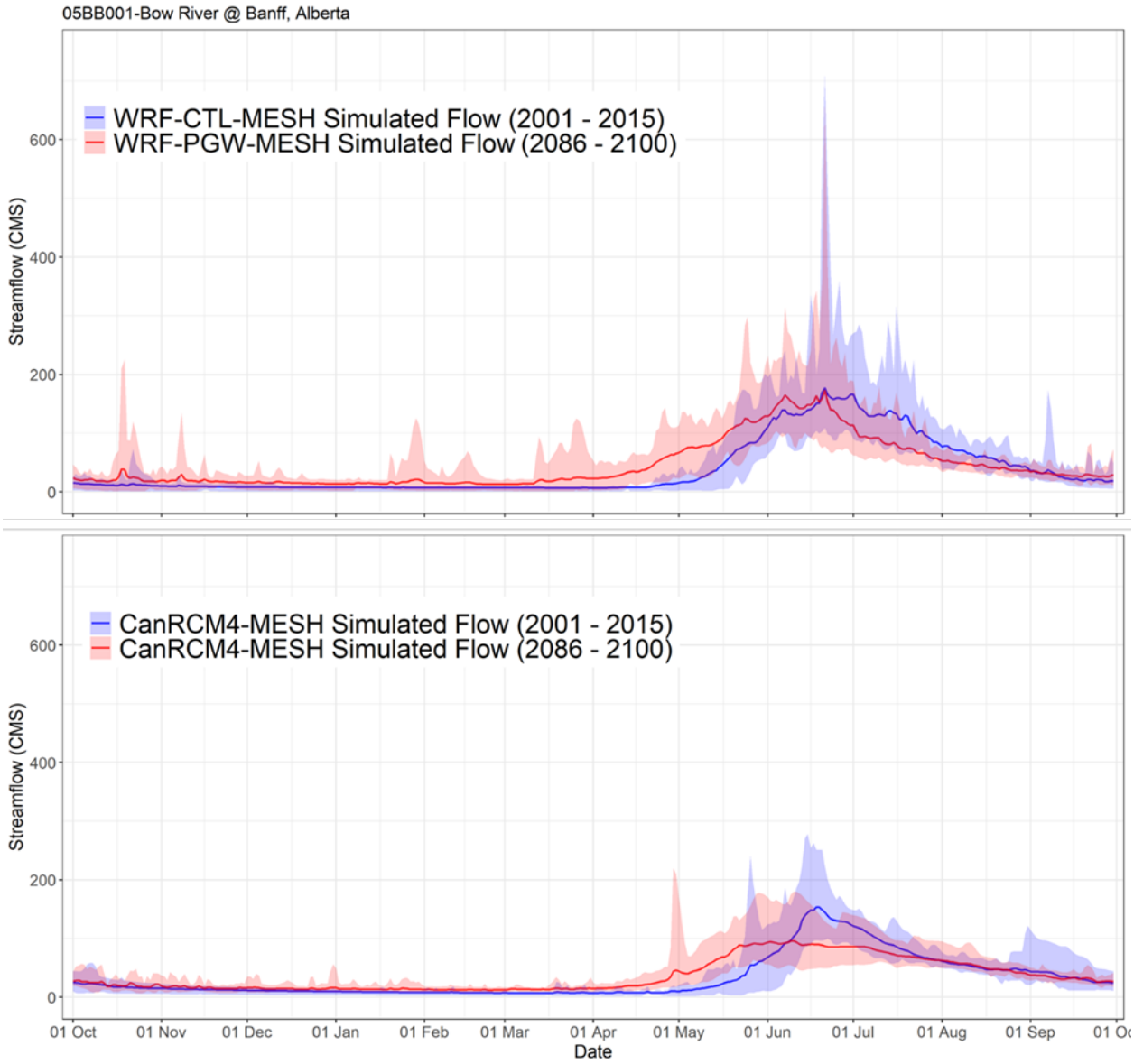

Figure 38. Minimum, mean and maximum daily streamflow of the Bow River at Banff for historical and future climates (top: WRF-MESH, bottom CanRCM4-MESH)

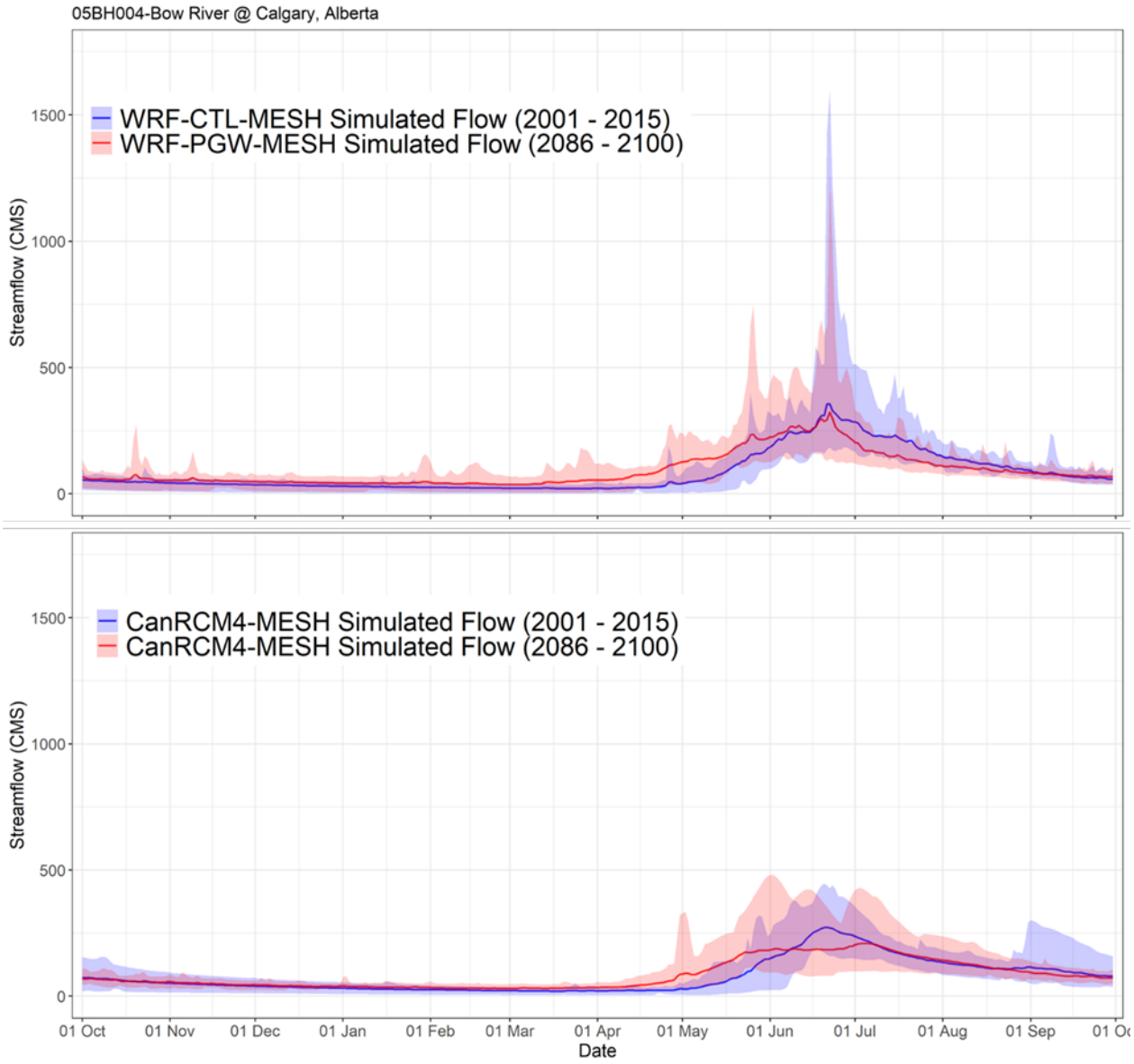

Figure 39. Minimum, mean and maximum daily streamflow of the Bow River at Calgary for historical and future climates (top: WRF-MESH, bottom CanRCM4-MESH)

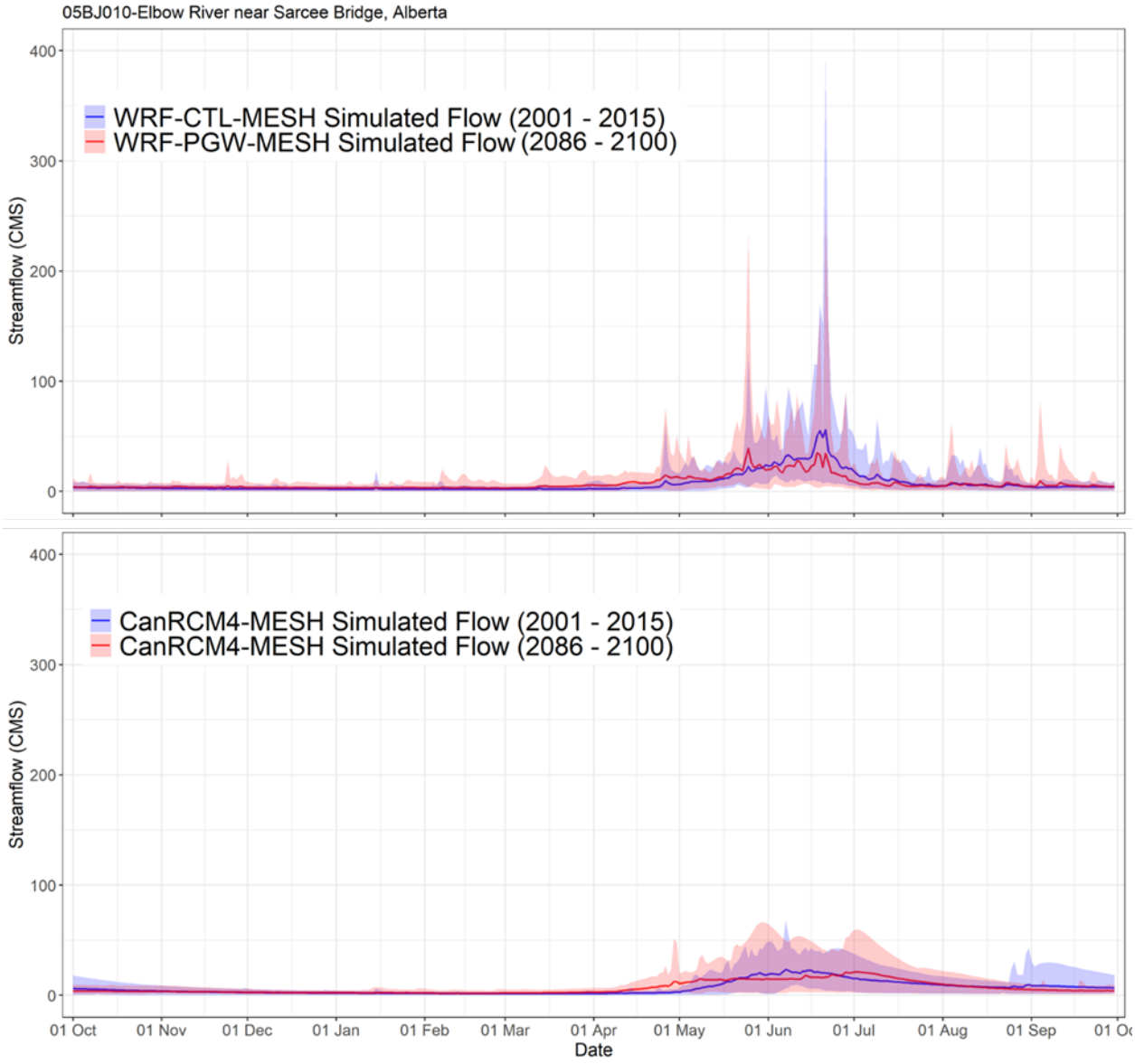

Figure 40. Minimum, mean and maximum daily streamflow of the Elbow River near Sarcee Bridge for historical and future climates (top: WRF-MESH, bottom CanRCM4-MESH)

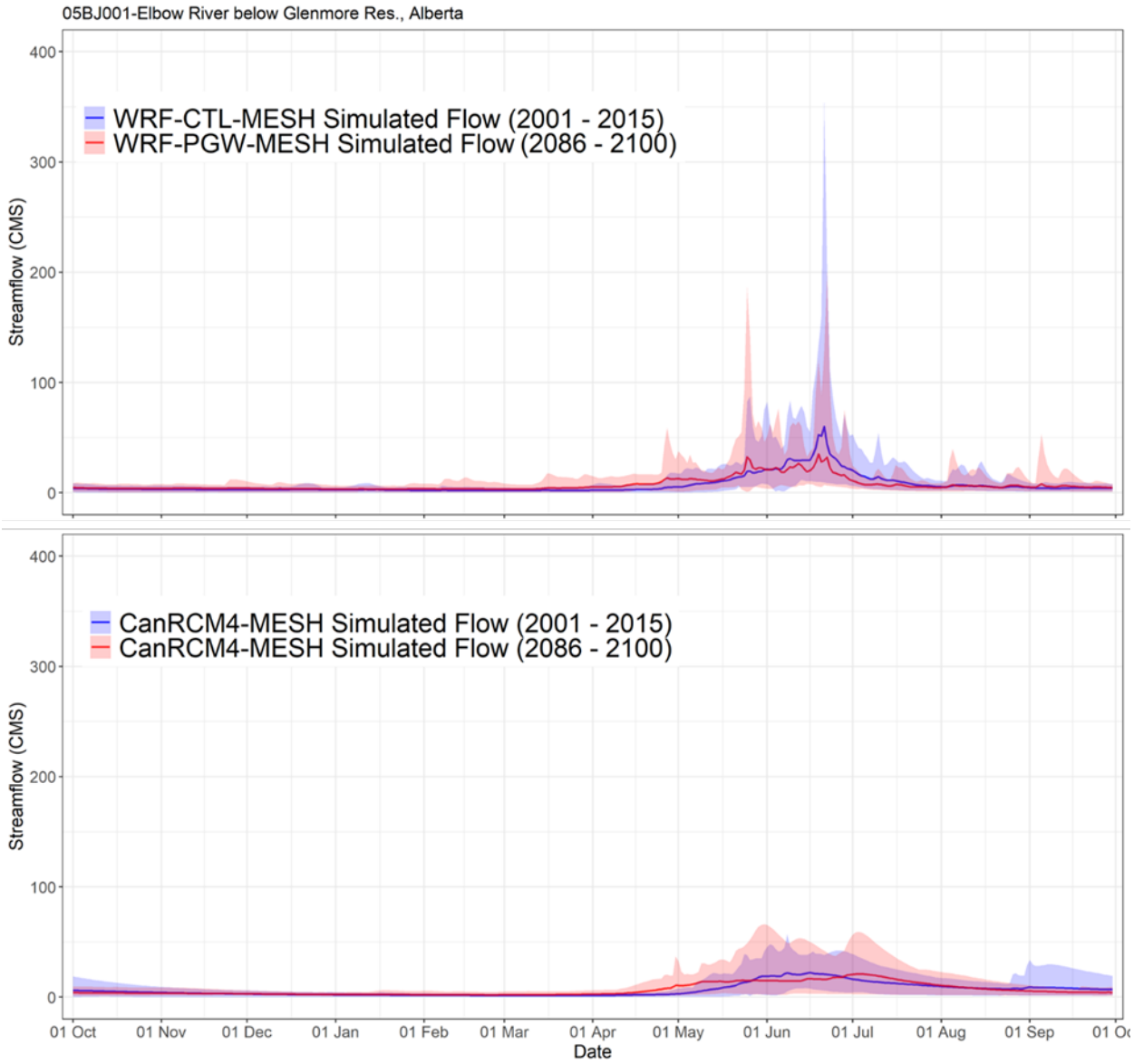

Figure 41. Minimum, mean and maximum daily streamflow of the Elbow River below Glenmore Reservoir for historical and future climates (top: WRF-MESH, bottom CanRCM4-MESH)

The spatial distribution of the centre of mass of local runoff over the whole Bow River Basin above Calgary under historical and future climates is shown in Figure 42. The effects of warmer temperatures and increases in precipitation in advancing the snow-free date by shortening the snow season are important to the hydrological processes that govern streamflow generation affecting the magnitudes and timing of the maximum snowpack and the centre of mass of runoff Relative to 2000 – 2015 conditions, at the end of the 21st century, the average centre of mass of flow (CT) is projected to be up to 45 days earlier for the partially glaciated high mountains, up to 30 days earlier in the foothills and up to 14 days later in the low elevation grassland and agricultural parts of the basin (Figure 42).

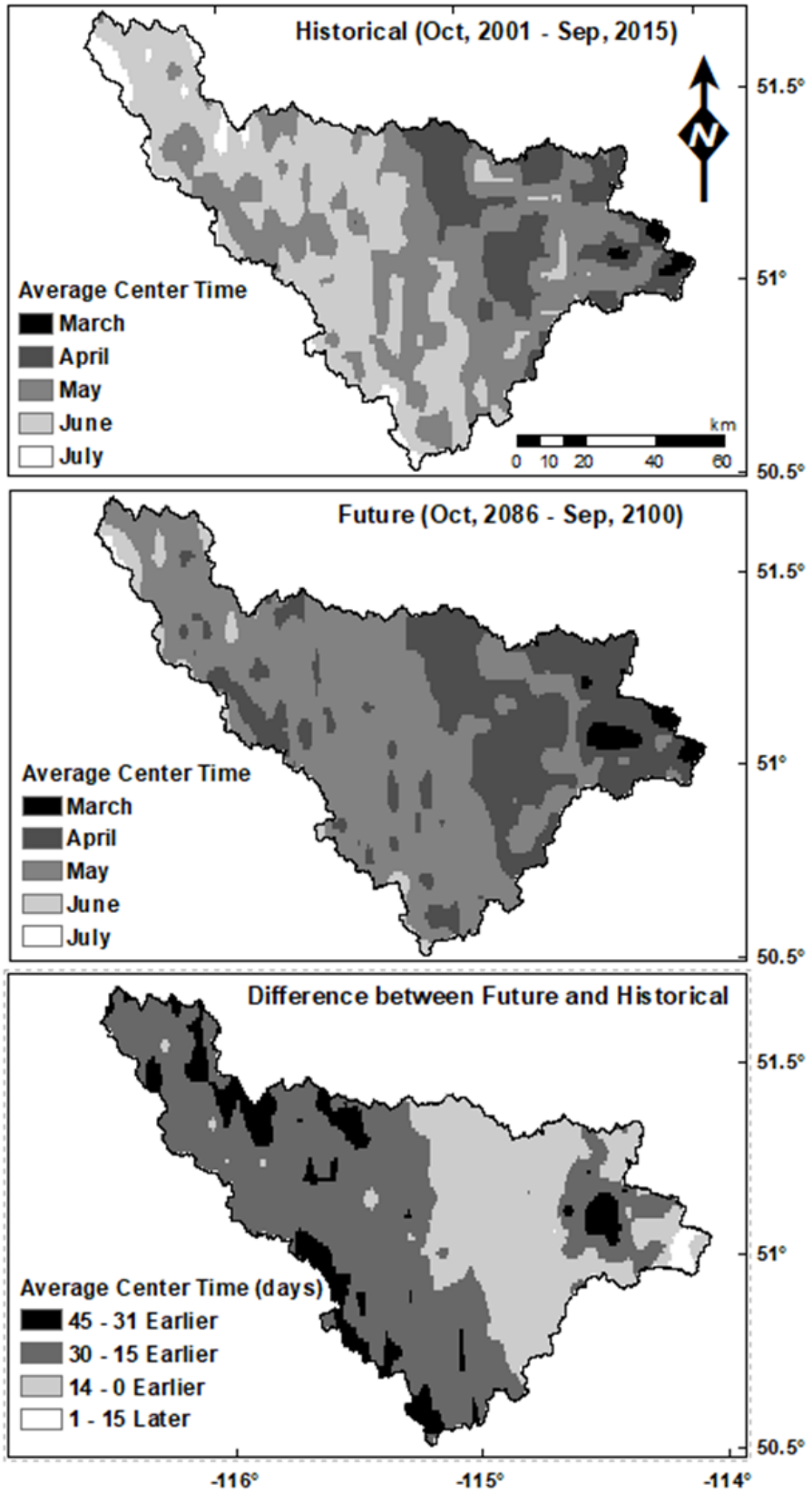

Figure 42. Timing of Centre of Mass of runoff and its change under WRF historical and future climate with fixed historical glacier coverage

4.4.3 **Future Change in Runoff Generation Mechanism**

There are currently far more SMR events in the high mountains than in the foothills and plains. In the future (2086 - 2100), the WRF-PGW-simulated climate is predicted to increase the frequency of SMR events at the highest elevations, where there is glacier coverage and to decrease the SMR frequency everywhere else. SMR events are projected to increase by up to six events per year in the high mountains and to decrease by up to fourteen events per year in the foothills as shown in (Figure 43).

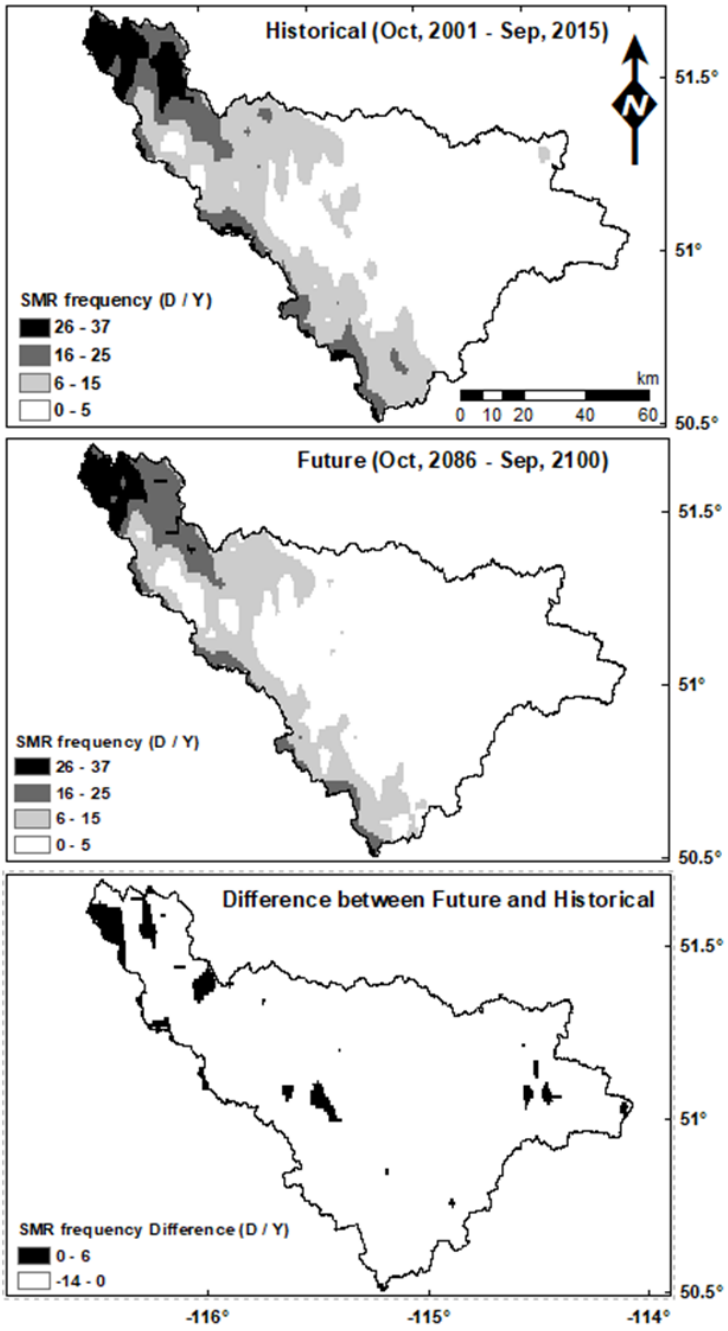

Figure 43. Change in snowmelt runoff (SMR) events under WRF historical and future climate and with fixed historical glacier coverage

Currently, ROS events are most frequent at the high mountain elevations. In the warmer, wetter future climate scenario, ROS events are predicted to be more frequent at higher elevations and in the foothills, particularly in the Bow River basin above Banff and the southwestern reaches of the basin (Figure 44) and less frequent at lower elevations in the plains region. This variation is due to the increase in rainfall being counterbalanced by the decreased snow-covered period with greater counterbalancing with the warmer initial climates found at lower elevations.

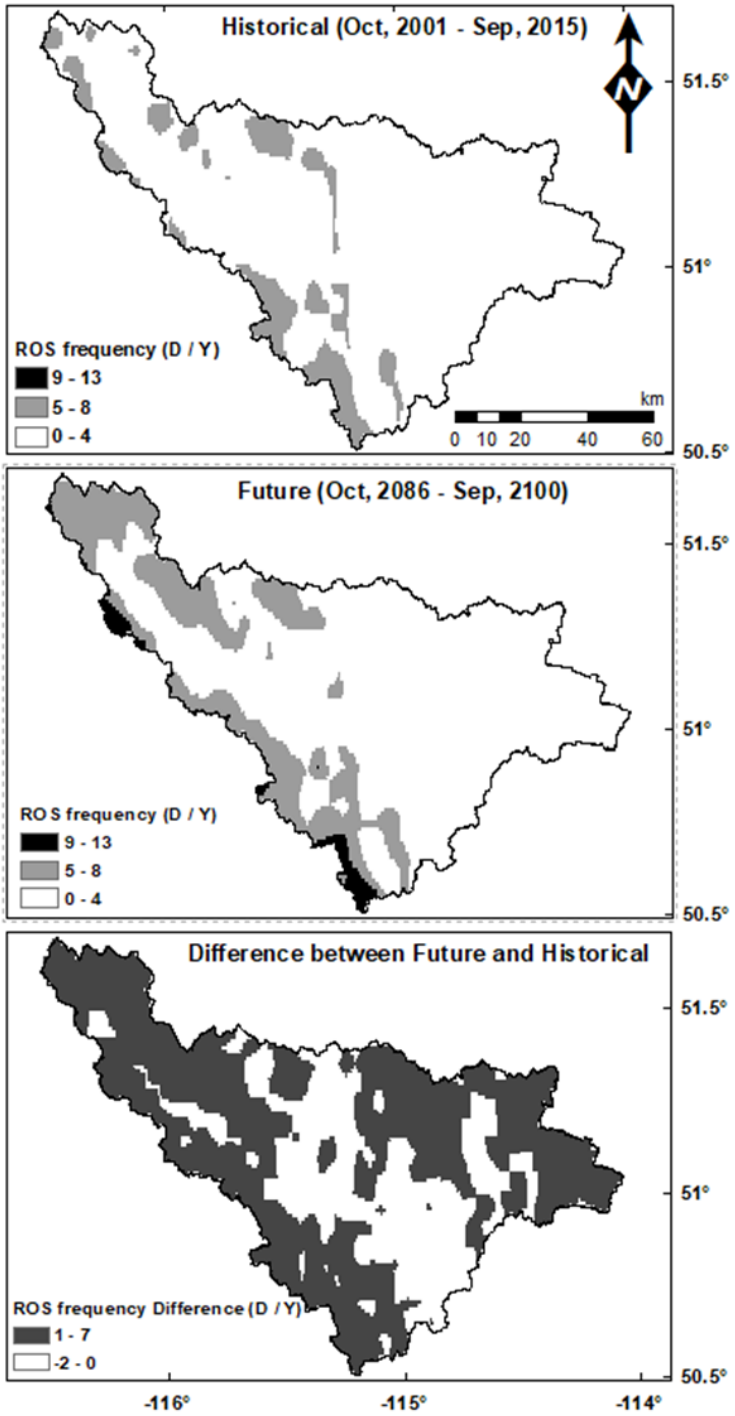

Figure 44. Change in Rain-On-Snow (ROS) events under WRF historical and future climate and with historical glacier coverage held constant.

Rainfall-runoff (RR) events are most frequent at lower elevations. Rainfall increases in the future are predicted to increase RR by up to six events per year over the mountains and foothills (Figure 45). Decreases of up to four events per year are projected for the plains due to higher temperatures and drier soil conditions that do not favour runoff generation. Increases in rainfall-runoff events of four events per year are projected for the whole Bow River Basin and five events per year for the Elbow River Basin.

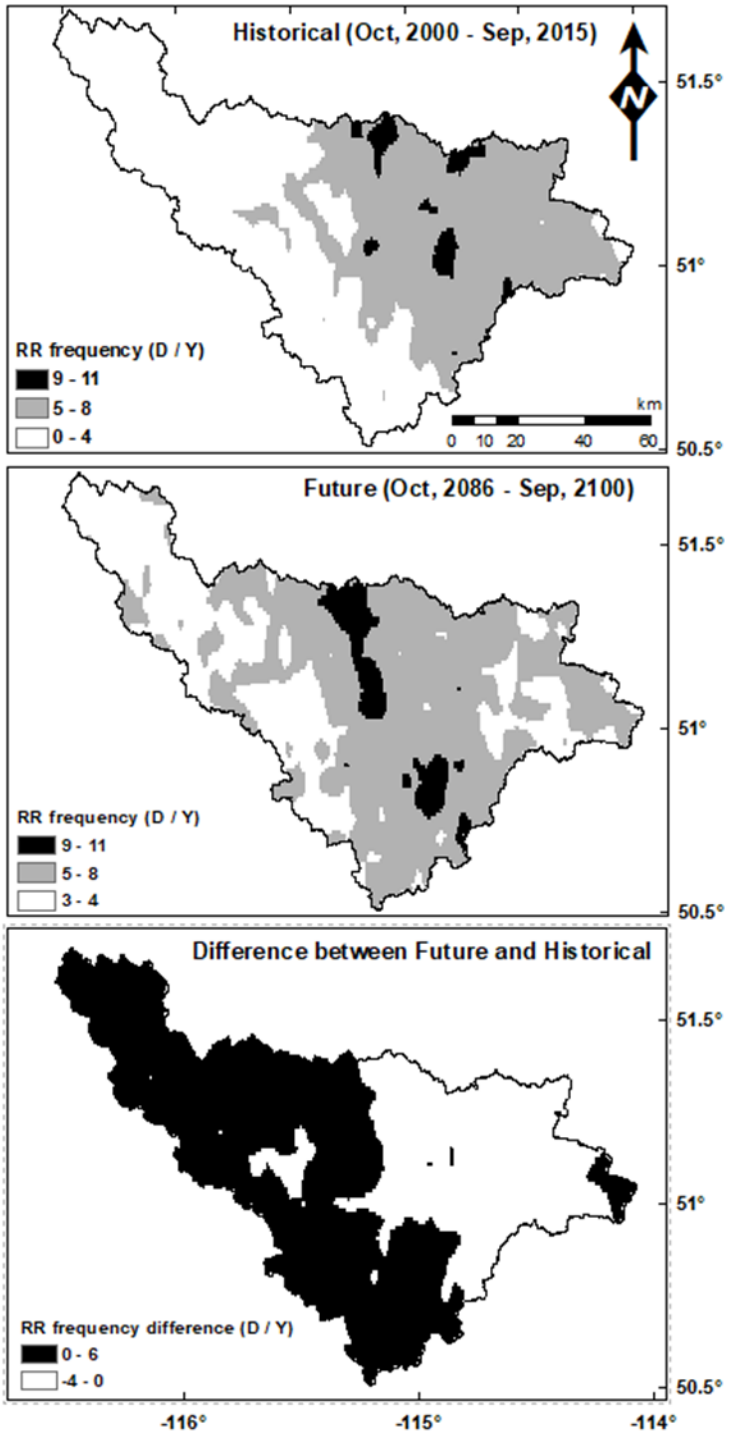

Figure 45. Change in Rain-Runoff (RR) events under WRF historical and future climates.

4.4.4 The 2005 and 2013 floods under a future climate

The 2005 Flood

Major floods in these basins are typically caused by heavy rain falling onto conditions of nearly-saturated soils, high water tables and remaining high elevation snowpacks in late spring when previous runoff has filled surface storage as was the case in 2005 (Shook, 2016). Figure 48 shows changes in rainfall and snowfall for a WRF PGW simulation of the 2005 flood event. In PGW the same weather is replayed but with a future atmosphere. The warmer future atmosphere can hold more water vapour and may have greater capacity to generate rainfall, but warmer winters and springs shorten the snowcovered season and reduce the seasonal snowpack. For the Bow River at Banff, with increased precipitation and warmer air temperatures in the future, compared to the historical 2005, the snowfall events become smaller as the precipitation phase changes from snowfall to rainfall. Under the PGW climate, precipitation over the two days (about 73 mm in June 17 & 18) is about 57 mm greater in the future than it was historically. For the Bow River at Calgary, snowfall decreases in the future compared with the historical period. Precipitation over the two days (June 17 & 18) is slightly greater and more spread out in the future than it was historically. For the Elbow River near Sarcee Bridge, both the precipitation and snowfall decrease for PGW compared with the historical period over the two days (June 17 & 18) and are more spread out in the future (Figure 48). It should be noted that modelled precipitation is unrealistically low for the flood event on the Elbow River and so these results should be interpreted with great care.

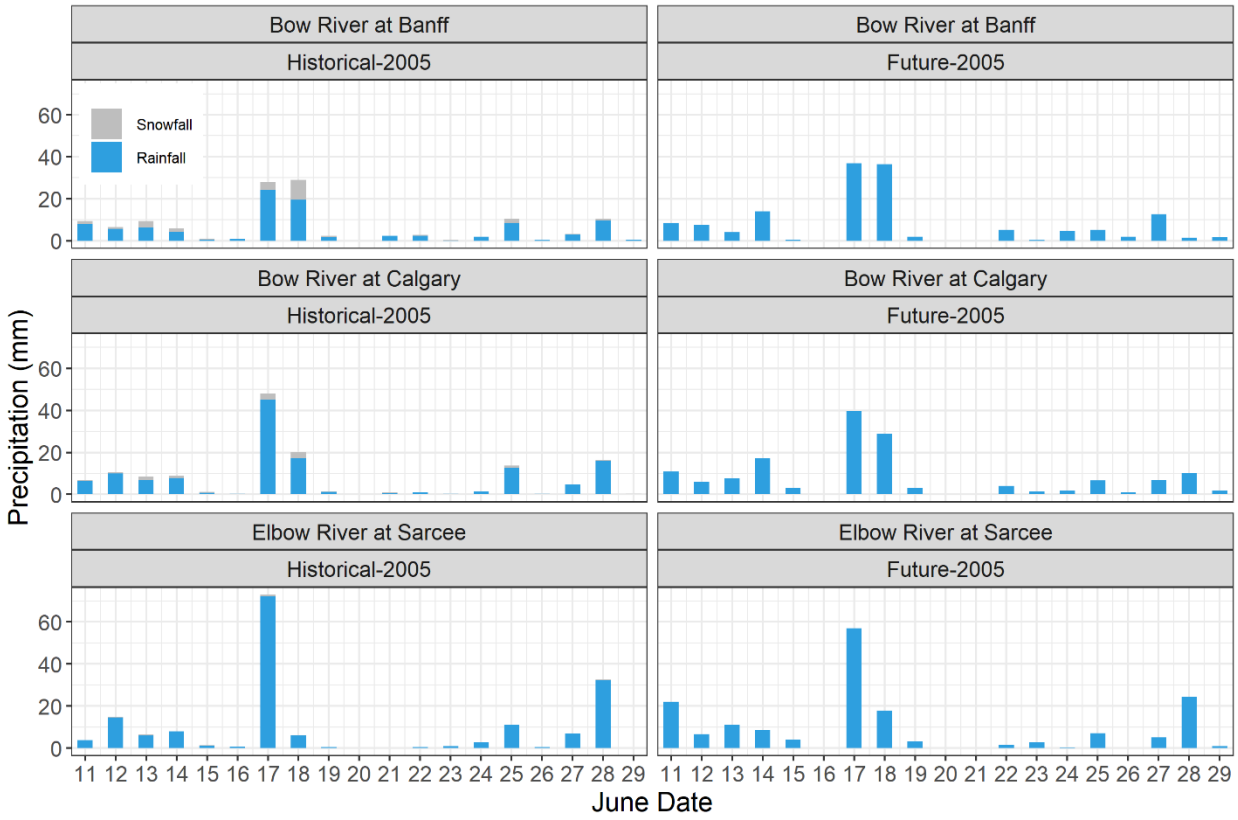

Figure 46. Rainfall and snowfall events around the 2005 flood for Bow River basin at Banff and Calgary, Elbow River basin near Sarcee Bridge calculated using WRF under the historical climate and pseudo global warming climate.

The 2005 event in the Bow River basin at Banff and Calgary (Figure 49) was predominantly due to ROS. Under the PGW future climate, the runoff increases due to an increase in precipitation, and the ROS and RR events are still the dominant mechanisms in Bow River at Banff and Calgary but with a greater contribution from mixed and RR events and a vastly reduced contribution from SMR before and after the event (Figure 49).

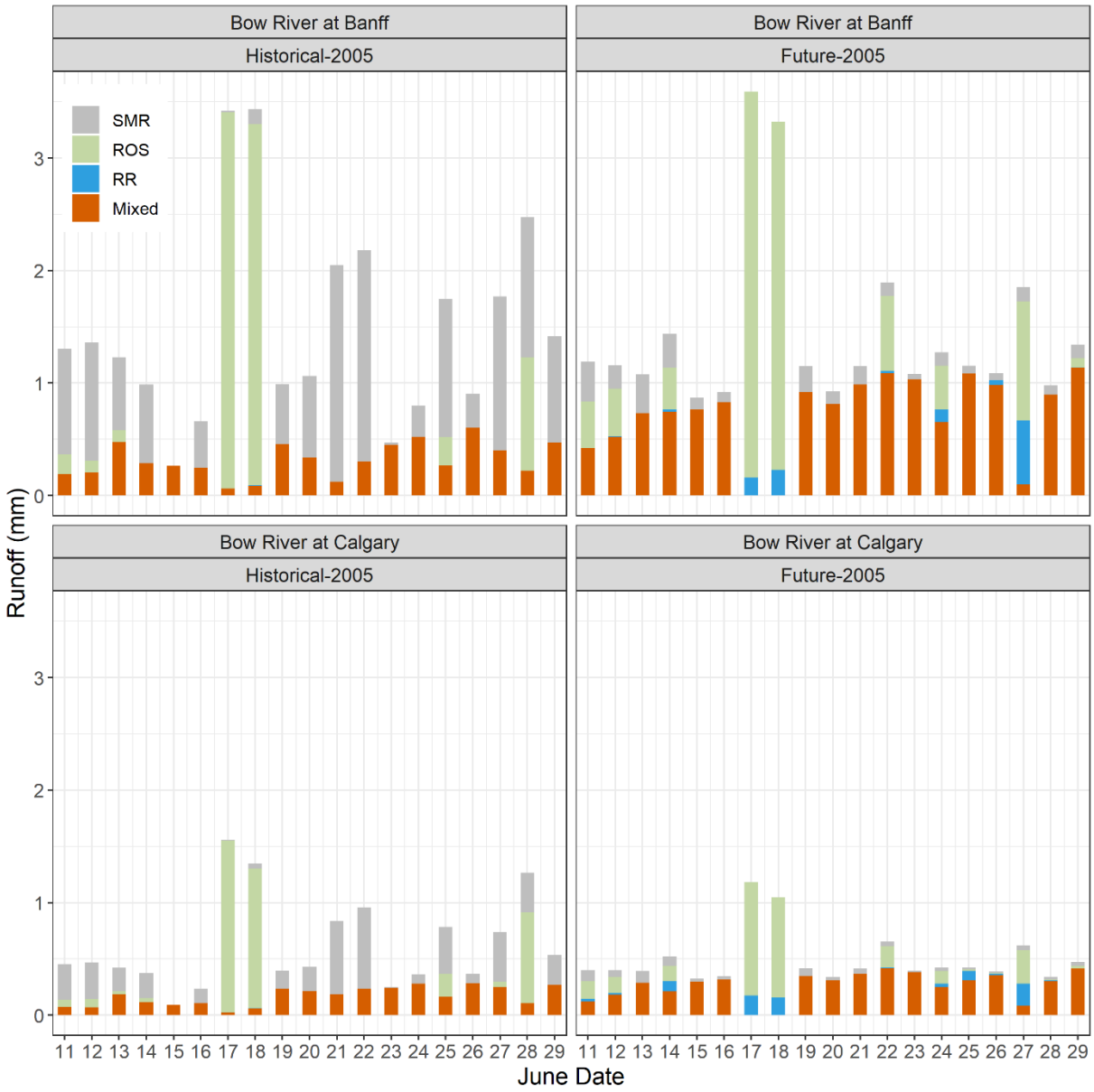

Figure 47. Snow melt runoff (SMR), rain-on-snow (ROS), rainfall-runoff (RR) and mixed runoff events for the Bow River basin at Banff and Calgary around the 2005 flood calculated using MESH with the WRF estimated actual weather and future weather calculated by WRF for the PGW climate (future atmosphere, same storm)

The 2005 flood in Elbow River basin near Sarcee Bridge was due to ROS and RR but modelled with very inaccurate precipitation (Figure 50). Under PGW conditions, the flood volume essentially disappears due to a decrease in precipitation, decrease in ROS, and reduced SMR before and

after the event (Figure 50). Lack of snowcover, drier soils and reduced storage almost certainly causes this flood event to cease under warmer PGW conditions despite similar precipitation amounts. Again, this result is highly uncertain due to unreliable precipitation estimates.

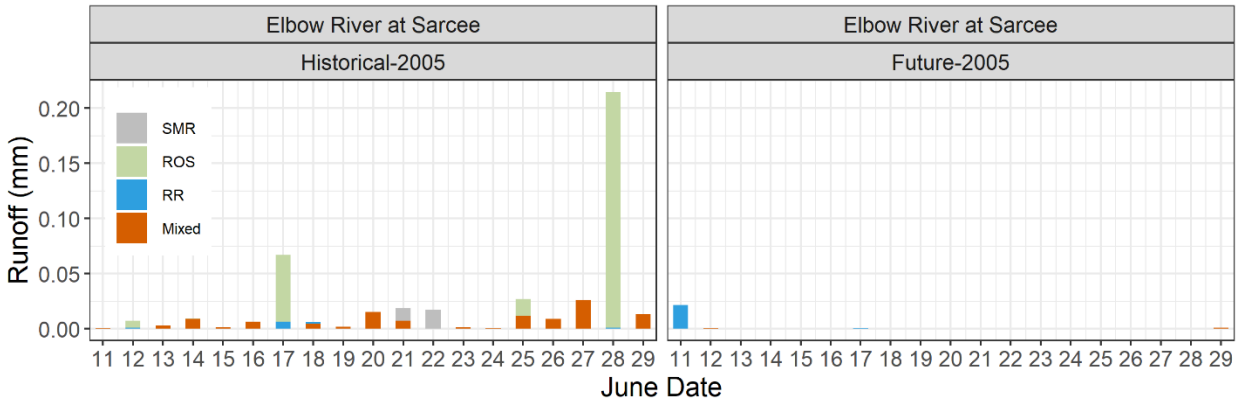

Figure 48. Snow melt runoff (SMR), rain-on-snow (ROS), rainfall-runoff (RR) and mixed runoff events for the Elbow River basin at Sarcee Bridge around the 2005 flood calculated using MESH with the WRF estimated actual weather and future weather calculated by WRF for the PGW climate (future atmosphere, same storm)

The 2013 Flood

The June 2013 flood produced the highest flows ever recorded in many regional streams including parts of the Bow River. Precipitation totals of up to 350 mm over the event were also record values for many gauges. Observations showed precipitation falling almost completely as rainfall except for snowfall at high elevations on the third day of heavy precipitation (Pomeroy et al., 2016). For WRF simulations of the Bow River basin above Banff, precipitation around the 2013 flood was mostly rainfall and was distributed over three days compared with the PGW future climate precipitation that concentrated precipitation over one day but with similar maximum rated (Figure 51). In the Bow River Basin above Calgary, the WRF historical precipitation (mostly rainfall) was distributed over the three days around the 2013 flood unlike the WRF PGW future climate where it was concentrated into one day with little snowfall and a much greater intensity (Figure 51). Like the Bow River at Calgary, PGW future precipitation over the Elbow River at Sarcee Bridge tended to be concentrated over a single, more intense day compared with the historical WRF-generated climate (Figure 51).

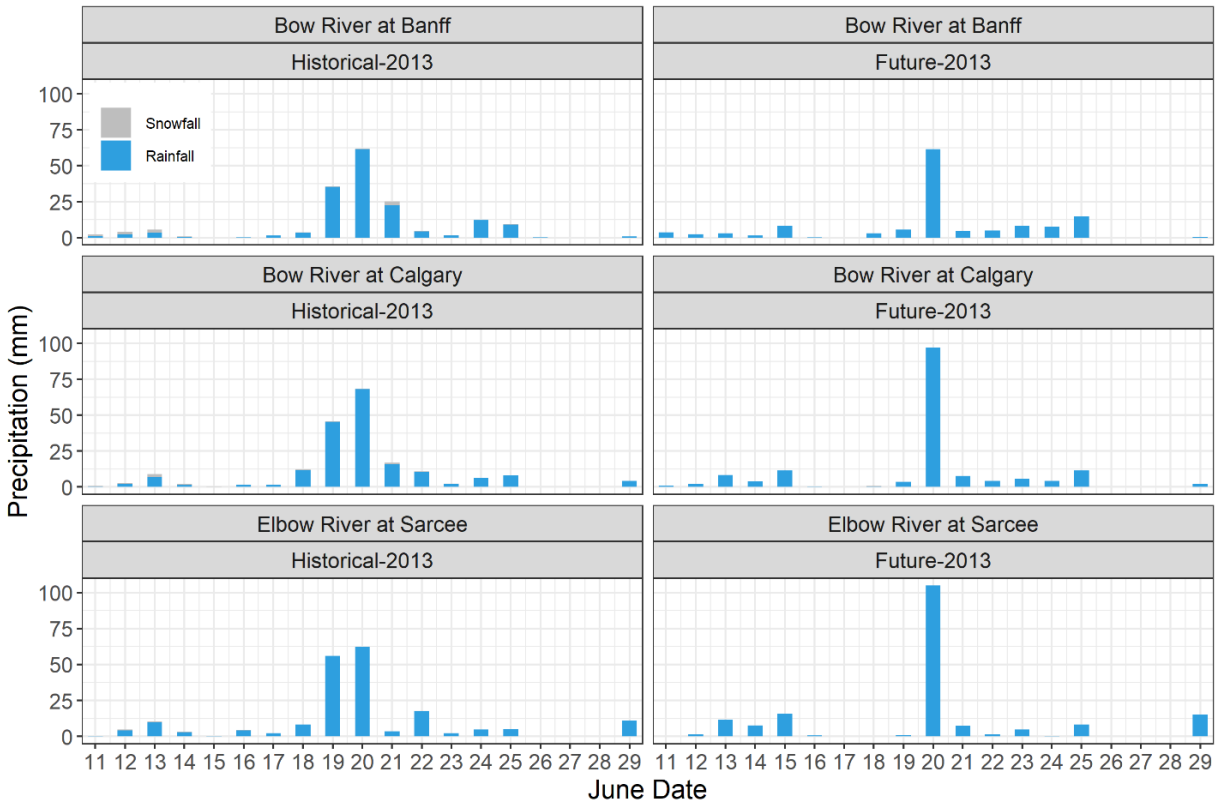

Figure 49. Rainfall and snowfall events around the 2013 flood of Bow River basin at Banff and Calgary, and Elbow River Basin near Sarcee Bridge calculated using WRF under the historical climate and pseudo global warming climate.

The historical WRF-MESH simulations of the 2013 flood at Banff show it was from a ROS event preceded and followed by SMR. WRF-MESH under PGW projects the event under a future atmosphere would be a larger ROS with more SMR beforehand and some contribution from RR. The historical WRF-MESH simulations of the 2013 flood of the Bow River at Calgary indicate it was from a ROS event with some contribution from rainfall-runoff. Simulations under a future climate with PGW show that ROS will still dominate but with a higher RR event contribution and much lower cumulative streamflow for the event which would cease to be considered a major flood (Figure 50).

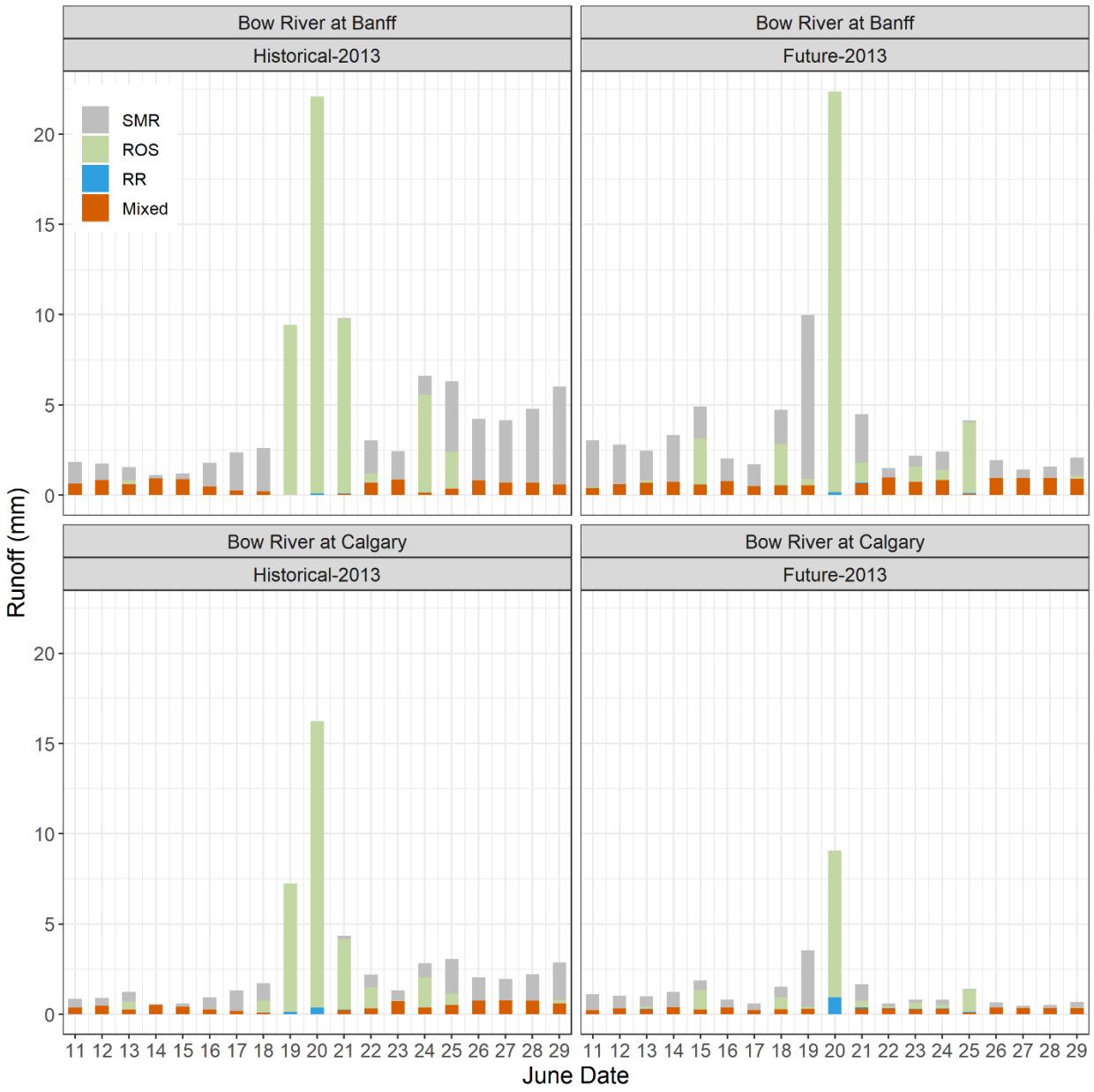

Figure 50. Snow melt runoff, rain-on-snow, rainfall-runoff and mixed events of runoff component of the Bow River basin at Banff and Calgary around 2013 flood calculated using MESH with the WRF estimated actual weather and future weather calculated by WRF for the PGW climate (future atmosphere, same storm).

The historical WRF-MESH simulations of the 2013 flood of the Elbow River at Sarcee show the historical event was a result of both ROS with a small RR contribution that was preceded by SMR. Unlike the historical 2013 flood on the Elbow, the PGW future climate produces vastly lower runoff volumes and only a small RR event (Figure 51).

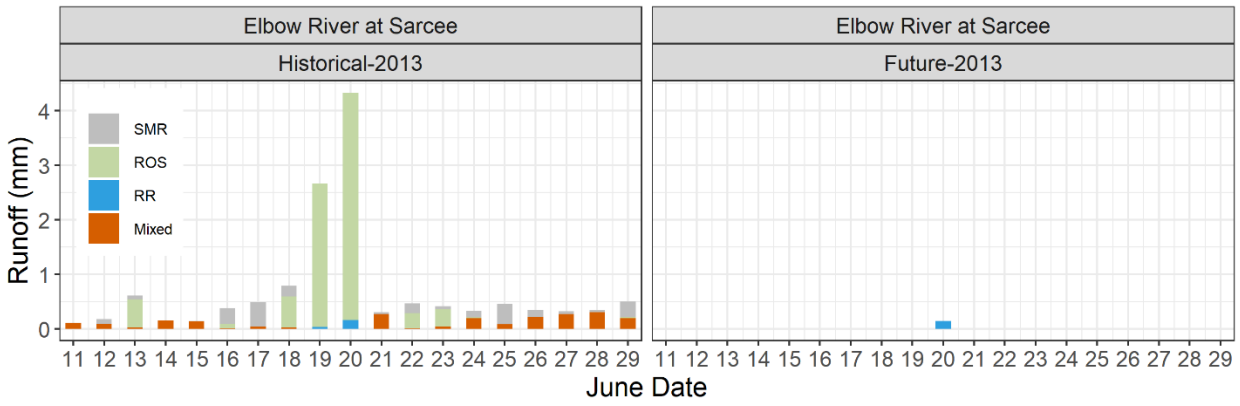

Figure 51. Snow melt runoff, rain-on-snow, rainfall-runoff and mixed events of runoff component of the Elbow River basin at Sarcee Bridge around the 2013 flood calculated using MESH with the WRF estimated actual weather and future weather calculated by WRF for the PGW climate (future atmosphere, same storm).

4.5 Combined Impact of Climate Change and Deglaciation on Future Streamflow Regimes

4.5.1 Impact of Deglaciation and Climate Change on Streamflow

Glacier mass balance projections for the RCP8.5 scenario in the upper Bow River Basin indicate accelerated mass loss throughout the 21st century, such that the glaciers will have vanished by the end of the century (Clarke et al., 2015). This study therefore simulated streamflow for future climates with the former glaciated area converted into barren land. For comparison to this highly likely scenario, a scenario with existing glacier coverage held fixed was also run – if such glacier coverage could exist in a warmer future climate there would be exceptionally high icemelt volumes. The results of the modelling experiment are summarized in Figure 52 and Figure 53 for Bow River at Banff and Calgary respectively. In general, a decrease in streamflow due to deglaciation for summer and fall months (June to August) can be observed consistently under both WRF-PGW and CanRCM4 future climates. The impact of deglaciation is greater in simulations driven by the CanRCM4 due to the MESH-CanRCM4's greater estimation of glacial ice wastage contribution to streamflow. The smaller glacier wastage contributions simulated by MESH with WRF driving meteorology are more consistent with estimates of previous glaciological and hydrological studies and also produce the most reliable mass balance estimates when compared to Peyto Glacier.

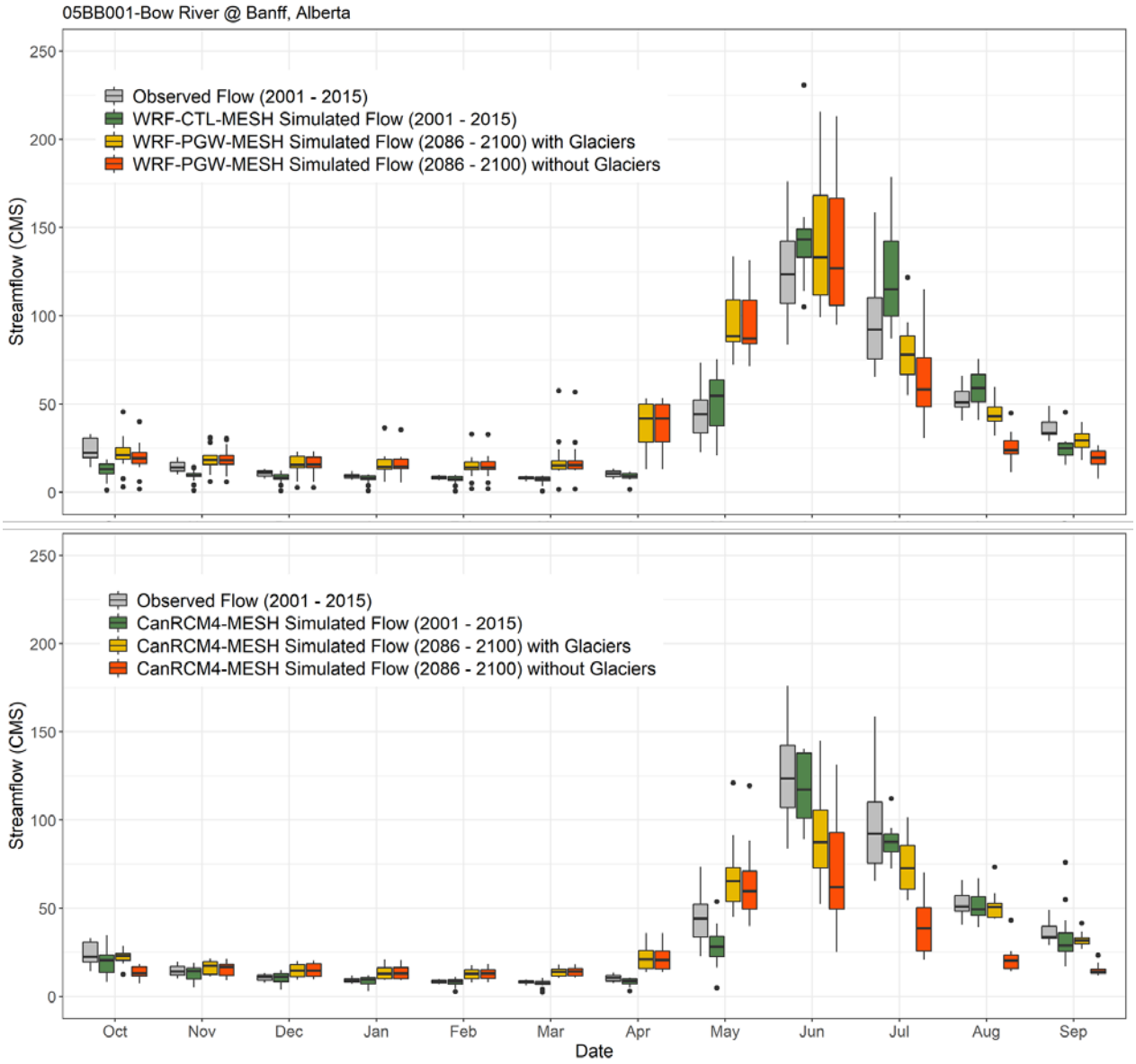

Figure 52. Box plots showing the seasonality of streamflow for Bow River at Banff by grouping monthly streamflow over 15 years into monthly bins. The band near the middle of the colored box shows the median and the bottom and top of the central rectangle spans the lower quartile to the upper quartile. Whiskers above and below the box show the location of the maximum and minimum simulations based on MESH driven by WRF current and PGW and CanRCM4 climate.

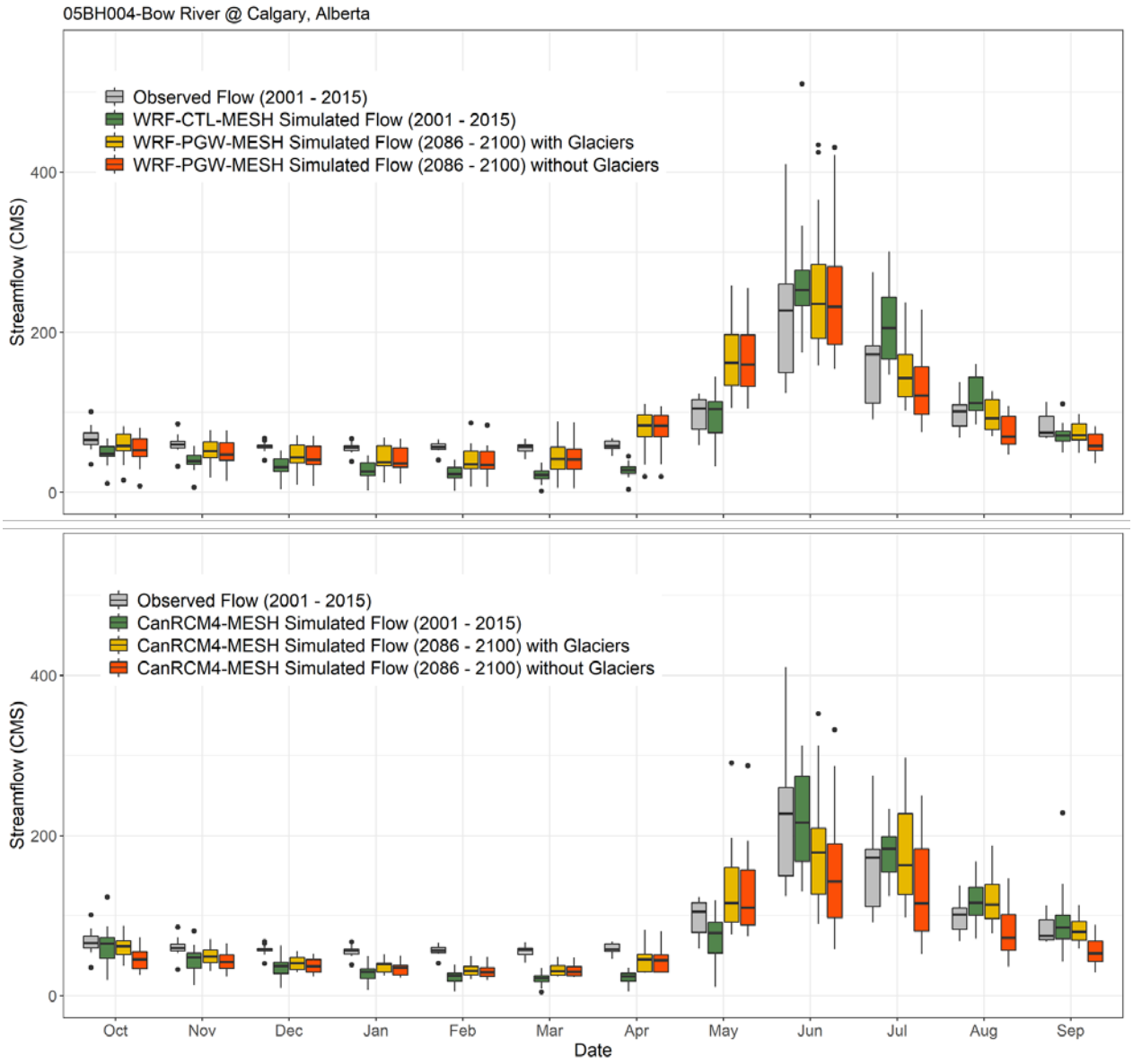

Figure 53. Box plots showing the seasonality of streamflow for Bow River at Calgary by grouping monthly streamflow over 15 years into monthly bins. The band near the middle of the colored box shows the median and the bottom and top of the central rectangle spans the lower quartile to the upper quartile. Whiskers above and below the box show the location of the maximum and minimum simulations based on MESH driven by WRF current and PGW and CanRCM4 climate.

The contributions of glacier wastage to annual streamflow volumes were assessed for both historical and future climates, assuming fixed glacier coverage, to assess the need to incorporate glacier change in future hydrological models of these basins. Under both future climate simulations (RCM and PGW), glacier ice wastage contributions increase from historical values due to increased temperatures and reduced snowcovers. The WRF simulated PGW climate driving MESH increased the glacier ice wastage contribution to 9.3% from the historical 2.5% for Bow River at Banff. Similarly, it increased the glacier ice wastage contribution of the Bow River at Calgary to 6.2% from its historical 1.8%. Based on CanRCM4 simulated climate driving MESH, the annual glacier contribution to the annual basin runoff increased to 25% and 16.5% from their

historical 13.2% and 9.2% for Bow River at Banff and Calgary, respectively. Of course, if glaciers are allowed to decrease to a negligible coverage which is anticipated from glacier models then the glacier ice wastage contribution drops to 0% (Table 8).

Table 8. Percentage of glacier ice wastage contribution to the annual streamflow volume at the outlet of the basin

Basins	Simulation Runs	Glaciers Contribution (%)		
		Historical Period (2001 - 2015) With Glacier	Future Period (2086 - 2100) With Glacier	Future Period (2086 - 2100) Without Glacier
Bow River at Banff	WRF - Mountain MESH	2.4	9.3	0
	CanRCM4 - Mountain MESH	13.5	25	0
Bow River at Calgary	WRF - Mountain MESH	1.8	6.3	0
	CanRCM4 - Mountain MESH	9.5	16.7	0

Figure 54 shows the spatial distribution of the impact of deglaciation on the local runoff generation by the end of the century. The mean annual runoff reduction varies from 232 to 825 mm/yr in glaciated grid cells.

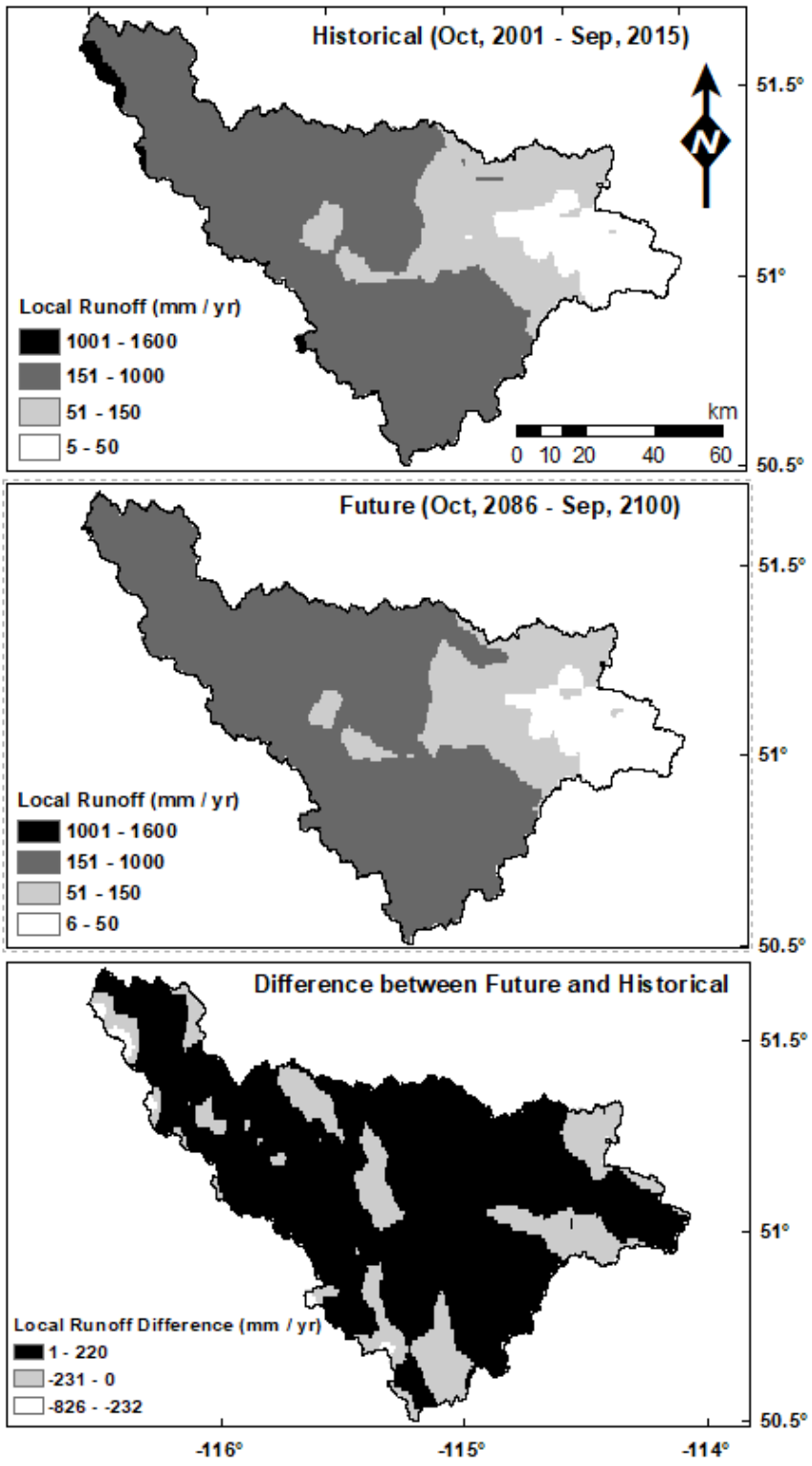

Figure 54. Local runoff simulated by MESH and change under WRF PGW with deglaciation

4.5.2 Bias Corrected Future WRF-PGW-MESH Simulated Streamflow

Bias corrections to future streamflow estimates are needed to produce reliable flood estimations for design and public safety purposes. Quantile-quantile mapping bias corrections in the Bow River Basin use over a century of Water Survey of Canada observations and advanced hydrological modelling driven by high resolution atmospheric models. Figure 55 shows the observed flow exceedance curve and the bias-corrected WRF-driven, MESH-estimated historical and future modeled flow duration curves with and without future glaciers. The bias-corrected historical simulations by WRF-MESH generally matched very well to the observed flow duration curves while the extreme values of the bias-corrected CanRCM4-MESH simulated flow duration curves for the historical climate showed only small deviations from the observed values (Figure 56). Based on the corrected flow duration curves, median and lower streamflow discharges will likely increase under future climate change at all gauging stations and both climate forcing datasets. High flows (i.e. exceeded less than 10% of the time) are projected to decline substantially, by up to 15% under WRF PGW-driven simulations and by up to 36% under CanRCM4-driven future climates. The changes are greatest for the Bow River at Banff and smallest for the Elbow River below Glenmore Reservoir. The effects of deglaciation on flow duration curves is to reduce streamflows, particularly medium to high flows, in future climates. As the flows of the Bow River at Calgary are strongly affected by upstream reservoirs any future streamflows will also be affected by changes in the future reservoir operation rules (after 2012) that are not considered here.

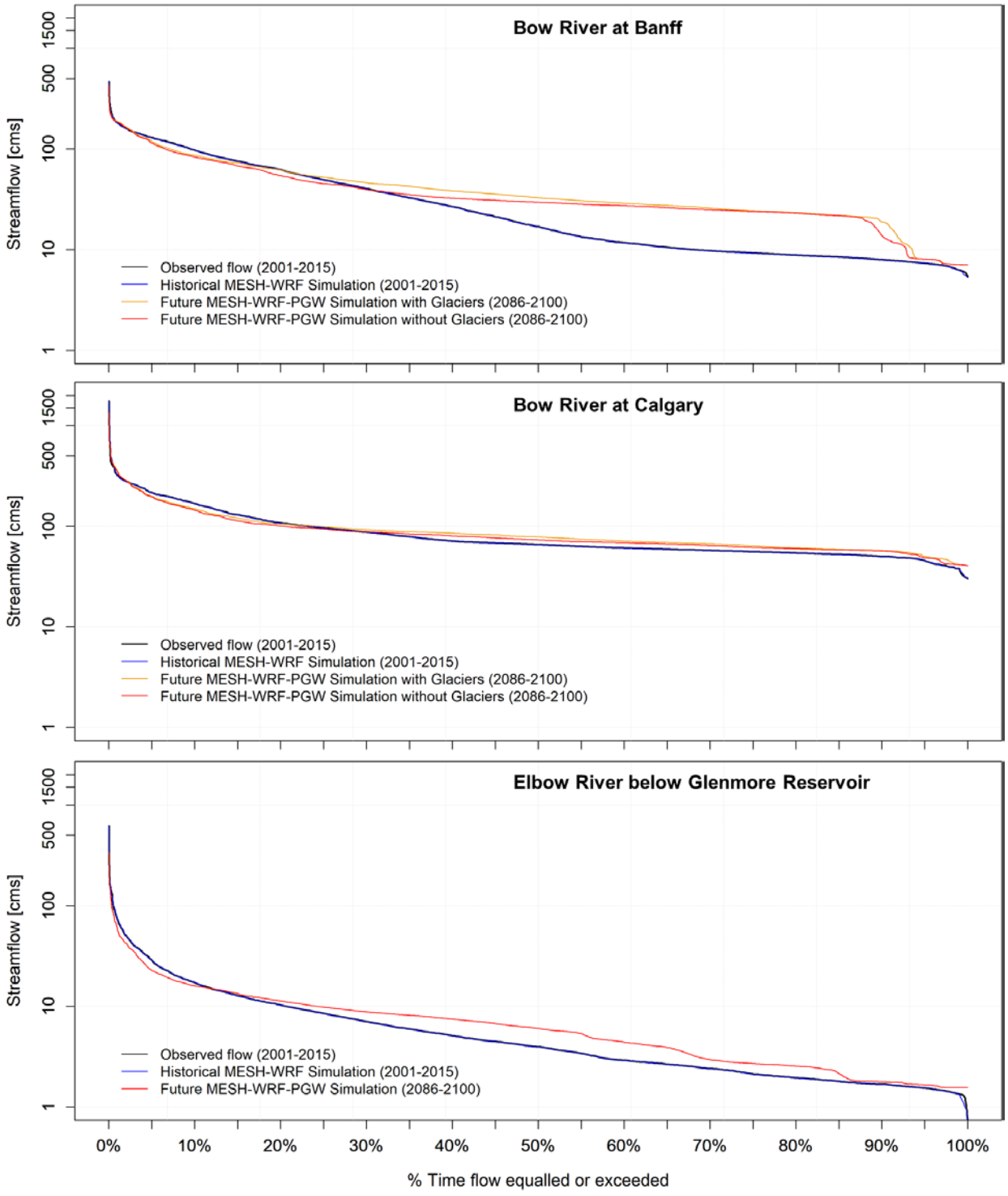

Figure 55. MESH-modelled flow duration curves for current WRF and future PGW WRF climate after streamflow bias correction for Bow River at Banff (top), Bow River at Calgary (middle) and Elbow River below Glenmore Reservoir (bottom). Simulation are with and without glaciers for the Bow River.

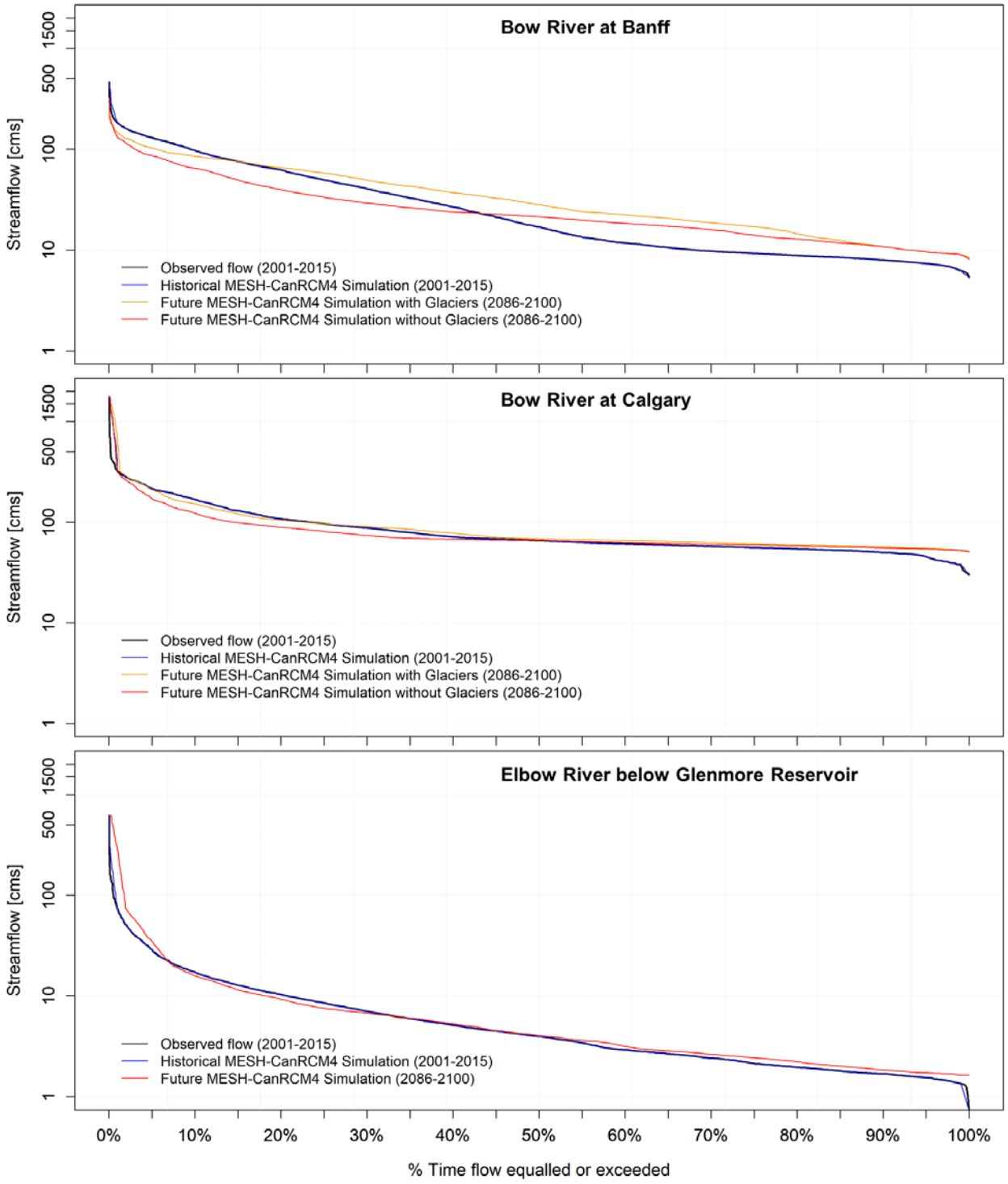

Figure 56. MESH-modelled flow duration curves for current and future CanRCM4 climate after streamflow bias correction for Bow River at Banff (top), Bow River at Calgary (middle) and Elbow River below Glenmore Reservoir (bottom). Simulation of the future Bow River flows include deglaciation and glaciated areas held constant.

Using the bias-corrected historical and future climate modelled flow duration curves, streamflows that were exceeded between 10 and 90% of the time were extracted, and the percent changes in

the streamflow quantiles between the current and future climates for both WRF and CanRCM4 driven MESH runs are given in Table 10. Selected quantiles of observed and bias-corrected simulated historical and future streamflow by MESH, driven by WRF and CanRCM4 climate, assuming deglaciation for all future streamflow simulations. Negative changes are shown in bold. All the results shown in the table include the simple reservoir model developed for this project and the historical reservoir discharge curves were kept constant for future climate simulations. The simulations also use the result of (Clarke et al., 2015) to remove all glaciers from the modelled results for late 21st C. The results show a decline in large flows, especially for the highest flows and those driven by CanRCM4 simulations and especially for the Bow at Banff, and an increase in medium to low flows especially for the WRF driven simulations and especially for the Bow at Banff. Decreases in the top 10% of flows ranged from 15% at Banff, 13% at Calgary and 7% for the Elbow for MESH-WRF and ranged from 33% at Banff to 26% at Calgary and 8% for the Elbow for MESH-CanRCM4.

Table 9. Selected quantiles of observed and bias-corrected simulated historical and future streamflow by MESH, driven by WRF and CanRCM4 climate, assuming deglaciation for all future streamflow simulations. Negative changes are shown in bold.

% Time Flow Equalled / Exceeded	QObs	WRF-MESH QS_{Hist}	WRF-MESH QS_{Futu}	% Change	CanRCM4-MESH QS_{Hist}	CanRCM4-MESH QS_{Futu}	% Change
Bow River at Banff							
10	97.6	97.6	83.3	**-14.7**	97.7	65.0	**-33.4**
20	62.5	62.5	54.5	**-12.9**	62.5	39.9	**-36.2**
30	40.3	40.4	39.6	**-2.0**	40.5	29.3	**-27.6**
40	26.7	26.7	32.5	21.7	26.7	24.0	**-10.3**
50	17.0	16.9	29.6	74.9	16.9	21.4	26.8
60	11.8	11.7	27.4	134.0	11.7	18.5	57.7
70	9.8	9.8	24.9	155.7	9.8	15.9	63.2
80	8.8	8.8	23.1	161.7	8.8	12.9	45.8
90	7.9	7.9	13.9	74.5	7.9	10.8	35.9
Bow River above Calgary							
10	167.9	167.1	145.1	**-13.2**	167.0	123.1	**-26.3**
20	107.6	107.0	100.9	**-5.7**	107.0	88.8	**-17.0**
30	87.6	87.5	88.1	0.6	87.5	73.9	**-15.6**
40	71.2	71.2	80.2	12.7	71.2	67.8	**-4.7**
50	65.8	65.7	73.2	11.5	65.7	65.8	0.2
60	61.0	60.9	68.7	12.9	60.9	62.9	3.2
70	57.6	57.5	64.4	12.0	57.5	60.4	5.1
80	54.2	54.2	60.0	10.6	54.2	58.3	7.5
90	50.0	49.9	56.9	14.0	49.9	55.6	11.4
Elbow River below Glenmore Reservoir							
10	17.3	17.3	16.0	**-7.3**	17.2	15.9	**-7.9**
20	10.3	10.3	11.3	10.1	10.3	9.3	**-10.0**
30	7.1	7.1	8.8	25.0	7.1	6.8	**-4.0**
40	5.1	5.1	7.5	46.1	5.1	5.3	3.7
50	4.0	4.0	6.0	52.7	4.0	4.0	1.9
60	2.9	2.9	4.4	51.6	2.9	3.2	8.8
70	2.4	2.4	3.0	22.9	2.4	2.6	9.7
80	2.0	2.0	2.6	31.0	2.0	2.2	13.9
90	1.7	1.7	1.8	6.0	1.7	1.8	9.2

5. Conclusions

Realistic simulations of future streamflows from mountain headwater basins are crucial for mitigation of flood damages and for improved management of water resources for ecosystems, communities and agriculture under a changing climate. Simulating the hydrological cycle in high relief cold regions is challenging for most models but is critical for predicting climate change impacts in these UNESCO World Heritage Site ecosystems. High resolution, coupled, physically based and Earth system models that include cold regions atmospheric, glaciological and hydrological processes are essential tools for such applications.

In this study, a coupled high resolution atmospheric model (WRF) and a physically based hydrological land surface scheme model (MESH) that was specially adapted for mountain terrain and topography, run at 4 km resolution, provided the most reliable estimates of streamflow for the Bow River Basin above Calgary, including the Elbow River. The coupled Mountain MESH-WRF model was able to estimate streamflow quite well with minimal calibration of parameters in a basin that include high mountain glaciated and snow-dominated headwaters, dense forests, grasslands, cultivated lands and urban areas and is partially regulated. Much of the basin has exceedingly sharp and complex topography. The improved Mountain MESH model included calculations of the effects of topography, slope and aspect on meteorological forcing fields and was set up, parameterised and run for the Bow River Basin using several meteorological datasets at varying spatial resolutions. The model setup incorporated simple empirical reservoir operation rules that were developed based on the relationship between the quantiles of historical storage and dam releases. The model calibration was based on a limited selection of soil, transpiration and routing parameters from the two dominant GRUs, out of the total of 11; the remaining GRUs used default parameters from literature or from previous studies. Observed streamflows for the Bow River at Banff and Elbow the River near Sarcee Bridge were used to calibrate and validate the model. The model performance in estimating glacier mass balance was also evaluated and it was found that by changing glacier coverage to barren land coverage the effects of deglaciation could be estimated. The performance of WRF-MESH was found to be suitable for exploration of future hydrological regimes and extreme events for various stations in the Bow River Basin above Calgary.

The WRF and CanRCM4 models project that the mean annual temperature of the Bow River Basin will increase by 4 - 5 °C from early 21st C values in the RCP 8.5 scenario by the end of the century. The mean monthly temperature of the Bow River basin at Banff is projected to increase by 4.2 °C in January and 5.3 °C in June by the end of the century. Similarly, the largest increases in the mean monthly temperature for Bow River at Calgary and Elbow River near Sarcee Bridge were in May, where it increased by 4.9 and 5.1 ºC respectively while the smallest increase was in July where it increased by 3.8 and 4 °C respectively. Coupled MESH-atmospheric model runs for future changes in climate show an advance in the timing of snowmelt runoff in the Bow River at Banff and Calgary and the Elbow River near Sarcee Bridge by weeks to months due to earlier and smaller snowmelt runoff. In a warmer future climate, rain-on-snow events will be less frequent at lower elevations and more frequent at middle and higher elevations whilst snowmelt runoff events will decline almost everywhere and rainfall-runoff events will increase everywhere. Glacier

contributions to runoff will decline dramatically at high elevation locations with concomitant deglaciation, providing notable declines in late summer streamflow above Banff, but should cause a reduction in annual streamflow volumes of less than 2% (44 million cubic metres based on modeled flow) for the Bow River at Calgary and will have no impact on the Elbow River.

A novel way was devised to use bias correction from streamflow observations to reduce the uncertainty of modelled flow duration curves. This bias correction was also applied to future streamflow simulations. The effects of climate change on future streamflow was to reduce the highest streamflows and to increase the medium and low flows. A detailed examination of historical floods in June of 2005 and 2013 for current and future climates showed increases in flood flows for the Bow River at Banff, but reductions in flows at Calgary in the Bow and Elbow rivers due to changes in the precipitation regime, and reduced rain-on-snow runoff and antecedent snowmelt runoff – both are consequences of warmer conditions. Increased rainfall-runoff was unable to compensate for reductions in snow-based runoff processes for this flood event.

This study does have some important limitations. The present reservoir operation rule model does not take future changes in reservoir management into account and it is acknowledged that these will change in the future and have changed recently to add flood flow mitigation to operating objectives. The other considerable source of uncertainty is to substitute barren land in the place of glacierised areas for simulations of future hydrology. It is expected that deglaciated zones will develop vegetation and soils over time, but was assumed to be at longer time scales than considered in this study. The uncertainty of the climate change includes many aspects. The emission/radiative forcing aspects range from RCP2.6 to 8.5 for low end to high-end emission scenario. The report has chosen to show the high-end emission scenario that the world is currently on track for, and so that was fixed for this investigation. Uncertainty is introduced by the climate sensitivity of each GCM in the CMIP5, which shows large differences among the models under the same RCP8.5 scenario. Uncertainty also exists in how climate changes differences amongst the GCMs influence to the WRF dynamical downscaling results, then to the streamflow simulation in MESH. To fully represent this uncertainty due to the climate sensitivity of the GCMs and dynamical downscaling models, an ensemble of dynamical downscaling and hydrological modelling is needed, which is exceedingly expensive in computation. Uncertainty is indeed important, but not easy to tackle through the dynamical downscaling approach. However, it is always a good practice to present the results in the context of the layers of uncertainty in the climate projection due to uncertain emission scenarios, different climate sensitivities of models, downscaling models, and hydrological modelling. The WRF pseudo global warming (PGW) technique essentially “replays” historical weather with a modified atmosphere and boundary conditions. So, whilst storms and droughts are modified, the same sequence of weather is run for “future climate” and no new or longer storms or droughts can be introduced to the future climate. This may introduce errors into assessment of extreme events, but PGW is currently the most sophisticated way to dynamically downscale atmospheric models to the finer scales needed to produce reliable precipitation in mountains. Another key limitation of WRF is that it has only a single run due to its very high computational cost and so an assessment of uncertainty in streamflow estimation was not possible for this project beyond comparing the impact of various

driving meteorological datasets. Hence, it is recommended to incorporate the future climate uncertainty from RCMs into subsequent WRF modeling exercises in order to quantify the uncertainty behind impact of future climates on streamflow. A companion report, Centre for Hydrology Report No. 17 does exactly this and should be considered along with this foundational report as part of the case study of how to estimate future flood streamflows using coupled climate and hydrological models.

Acknowledgements

The authors wish to acknowledge the very helpful advice from the project committee composed of members of NRCan, ECCC, AEP, and the City of Calgary.

6. References

Asong ZE, Elshamy ME, Princz D, Wheater HS, Pomeroy JW, Pietroniro A, Cannon A. (2020). High-resolution meteorological forcing data for hydrological modelling and climate change impact analysis in the Mackenzie River Basin. Earth System Science Data, 12(1), 629-645. https://doi.org/10.5194/essd-12-629-2020

Bash, E.A., Marshall, S.J. (2014). Estimation of glacial melt contributions to the Bow River, Alberta, Canada, using a radiation-temperature melt model. Annals of Glaciology 55, 138–152. https://doi.org/10.3189/2014AoG66A226

Bernier, N.B., Bélair, S., Bilodeau, B., Tong, L. (2011). Near-Surface and Land Surface Forecast System of the Vancouver 2010 Winter Olympic and Paralympic Games. Journal of Hydrometeorology. 12, 508–530. https://doi.org/10.1175/2011JHM1250.1

Brutsaert W. (1975). On a derivable formula for longwave radiation from clear skies. Water Resources Research 11: 742–744. https://doi.org/10.1029/WR011i005p00742

Bolch T., Menounos B. and Wheate R. (2010). Landsat-based inventory of glaciers in western Canada, 1985–2005. Remote Sensing of Environment, 114(1), 127–137. https://doi.org/1016/j.rse.2009.08.015

Buck, A.L. (1981). New Equations for Computing Vapor Pressure and Enhancement Factor. Journal of Applied Meteorology, 20, 1527-1532. https://doi.org/10.1175/1520-0450(1981)020<1527:NEFCVP>2.0.CO;2

Canadian Dam Association (2019). Inventory of Large Dams in Canada 2019. Presented at the 87 th Annual Meeting and Symposium of the International Commission on Large Dams (ICOLD), Ottawa, Canada, June 9 to 14, 2019, p. 76. https://www.cda.ca/EN/Publications_Pages/Dams_in_Canada_2019.aspx

Clarke, G. K. C., Jarosch, A. H., Anslow, F. S., Radić, V., and Menounos, B. (2015). Projected deglaciation of western Canada in the twenty-first century. Nature Geoscience, 8, 372–377. https://doi: 10.1038/ngeo2407

Comeau, L.E.L., Pietroniro, A., Demuth, M.N. (2009). Glacier contribution to the North and South Saskatchewan Rivers. Hydrological Processes, 23, 2640–2653. https://doi.org/10.1002/hyp.7409

Côté, J., Gravel, S., Méthot, A., Patoine, A., Roch, M., Staniforth, A. (1998). The Operational CMC–MRB Global Environmental Multiscale (GEM) Model. Part I: Design Considerations and Formulation. Monthly Weather Review, 126, 1373–1395. https://doi.org/10.1175/1520-0493(1998)126<1373:TOCMGE>2.0.CO;2

DeBeer, C.M., Pomeroy, J.W. (2017). Influence of snowpack and melt energy heterogeneity on snow cover depletion and snowmelt runoff simulation in a cold mountain environment. Journal of Hydrology, 553, 199–213. https://doi.org/10.1016/j.jhydrol.2017.07.051

Demuth, Michael, Pinard, V, A.Pietroniro, Luckman, Brian, Hopkinson, Chris, Dornes, Pabo & Comeau, L. (2008). Recent and past-century variations in the glacier resources of the Canadian Rocky Mountains: Nelson River system. Terra Glacialis. Special Issue. 27-52.

Dornes, P.F., Pomeroy, J.W., Pietroniro, A., Carey, S.K., Quinton, W.L. (2008a). Influence of landscape aggregation in modelling snow-cover ablation and snowmelt runoff in a sub-arctic mountainous environment. Hydrological Sciences Journal, 53(4), 725–740. https://doi.org/10.1623/hysj.53.4.725

Dornes, P.F., Pomeroy, J.W., Pietroniro, A., Verseghy, D.L. (2008b). Effects of Spatial Aggregation of Initial Conditions and Forcing Data on Modeling Snowmelt Using a Land Surface Scheme. Journal of Hydrometeorology, 9, 789–803. https://doi.org/10.1175/2007JHM958.1

Essery, R., Li, L., Pomeroy, J. (1999). A distributed model of blowing snow over complex terrain. Hydrological Processes, 13, 2423–2438. https://doi.org/10.1002/(SICI)1099-1085(199910)13:14/15<2423::AID-HYP853>3.0.CO;2-U

Farjad, B., Gupta, A., Marceau, D.J. (2015). Hydrological Regime Responses to Climate Change for the 2020s and 2050s Periods in the Elbow River Watershed in Southern Alberta, Canada, in: Ramkumar, Mu., Kumaraswamy, K., Mohanraj, R. (Eds.), Environmental Management of River Basin Ecosystems, Springer Earth System Sciences. Springer International Publishing, Cham, pp. 65–89. https://doi.org/10.1007/978-3-319-13425-3_4

Farjad, B., Gupta, A., Razavi, S., Faramarzi, M., & Marceau, D. J. (2017). An integrated modelling system to predict hydrological processes under climate and land-use/cover change scenarios. *Water*, *9*(10), 767.

Fassnacht S.R, Snelgrove K.R., Soulis E.D. (2001). Daytime longwave radiation approximation for physical hydrological modelling of snowmelt: a case study of southwestern Ontario. Proceedings Sixth IAHS Scientific Assembly Symposium, IAHS 270. IAHS: Maastricht; 279–286

Freudiger, D., Kohn, I., Stahl, K., and Weiler, M. (2014). Large-scale analysis of changing frequencies of rain-on-snow events with flood-generation potential, Hydrology and Earth System Sciences, 18(7), 2695–2709. https://doi.org/10.5194/hess-18-2695-2014, 2014

Garnier, B.J., Ohmura, A. (1970). The Evaluation of Surface Variations in Solar Radiation Income. Solar Energy, 13(1), 21–34. https://doi.org/doi.org/10.1016/0038-092X(70)90004-6

Garnier, B.J., Ohmura, A. (1968). A Method of Calculating the Direct Shortwave Radiation Income of Slopes. Journal of Applied Meteorology, 7, 796-800. https://doi.org/10.1175/1520-0450(1968)007<0796:AMOCTD>2.0.CO;2

Gizaw, M.S., Gan, T.Y. (2016). Possible impact of climate change on future extreme precipitation of the Oldman, Bow and Red Deer River Basins of Alberta. International Journal of Climatology, 36(1), 208–224. https://doi.org/10.1002/joc.4338

Granger, R.J., Gray, D.M. (1990). A net radiation model for calculating daily snowmelt in open environments. Hydrology Research, 21(4-5), 217–234. https://doi.org/10.2166/nh.1990.017

Gudmundsson, L.; Bremnes, J. B.; Haugen, J. E. & Engen-Skaugen, T (2012). Technical Note: Downscaling RCM precipitation to the station scale using statistical transformations - a comparison of methods. Hydrology and Earth System Sciences, 16, 3383-3390. https://doi:10.5194/hess-16-3383- 2012

Haghnegahdar, A., Razavi, S., Yassin, F., Wheater, H. (2017). Multicriteria sensitivity analysis as a diagnostic tool for understanding model behaviour and characterizing model uncertainty. Hydrological Processes, 31(25), 4462-4476. https://doi.org/10.1002/hyp.11358

Hopkinson, C., & Young, G. J. (1998). The effect of glacier wastage on the flow of the Bow River at Banff, Alberta, 1951–1993. Hydrological Processes, 12 (10-11), 1745 - 1762. https://doi.org/10.1002/(SICI)1099-1085(199808/09)12:10/11<1745::AID-HYP692>3.0.CO;2-S

Li, Y., Li, Z., Zhang, Z., Chen, L., Kurkute, S., Scaff, L., & Pan, X. (2019). High-resolution regional climate modeling and projection over western Canada using a weather research forecasting model with a pseudo-global warming approach. Hydrology and Earth System Sciences, 23(11), 4635–4659. https://doi.org/10.5194/hess-23-4635-2019

Harder, P., Pomeroy, J.W., Westbrook, C.J. (2015). Hydrological resilience of a Canadian Rockies headwaters basin subject to changing climate, extreme weather, and forest management. Hydrological Processes, 29, 3905–3924. https://doi.org/10.1002/hyp.10596

Hopkinson, C., Young, G.J. (1998). The effect of glacier wastage on the flow of the Bow River at Banff, Alberta, 1951–1993. Hydrological Processes, 12, 1745–1762. https://doi.org/10.1002/(SICI)1099-1085(199808/09)12:10/11<1745::AID-HYP692>3.0.CO;2-S.

Ihaka, R., Gentleman, R. (2007). R: A Language for Data Analysis and Graphics. Journal of Computational and Graphical Statistics, 5(3), 299–314. https://doi.org/10.1080/10618600.1996.10474713

Islam, M.Z. (2013). Modeling the Hydrology and Water Resources Management of South Saskatchewan River Basin under the Potential Combined Impacts of Climate Change and Climate Anomalies [Doctoral dissertation, University of Alberta, Edmonton]. https://doi.org/10.7939/R31353

Islam, Z., Gan, T.Y. (2014). Effects of Climate Change on the Surface-Water Management of the South Saskatchewan River Basin. Journal of Water Resources Planning and Management, 140(3), 332–342. https://doi.org/10.1061/(ASCE)WR.1943-5452.0000326

López-Moreno, J.I., Pomeroy, J.W., Revuelto, J., Vicente-Serrano, S.M. (2013). Response of snow processes to climate change: spatial variability in a small basin in the Spanish Pyrenees. Hydrological Processes, 27(18), 2637–2650. https://doi.org/10.1002/hyp.9408

Liston, G.E., Elder, K. (2006). A Meteorological Distribution System for High-Resolution Terrestrial Modeling (MicroMet). Journal of Hydrometeorology, 7, 217–234. https://doi.org/10.1175/JHM486.1

Marty, C., Philipona, R., Fröhlich, C., Ohmura, A. (2002). Altitude dependence of surface radiation fluxes and cloud forcing in the alps: Theoretical and Applied Climatology, 72, 137-155. https://doi.org/10.1007/s007040200019

Mahfouf, J.-F., Brasnett, B., Gagnon, S. (2007). A Canadian Precipitation Analysis (CaPA) Project: Description and Preliminary Results. Atmosphere-Ocean, 45(1), 1–17. https://doi.org/10.3137/ao.v450101

Marsh, C.B,, Pomeroy, J.W., Wheater, H. (2020) The Canadian Hydrological Model (CHM) v1.0: a multi-scale, multi-extent, variable-complexity hydrological model – design and overview. Geosci. Model Dev., 13, 225–247, https://doi.org/10.5194/gmd-13-225-2020

Marshall S., White, E.C., Demuth, M.N., Bolch, T., Wheate, R., Menounos, B., Beedle, M.J., Shea, J.M. (2011). Glacier water resources on the eastern slopes of the Canadian Rocky Mountains. Canadian Water Resources Journal, 36(2), 109–134. https://doi: 10.4296/cwrj3602823

Matott, L.S. (2017). OSTRICH: an Optimization Software Tool, Documentation and User's Guide, Version 17.12.19, 79 pages, University at Buffalo Center for Computational Research. www.eng.buffalo.edu/~lsmatott/Ostrich/OstrichMain.html

Musselman, K.N., J.W. Pomeroy, N. Leroux, R. Essery (2015), Impact of windflow calculations on simulations of alpine snow accumulation, redistribution and ablation. Hydrological Processes, 29(18), 3983-3999. DOI: 10.1002/hyp.10595

Nazemi, A. and Wheater, H.S. 2014. How can the uncertainty in the natural inflow regime propagate into the assessment of water resource systems? Adv. Water Resour., 63: 131-142, doi: http://dx.doi.org/10.1016/j.advwatres.2013.11.009.

Oliphant, A.J., Spronken-Smith, R.A., Sturman, A.P., Owens, I.F. (2003). Spatial Variability of Surface Radiation Fluxes in Mountainous Terrain. Journal of Applied Meteorology, 42, 113–128. https://doi.org/10.1175/1520-0450(2003)042<0113:SVOSRF>2.0.CO;2

Peel, M.C., Finlayson, B.L., McMahon, T.A. (2007). Updated world map of the Köppen-Geiger climate classification. Hydrology and Earth System Sciences, 11(5), 1633–1644. https://doi.org/10.5194/hess-11-1633-2007

Pietroniro, A., Fortin, V., Kouwen, N., Neal, C., Turcotte, R., Davison, B., Verseghy, D., Soulis, E.D., Caldwell, R., Evora, N., Pellerin, P. (2007). Development of the MESH modelling system for hydrological ensemble forecasting of the Laurentian Great Lakes at the regional scale. Hydrology and Earth System Sciences, 11(4), 1279–1294. https://doi.org/10.5194/hess-11-1279-2007

Pomeroy, J.W., Gray, D.M., Landine, P.G. (1993). The Prairie Blowing Snow Model: characteristics, validation, operation. Journal of Hydrology, 144(1-4), 165–192. https://doi.org/10.1016/0022-1694(93)90171-5

Pomeroy, J. W., Toth, B., Granger, R. J., Hedstrom, N. R., Essery, R. L. H. (2003). Variation in surface energetics during snowmelt in a subarctic mountain catchment. Journal of Hydrometeorology, 4(4), 702-719.

Pomeroy, J.W., Stewart, R.E., Whitfield, P.H. (2015). The 2013 flood event in the South Saskatchewan and Elk River basins: Causes, assessment and damages. Canadian Water Resources Journal / Revue canadienne des ressources hydriques, 41(1-2), 105–117. https://doi.org/10.1080/07011784.2015.1089190

Rasmussen, R., Liu, C., Ikeda, K., Gochis, D., Yates, D., Chen, F., et al. (2011). High-Resolution Coupled Climate Runoff Simulations of Seasonal Snowfall over Colorado: A Process Study of Current and Warmer Climate. Journal of Climate, 24(12), 3015–3048. https://doi.org/10.1175/2010JCLI3985.1

Rasmussen, R., Ikeda, K., Liu, C., Gochis, D., Clark, M., Dai, A., et al. (2014). Climate Change Impacts on the Water Balance of the Colorado Headwaters: High-Resolution Regional Climate Model Simulations. Journal of Hydrometeorology, 15(3), 1091–1116. https://doi.org/10.1175/JHM-D-13-0118.1

Rasouli, K., Pomeroy, J.W., Marks, D.G. (2015). Snowpack sensitivity to perturbed climate in a cool mid-latitude mountain catchment. Hydrological Processes, 29, 3925–3940. https://doi.org/10.1002/hyp.10587

Rasouli, K., Pomeroy, J. W., Whitfield, P. H. (2019). Hydrological responses of headwater basins to monthly perturbed climate in the North American cordillera. Journal of Hydrometeorology, 20(5), 863-882.

Schirmer, M., Pomeroy, J. W. (2020). Processes governing snow ablation in alpine terrain–detailed measurements from the Canadian Rockies. Hydrology and Earth System Sciences, 24(1), 143-157.

Sheer, A.M.S., Nemeth, M.W., Sheer, D.P., Ham, M.V., Kelly, M., Hill, D., Lebherz, S.D. (2013). Developing a New Operations Plan for the Bow River Basin Using Collaborative Modeling for Decision Support. Journal of the American Water Resources Association, 49(3), 654–668. https://doi.org/10.1111/jawr.12068

Shook, K. (2016). The 2005 flood events in the Saskatchewan River Basin: Causes, assessment and damages. Canadian Water Resources Journal / Revue canadienne des ressources hydriques 41(1-2), 94–104. https://doi.org/10.1080/07011784.2014.1001439

Tanzeeba, S., Gan, T.Y. (2012). Potential impact of climate change on the water availability of South Saskatchewan River Basin. Climatic Change, 112, 355–386. https://doi.org/10.1007/s10584-011-0221-7

Tesfa, T. K., Leung, L. R., & Ghan, S. J. (2020). Exploring topography-based methods for downscaling subgrid precipitation for use in Earth System Models. Journal of Geophysical Research: Atmospheres, 125, e2019JD031456. https://doi.org/10.1029/2019JD031456

Thornton, P.E., Running, S.W., White, M.A. (1997). Generating surfaces of daily meteorological variables in complex terrain. Journal of Hydrology, 190(3-4), 214–251. https://doi.org/10.1016/S0022-1694(96)03128-9

Tolson, B.A., Shoemaker, C.A. (2007). Dynamically dimensioned search algorithm for computationally efficient watershed model calibration. Water Resources Research, 43(1), 1–16. https://doi.org/10.1029/2005WR004723

Valeo, C., Xiang, Z., Bouchart, F.J.-C., Yeung, P., Ryan, M.C. (2007). Climate Change Impacts in the Elbow River Watershed. Canadian Water Resources Journal / Revue canadienne des ressources hydriques, 32(4), 285–302. https://doi.org/10.4296/cwrj3204285

Veiga, V.B., Hassan, Q.K., He, J. (2015). Development of Flow Forecasting Models in the Bow River at Calgary, Alberta, Canada. Water, 7(1), 99–115. https://doi.org/10.3390/w7010099

Weedon, G. P., Gomes, S., Viterbo, P., Österle, H., Adam, J.C., Bellouin, N., Boucher, O. and M. Best, M. (2010). The WATCH forcing data 1958–2001: A meteorological forcing dataset for land surface and hydrological models. Technical Report No. 22, 41 pp

Weedon, G. P., Gomes, S., Viterbo, P., Shuttleworth, W. J., Blyth, E., Osterle, H., Adam, J. C., Bellouin, N., Boucher, O., and Best, M. (2011). Creation of the WATCH forcing data and its use to assess global and regional reference crop evaporation over land during the twentieth century. Journal of Hydrometeorology, 12, 823–848. https://doi.org/10.1175/2011JHM1369.1

Whitfield, P.H., Pomeroy, J.W. (2016). Changes to flood peaks of a mountain river: implications for analysis of the 2013 flood in the Upper Bow River, Canada. Hydrological Processes, 30, 4657–4673. https://doi.org/10.1002/hyp.10957

Whitfield, P.H, Pomeroy, J.W. (2017) Assessing the quality of the streamflow record for a long-term reference hydrometric station: Bow River at Banff, Canadian Water Resources Journal, 42:4, 391-415, DOI:10.1080/07011784.2017.1399086.

Yanping Li, Zhenhua Li, Zhe Zhang, Liang Chen, Sopan Kurkute, Lucia Scaff, and Xicai Pan, (2019). High-Resolution Regional Climate Modeling and Projection over Western Canada using a Weather Research Forecasting Model with a Pseudo-Global Warming Approach. Hydrology and Earth System Sciences, 23(11), 4635-4659. https://doi.org/10.5194/hess-23-4635-2019

Zhang, X., Harvey, K.D., Hogg, W.D., Yuzyk, T.R. (2001). Trends in Canadian streamflow. Water Resources Research, 37(4), 987–998. https://doi.org/10.1029/2000WR900357

Zhang, Z., Li, Y., Chen, F. et al. (2018). Evaluation of convection-permitting WRF CONUS simulation on the relationship between soil moisture and heatwaves. Climate Dynamics. https://doi.org/10.1007/s00382-018-4508-5

Zhang, T., Li, B., Yuan, Y., Gao, X., Sun, Q., Xu, L., & Jiang, Y. (2018). Spatial downscaling of TRMM precipitation data considering the impacts of macro-geographical factors and local elevation in the Three-River Headwaters Region. Remote Sensing of Environment, 215, 109–127. https://doi.org/10.1016/j.rse.2018.06.004.

7. Appendix A: Model Parameters

A.1 Calibrated model Parameters for Various Forcing

Land Cover	Parameter	CanRCM4	GEM-CaPA	WFD-CRU	WFDEI	WRF	WFDEI-GEM-CaPA	CanRCM4-WFDEI-GEM-CaPA
Barren land	ZSNL	0.3	0.04	0.47	0.26	0.48	0.06	0.46
	ZPLS	0.11	0.09	0.09	0.19	0.2	0.12	0.08
	ZPLG	0.15	0.1	0.1	0.16	0.2	0.17	0.11
	SDEP	0.6	0.9	0.5	0.5	0.4	0.63	0.5
	KSAT	3.20E-05	1.90E-04	3.40E-05	6.80E-05	6.50E-03	9.30E-05	2.80E-05
	DDEN	75	11	86	85	3	45	98
Forest	ROOT	1.5	1.8	1.9	0.8	1	1.2	2
	RSMN	223	220	207	216	176	221	200
	SDEP	1.8	3.4	3.4	1	1	1.2	1.7
	KSAT	9.10E-06	4.10E-03	3.40E-05	3.10E-04	1.70E-04	3.20E-03	1.70E-04
	DDEN	90	98	100	30	23	35	4
	MANN	0.11	0.24	0.23	0.29	0.16	0.12	0.14
Two River Class Routing	PWR1	1.1	2.4	1.6	2.1	2.9	2.4	1.8
	FLZ1	2.43E-05	2.02E-04	5.86E-06	1.33E-07	8.39E-03	1.28E-03	1.43E-04
	R2N1	0.15	0.07	0.16	0.03	0.1	0.04	0.11
	R1N	0.52	0.1	0.28	0.07	0.12	0.1	0.41
	PWR2	2.8	2.7	1.4	3	1.5	2.6	1.8
	FLZ2	1.05E-07	4.63E-03	5.60E-07	8.48E-03	1.81E-06	6.55E-03	9.04E-06
	R2N2	0.15	0.01	0.1	0.04	0.08	0.02	0.12
	R1N2	0.52	0.05	0.18	0.07	0.21	0.05	0.31

A.2 Parameters used for blowing snow model

GRUs Name & their Orders	Fetch (m)	Veg. Height (m)	Stalk Density (# / m ^{2})	Stalk Diameter (m)	Distribution Factor
Urban	1000	6	320	0.003	0
Glaciers	1000	0.2	320	0.003	1
Barren land, North Facing	1000	0.1	320	0.003	1
Barren land, South Facing	1000	0.1	320	0.003	1
Barren land, Flat	1000	0.1	320	0.003	1
Cropland, Flat	1000	0.35	320	0.003	1
Grassland, Flat	500	0.4	200	0.003	1
Forest, South Facing	300	6	100	0.01	1

Forest, North Facing	300	6	100	0.01	1
Forest, South Facing	300	6	100	0.01	1
Water	300	6	1	0	1

A.3 Other vegetation Parameters used in this modeling exercise derived from literature and CLASS default values

Parameters	**Forest**	**Barren land**	**Crop**	**Grass**	**Water**	**Urban**	**Glacier**
RSMN	Calibrated		85	100	-	-	-
QA50	30		30	30	-	-	-
VPDA	0.65		0.5	0.5	-	-	-
VPDB	1.05		1.0	1.0	-	-	-
PSGA	100		100	100	-	-	-
PSGB	5.0		5.0	5.0	-	-	-
LAMX	2.0		1.5	1.5	-	-	-
LAMN	1.6		0.0	1.5	-	-	-
LNZ0	0.41	-4.605	-2.53	-4.60	-6.90	1.35	-6.215
ALVC	0.02		0.043	0.062	0.07	0.09	0.40
ALIC	0.18		0.276	0.263	0.14	0.15	0.20
CMAS	12.0		2.0	0.2	-	-	-
ROOT	1.0		1.0	0.1	-	-	-
MANN	Calibrated	0.027	0.035	0.03	0.04	0.015	0.027